REALISATION OF AN EFFICIENT TERAHERTZ SOURCE USING QUANTUM DOT DEVICES

NASIR GARBA BELLO

Doctor of Philosophy

ASTON UNIVERSITY

December 2021

Abstract

The development of a compact, tunable, room-temperature operating THz source remains one of the key unsolved tasks in the scientific community to unlock the numerous advantages and applications of THz radiation in spectroscopy, communication, sensing, and imaging among others. Pulsed terahertz systems requires femtosecond optical pumping from mainly bulky lasers, while earlier approaches of continuous-wave(CW) THz generation involved using pumped gas lasers which were very bulky and barely tunable. However, more recent sources of CW THz mostly use Quantum Cascade lasers (QCL) and Photoconductive antennas (PCA); The QCL suffers from cryogenic operating conditions and production complexity that keeps it out of commercial reach while conventional Photoconductive antennas are mainly limited by low optical-terahertz conversion efficiency.

The use of quantum dots (QD) in PCA substrate material for THz generation has been implemented by research in this thesis to achieve both pulsed and continuous wave terahertz radiation, to provide access to optical pumping from compact semiconductor lasers and more importantly to reduce the carrier lifetime in PCAs to enable more efficient and optimised photoconductive antenna for THz generation.

This research has demonstrated a tunable continuous-wave Quantum Dot external cavity laser emitting at two frequencies as an optical pump for continuous wave terahertz generation. The external cavity QD Laser has been characterised with tunability of 152nm and a tuning range from 1143nm-1295nm that lies within the THz difference frequency for the generation of THz radiation from PCAs.

This research work also presents the enhancement of THz PCA's power output with Quantum dots at pump powers and operating conditions that are analogous to that of semiconductor lasers for a compact THz system. The generation of pulsed THz radiation from the designed quantum dot pho-

toconductive antennas (PCAs) pumped at 800nm and 700nm and optical pump power of 1mW-10mW with an applied bias voltage of 2V-20V has been recorded and presented in chapter 4.
This PhD project investigates the output and characteristics of the generated THz from the QD PCAs alongside a comparison with a commercial antenna from Teravil with low-temperature grown GaAs substrate. The QD PCAs outputs significantly higher THz power than the commercial PCA at low pump powers that are representative of semiconductor lasers. This provides a significant step towards the realisation of an efficient compact THz system.

Acknowledgement

All praises and thanks are due to God who has given me the blessing of life and health to be able to carry out this PhD research project. Furthermore, I would like to start by thanking my parents Hon. Garba Bello Yabo and Mrs Fatima Garba Bello for being my pillar of support and fountain of solace throughout my life; your relentless support psychologically, socially and economically has been benevolent. I would also like to thank my family at large, especially my Uncle Dr Ahmed Mohammed and his family, who became my second home in the UK.

My sincere thanks and gratitude to my Supervisor Prof Edik Rafailov and Associate Supervisor Prof Sergei Turitsyn for giving me the opportunity to work on this research project. I would like to especially thank Prof Edik Rafailov for his guidance, support and an open-door policy that made me feel always welcome to seek his help and assistance.

I would also like to thank my research group members and Postdocs Dr Amit Yadav and especially Dr Semyon Smirnov who has given immense support and guidance to me throughout the course of this project. I would also like to thank Dr Andrei Gorodetsky for all his amazing contributions and support.

Nomenclature

THz - Terahertz
GHz - Gigahertz
mm - millimetre
µm - micrometre
nm - nanometre
TD - Time-domain
TDS - Time-domain spectroscopy
PCA - Photoconductive Antennas
QD - Quantum Dot
QW - Quantum well
QCL - Quantum Cascade Laser
RTD - Resonant tunneling diode
CW - Continuous wave
EC - External cavity
ECDL - External cavity diode laser
DG - Diffraction gratings
LO - Longitudinal-optical
LTG - Low temperature grown
MBE - Molecular beam epitaxy
SI - Semi-insulating
TEC - Thermoelectric cooler
APE - Angewandte Physik & Elektronik GmbH
LD - Laser diode
GaAs - Gallium Arsenide
NH_3 - Ammonia
CH_3F - Fluoromethane
CH_3F_2 - Difluoromethane
CH_3OH - Methanol
CH_3I - Iodomethane

$LiNBO_3$ - Lithium niobium trioxide or Lithium niobate
RD - Radiation damaged
InAs - Indium Arsenide
IV - Current-Voltage
SNR - Signal to noise ratio
QD_Bt1 - Quantum dot bow-tie antenna 1
QD_Bt1 - Quantum dot bow-tie antenna 2
QD_id - Quantum dot antenna with interdigitated electrodes
QD_Pl - Quantum dot antenna with plasmonic gratings

List of Figures

List of Tables

Contents

Chapter 1

1.1 Introduction

The motivation behind this PhD research project is to facilitate the realisation of compact and efficient THz devices for biomedical applications. The non-ionising, non-invasive feature of THz diagnostic technology makes it a strong candidate for a safe medical imaging system. THz imaging devices can pave the way towards early cancer detection due to the increase in water content in cancerous cells and the strong absorption of THz waves by water. However, electromagnetic waves at THz frequencies have long had a bottleneck in efficient generation and detection, which led to the term THz gap, high band-gap energy in optical based sources and high parasitic losses in electronic sources means techniques such as up-conversion from electronic sources or downconversion from optical sources need to be implemented in order to generate THz. This research focuses on the use of Quantum dots to optimise the optical to THz efficiency in PCAs and also the use of QDs as active region for laser diodes as optical pump sources for THz generation.

Thesis overview

This thesis starts with an introduction and overview of the fundamental literature underpinning THz science and technology in chapter 1. This chapter looks at THz generation methods, detection methods and application.

Chapter 2 starts by establishing the usage of photoconductive antenna as the method of choice towards realising a compact, tunable and efficient terahertz source. It identifies the optical to THz conversion efficiency of the PCA as the main drawback with this technology. Furthermore, it establishes the use

of Quantum dot devices in Photoconductive antenna substrates to optimize the optical to THz efficiency of PCAs and also to pave the way for bandgaps that will allow using pump sources such as fiber lasers and semiconductor lasers.

In Chapter 3, continuous wave THz system is presented with the potential for realising compact THz sources due to the lack of requirement of femtosecond laser sources that are bulky and mostly require liquid cooling. A quantum dot dual wavelength laser diode was designed and characterised at THz difference frequencies for integration in a THz CW system.

Chapter 4 deals with the testing and comparison of the designed quantum dot antennas with a commercial Teravil antenna. Coherent and incoherent terahertz detection techniques were used by the aid of a PCA and a Golay cell respectively to obtain the amplitude and phase of the generated THz radiation as well as the intensity.

Finally, the thesis culminates with a conclusion of the undertaken research project and a future outlook for the advancement of this research.

1.2 Introduction to Terahertz

Terahertz (THz) refers to the region in the electromagnetic spectrum that is defined from around 300GHz – 10THz in frequency, 1mm - 30µm in wavelength, 9.9cm^{-1} - 330cm^{-1} in wave number and 1.24meV - 41.4meV in photon energy. It lies between the microwave and optical infrared frequencies, which gives it properties that make the generation of coherent and high-power THz radiation more difficult than its surrounding frequencies. The position of terahertz on the Electromagnetic spectrum is shown in Fig 1.1 below as the purported THz gap [7]. Based on classical electrodynamics, the terahertz region is the highest frequency where emission of electromagnetic radiations can be achieved using an electric dipole. This has made it challenging to realise high frequency antennas, especially at terahertz frequencies, which is because common architectures used at microwave frequencies present extremely high losses at high frequencies due to the strong dielectric absorption. However, recent research from both sides of the spectrum surrounding terahertz has seen microwave technologies and optical technologies shrink what has been referred to as the ‘’Terahertz gap”; but THz technologies still face some serious limitations that will be highlighted in this report [7]. Terahertz radi-

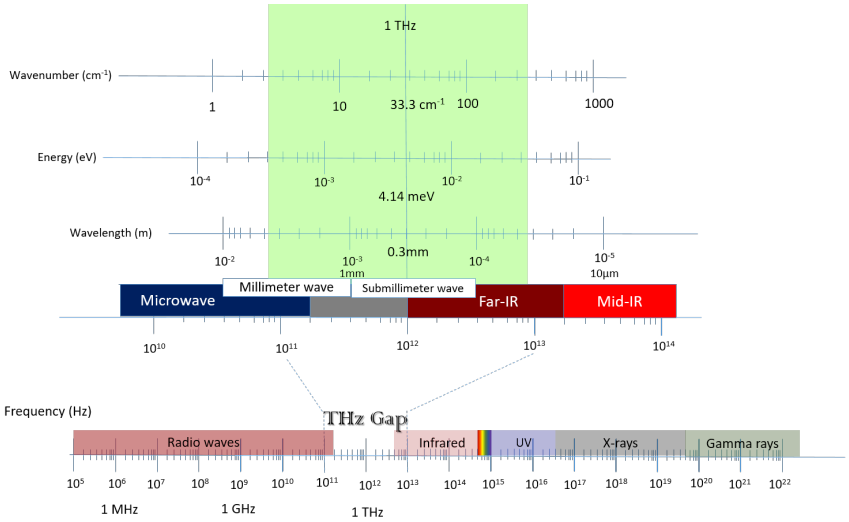

Figure 1.1: The THz frequency regime on the electromagnetic spectrum [7]

ation has a wide range of applications from security sensing to high data-rate short-range communication, to seeing through layers of artwork. Moreover, its characteristic reactions with molecules and low photon energy have given it a lot of potential in biomedical applications. These applications are still limited due to the lack of enablement by robust and practically usable terahertz devices. A fundamental breakthrough in terahertz technology is in the realisation of an ultra-compact high power room temperature operable THz source [8][9]. It remains one of the least developed spectral regions, although there has been a surge of activity in the past decade; immensely desired for many applications is a compact, coherent, continuous wave (cw) solid-state source, analogous to the semiconductor laser diode in the visible and infrared, or to transistor oscillators and amplifiers in the microwave[7].

1.3 Terahertz Generation Methods

In the last few decades, numerous works and research in the terahertz field has led to advances in terahertz generation methods using both optical and electronic sources. This section will focus on the methods of generation of terahertz and give a particular emphasis to why the method of choice for this research was chosen to be the use of Photoconductive antennas. Elec-

tronic solid sources that are based on semiconductors such as oscillators and amplifiers exhibit high frequency roll-off resulting from reactive parasitics or transit times as shown in Fig 1.2 below, another drawback in these sources is the simple resistive losses that dominates the device impedance at higher frequencies such as in the terahertz range of frequencies [8, 7]. Optical sources require operation in a level that is so low at meV range that they are comparable to that of the lattice phonons i.e. the relaxation energy in the crystal; this necessitates the use of cryogenic cooling to overcome this problem. Tube sources face physical scaling problems, metallic losses, as well as the need for both extremely high electric and magnetic fields. The main successful approaches of generating THz radiation are frequency up conversion from millimetre wavelengths and frequency down conversion from the optical wavelengths[10].

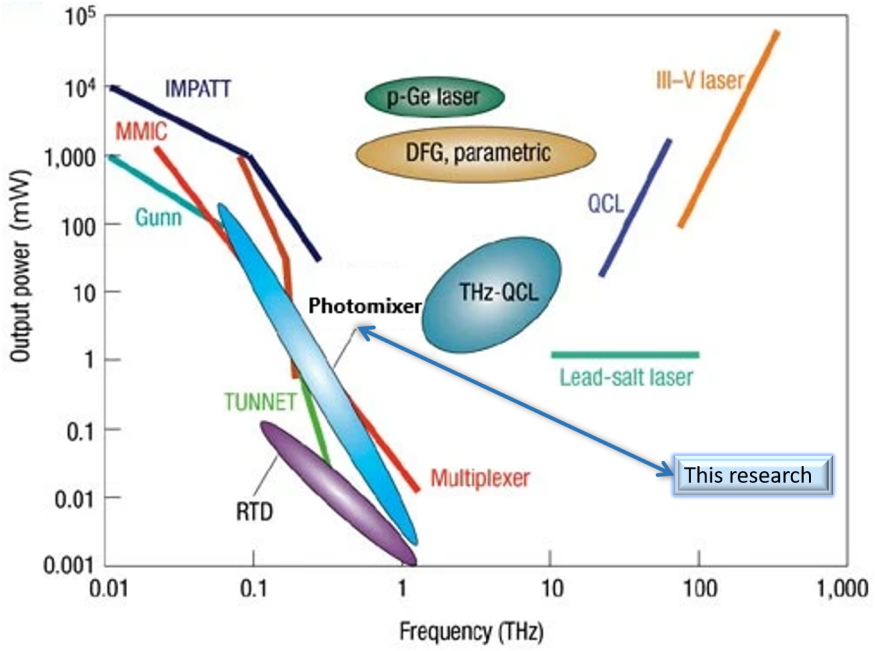

Figure 1.2: Terahertz Generation methods power vs frequency plot [11]

1.4 Terahertz sources

This research will review optical and electronic methods of terahertz generation particularly using Quantum Cascade lasers and Photoconductive Antennas as these are the most widely used methods and propose a terahertz generation method using Quantum dot Photoconductive Antennas pumped by a Quantum dot laser. Table 1.1 summarises the power output, frequency and temperature operating conditions of the THz sources discussed in section 1.4.

1.4.1 Electron Beam Sources

Free Electron Lasers (FELs), Gyrotrons, Backward wave oscillator (BWO) are terahertz sources based on electron beam that generate relatively high power signals. Energy transfer occurs between the electron beam and the electromagnetic wave from the interaction of a high energy electron beam with a strong magnetic field inside resonant cavities or waveguides.

Free Electron Laser:

The FEL as opposed to a conventional laser produces coherent radiation from a beam of free electrons rather than electrons bounded to atoms or molecules. For an FEL THz source, pulses of electrons are generated by an injector, then accelerated inside an RF accelerator to relativistic velocities[8].The electron bunch pulses are then injected into the undulator following the accelerator. The undulator or wiggler is a series of magnets that produces a magnetic field that is transverse to the direction of a relativistic beam.The electron bunch is forced into a 'wiggling' motion that causes the electrons to radiate independently [17]. The radiation wavelength for the FEL is determined by the wiggler period, magnetic field strength and the electron beam energy. The FEL operates in pulse mode and provide wide tenability and high-power, however, the requirement for electron accelerators makes it not feasible for standard laboratory usage[18].

Gyrotrons:

As early as the 1970s and 1980, Gyrotrons have been used to generate waves at 0.33 – 0.65 THz. Gyrotrons are powerful sources of coherent radiation

Table 1.1: Terahertz sources and reported power outputs [1, 2]

Source	Technology	THz	Temperature condition	THz Output Power	Ref
BWO	Vacuum electronic	0.65	Room	50mW	[12]
		0.1	Room	1.56 mW	
		0.2	Room	10 kW	
Free electron lasers	Vacuum electronic	0.1–4.8	Room	5 kW	[13]
		1.28–2.73	Room	20 W	
Frequency multiplication devices	Solid state electronic	0.7–1.1	Room	0.625 mW	[2]
		0.1–0.17	Room	16 mW	
Quantum cascade Lasers	Lasers	4.4	8 K	2mW(peak)	[14]
		4.4	10 K	0.02mW (average)	[15]
THz Photoconductive Antennas	Photoconductive switching	0.05THz-6THz	Room	1 µW at 10mW optical pump power	[16]
	Photomixing CW	0.25–2.4 THz tunable	Room	100 µW at 1THz and 100mW Optical pump power	[1]

in both pulsed and continuous wave regime. Gyrotron works based on the phenomena of Electron Cyclotron Resonance Maser ECRM instability, it employs a cathode emitting electron beam that enters into a cross electric and magnetic field, the electrons gyrate in the longitudinal magnetic field at their cyclotron resonance frequency, radiate then interact with the EM field

in the cavity. The frequency of the emitted radiation is determined by the magnetic field strength, in the case of THz frequencies, the strong magnetic field is needed or by using the harmonics of the fundamental frequency to obtain some THz power[19][20].

Backward wave oscillator:

The BWO is used to produce tuneable terahertz radiation by the utilisation of electrons and an applied DC voltage to transfer energy to an electromagnetic wave. The alteration of the DC voltage across the system alters the velocity of the electrons and hence determining the frequency of the electromagnetic wave, which allows for tuning over a range of frequencies. BWO have a limited spectral range over the terahertz frequencies, which means multiple BWOs are required for covering the THz range[7][21]. As can be seen Fig 1.3, the BWO operates by the extraction of energy from a bunched electron beam to a high frequency RF electric field, the drift velocity of the electrons has to be slightly higher than the phase velocity of the electromagnetic field for an effective energy transfer. Electrons emitted from a heated cathode at

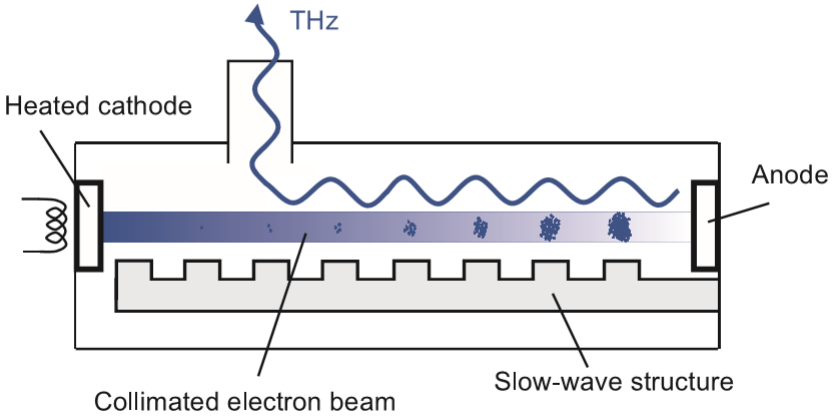

Figure 1.3: A schematic of a THz Backward wave oscillator [8]

one end of a vacuum tube are collimated by a magnetic field and accelerated towards an anode at the other end of the vacuum tube. A periodic structure is designed such that one component of the E-field, a backward-travelling wave, has the required phase velocity from the electrons. A waveguide is

utilised to couple out the amplified THz wave. BWOs are mostly used at frequencies below 1THz. Operating Frequencies ranging from 0.03 - 1THz and output power of up to 100mW below 200 GHz with 1mW power at 1THz have been reported [22] .

1.4.2 Up conversion

A successful technique of generating THz radiation is up-conversion of high frequency microwave signals from electronic sources to THz radiation. This is achieved via nonlinear reactive of lower frequency oscillators [10], as will be described in further details in section 1.4.3 below.

1.4.3 Frequency Multiplication:

This is based on the use of non-linear devices that generate harmonics of an input signal and suppress undesired ones. An electronic device with a non-linear response normally the Schottky barrier diode is used to upconvert microwave frequencies from sources such as Gunn diodes, Impatt diodes and Resonant tunnelling diodes into THz frequencies. The Schottky diode uses a metal semiconductor junction which is called the Schottky barrier, and the high conductivity of the metal contact leads to very high switching rates. Either the non-linear capacitance (varactor) or the non-linear resistance (varistor) of the device is utilised for the frequency multiplication. THz radiation can be generated by the up-conversion of microwave frequencies in nonlinear devices (frequency multipliers) mainly in the form of two-terminal solid-state devices such as Gunn diodes, impatt diodes and resonant tunnelling[8]. diodes.[7][8].

Gunn Diodes:

These are 2-terminal negative differential resistance (NDR) devices that generate radio frequency power when coupled with a suitable tuned AC resonator. A gunn diode will normally consist of a uniformly doped n-type material such as GaAS or InP sandwiched in-between highly doped regions at each terminal. Diode frequency multipliers generate the harmonics of an imput signal by utilising the reactive and/or the resistive nonlinearity of the diode[7, 8]. GaAs Gunn diodes operating from 10GHz- 100GHz have been

reported, and GaN based gunn diodes of above 300GHz with -840mW power output at 88GHz have been reported [23].

IMPATT Diodes:

(Impact ionisation transit time) have relatively high power capability, and they attain NDR from time delays achieved by applying an AC signal with a mean value just below the avalanche breakdown, the avalanche breakdown results from having a reverse bias across the pn-junction over a certain threshold value, this results in a large number of carriers in the avalanche region that moves through the drift region to the anode over a period of the transit-time delay. With the application of an AC signal just below avalanche breakdown[7, 8].

Resonant Tunnelling diodes:

are based on the formation of quantum well from layers of un-doped materials between two thin barriers. Resonant tunnelling occurs when an energy level in the quantum well is close to the energy of the electrons in the conduction band. In lieu with other NDR devices, a resonant tunnelling diode can generate electromagnetic radiation in an external resonant circuit. RTD produce the highest oscillations from the aforementioned microwave diode sources due to the tunnelling being a very fast process[8].

1.4.4 Lasers

THz can be generated using some direct lasers such as Far-IR gas lasers, P type germanium lasers and Quantum Cascade lasers. Far-IR lases operates on the molecular rotation of energy levels whose transition frequencies are in the THz region. P-type germanium lasers population inversion from two Landau levels formed by hot carriers that are submerged in crossed electric and magnetic field. Quantum cascade lasers operate based on transitions of sub-bands in semiconductor heterostructures, electrons undergo a successive intersubband transitions for the generation of THz.

Far-IR Gas Lasers

Optically pumped far-IR gas lasers emits THZ radiation based on the rotational transitions of gas molecules that have permanent electric dipole mo-

ment such as NH_3, CH_3F,CH_2F_2,CH_3OH and CH_3I, their rotational transitions are directly coupled to electromagnetic radiation via dipole interactions. The molecules are excited by optical pumping with usually CO_2 gas laser to take the molecules from the lowest excited vibrational state to the first excited vibrational state. THz radiation is emitted as a result of population inversion between the rotational states corresponding to the excited vibrational level. Power levels of 1-20mW are common for 20-100W laser pump power[24, 7].

P-type Germanium Laser

Another type of Terahertz laser is the p-type germanium laser, which is a tunable, solid state electrically pumped laser. It lases, based on the streaming motion and population inversion of hot carriers in p-type Ge crystals that are submerged in crossed electric and magnetic field. The THz photons are generated from the stimulated transitions between two light-hole landau levels, which is a discrete quantum mechanical energy level as a result of spatial confinement. P-type germanium lasers are tunable over 1-4 THz by changing the applied electric/magnetic field. Cryogenic cooling is required in the operation of p-type germanium lasers to avoid optical and acoustic lattice scattering[8][7].

Quantum Cascade Laser

Quantum cascade laser was first demonstrated at Bell laboratories in 1994 with a short wavelength of 4µm, they rely on only one type of carrier and on electronic transitions between conduction band states arising from size quantisation in semiconductor heterostructures[3, 25, 2, 26]. Quantum cascade lasers are semiconductor heterostructure lasers consisting of a periodically alternating layers of dissimilar semiconductors. Transition between subbands of these semiconductor nanostructures involve THz photons. In a QCL, electrons go under a successive intersubband transition to generate coherent THz radiation[7]. Over the years, immense contribution has been made by researchers towards achieving room temperature THz Quantum Cascade laser. The works of Mikhail A. Belkin, Federico Capasso, Alessandro Teriducci, M. Razeghi and other pioneers in THz Quantum cascade laser have made an outstanding contribution towards a room temperature THz QCL.

Room temperature THz Quantum Cascade Laser using III-Nitrides

A substantial development has been made in GaAs/AlGaAs based THz Quantum Cascade lasers with an operating temperature close to 200K [27]. Table 1.2 on page 25 shows THz power outputs from Quantum cascade lasers, as well as their operating temperatures. Khorami et al. designed a GaAs/AlGaAs quantum cascade laser for operation at high temperatures [28]. However, higher temperatures are severely limited by a small longitudinal-optical phonon energy in GaAs/AlGaAs (36meV). III-Nitrides are promising candidates for a room temperature THZ quantum cascade laser with their much larger longitudnal-optical phonon energy of around 90meV. Also, the use of difference frequency generation through two mid-infrared wavelengths in InP is promising towards realising highly efficient and high temperature THz quantum cascade laser[27, 29]. A THz Quantum cascade laser with an

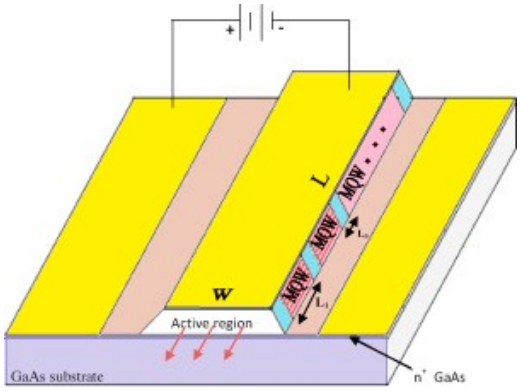

Figure 1.4: A GaAs/AlGaAs THz Quantum Cascade laser [28]

active region of GaAs/AlGaAs implemented towards realising a room temperature operation can be seen in Figure 1.4 above.

1.4.5 Down conversion

Another successful technique of generating terahertz radiation is by down conversion from optical sources, mainly using photoconductive devices and non-linear crystals.

Table 1.2: THz Quantum Cascade Lasers and their temperature performance and Optical Power output[3, 2]

Frequency(THz)	Operating Temperature (K)	Power Output	Year of Publication
4.4	8	2mW	2002
4.4	10	0.02mW	2006
3.4	10	139 mW CW	2014
3.4	77	248 mW (pulsed)	2014
3	178	1 W (pulsed)	2008
3.15	129	20 mW	2014
3	225	420 mW	2009
5	250	1µW	2008
	80	7 µW	2008

Optical Rectification in non-linear crystals

Terahertz radiation can be generated by optical rectification based on a second order non-linear effect. In this process, a train of visible or near IR ultrashort pulses are focused on a second order non-linear materials such as dielectric crystals. Material such as $LiNbO_3$, $LiTaO_3$, ZnTe have been used in the generation of THz via optical rectification. THz radiation can be generated in pulse regime from pulsed pump laser sources and also in continuous wave through difference frequency generation[8, 7]. Optical rectification has been widely implemented as an efficient approach of terahertz generation and generating high energy THz at low THz frequencies (0.2-0.8THz) that are more suitable for spectroscopy [30].The common nonlinear materials used for OR are ZnTe and $LiNbO_3$; ZnTE presents a problem of free carrier absorption while $LiNBO_3$ shows advantages in high damage threshold, low THz absorption, but it requires tilted front pumping technique to match the phase of the IR pump and THz wave. Because of the ability to cascade the non-linear process, high photon conversion efficiency can be achieved[31]. Jewariya et al. generated efficient terahertz conversion via a non-linear process in $LiNbO_3$ with a phased controlled femtosecond Ti:Sapphire laser pulse [32]. Shu Wei Huang also demonstrated a high conversion efficiency, high energy terahertz using cryogenically cooled $LiNbO_3$[31].

Photoconductive emitters

The first demonstration of generating pulsed terahertz radiation was by Auston et al. in 1984, where they used a PCA with a 10 µm gap size illuminated by a femtosecond laser; it will be until 1993 that E.R. Brown et al. will demonstrate coherent THz generating by employing the photomixing technique also referred to as optical heterodyne conversion. This method also capitalises on the use of PCAs illuminated by a laser to achieve THz generation[33, 34] The THz PCA allows for the generation of both CW and pulsed THz radiation by down conversion from a suitable optical pump. As PCAs are the method of choice for this PhD research, there will be a more comprehensive overview of PCAs in chapter 2 and the generation of CW THz via photomixing in PCA is discussed in Chapter 3.

Table 1.3: Comparison of Terahertz Generation methods with key advantages and disadvantages [4, 5]

	PCAs	Optical rectification
THz radiation properties	• Asymmetric quasi half-cycle THz pulses with peak field of few hundreds kVcm^{-1} • Low THz frequencies (0.1-1 THz) • Picosecond pulse duration • Large spot size ($\geq$2.5 mm)	• Single to multi–cycle THz pulses with peak fields from several 100 kVcm^{-1} up to several MV cm^{-1} • Broad bandwidth, from 0.1 THz to 6 THz, depending on the nonlinear crystal
Advantages	• High stability • Extraction of THz energy from the bias voltage	• High optical-terahertz conversion efficiency • Simple experimental configuration • High stability
Disadvantages	• Relatively low THz peak electric field of below 1.5 MV/m as compared to over 40 GV/m • Laser damage threshold of the antenna • High electromagnetic noise • THz radiation saturation at low optical fluence • Short life-time of the emitter	• Laser damage threshold of the nonlinear medium • Complicated phase matching conditions for some crystals • Thermal damage and multi-photon absorption from increase in free carrier density in the crystals when pumping at high laser intensities above 10GW/cm^2

1.5 Terahertz Detection Methods

Terahertz detection techniques are conventionally classified into two, i.e. coherent or incoherent (homodyne). The coherent methods measure the amplitude and phase of the input field, while the incoherent measures the intensity. For the purpose of this research, the coherent detection was carried out by

employing a PCA and the incoherent detection was carried out with the aid of a commerical Golay cell from Tydex.[8]. THz detection methods have been achieved by utilising microwave techniques such as rectification; a rectifier such as the Schottky diode is used by exploiting the non-linear I-V relationship to produce an output voltage proportional to the input current induced from an incident THz radiation[7].

Thermal detectors

Thermal devices are usually used for the detection of CW THz radiation, the devices employ the use of an absorber that exploits thermal dependant properties such as electrical resistivity for bolometers, electrical polarisation for pyroelectric detectors and gas pressure for Golay cell. These devices generally have a broad spectral response, but can be relatively slow due to the requirement for the absorbing element to reach thermal equilibrium before measurements can be taken. The main parameter in thermal detectors is their noise equivalent power NEP[7, 8].

Bolometer

In a bolometer, a material whose electrical resistivity is sensitive to temperature is used as an absorber; and a resistance thermometer is used to measure the temperature change due to the incident radiation. For highly sensitive detection, it requires L-He temperatures. Bolometer is the most sensitive detection method in the THz range, and hence why the Golay cell used in the experiments for this doctoral research was calibrated using a bolometer to ensure the accuracy of the obtained results[35].

Golay Cell

Golay cells are sensitive pneumatic radiation detectors that operates from millimeter waves to near IR. They are really important and wide spread in THz applications and THz systems as the Golay cell is the most sensitive thermal radiation detector that operates at room temperature and owing to this the golay cell was implemented for the detection of the THz output power in this research as will be seen in chapter 4[7]. A golay cell uses a semi-transparent absorbing film placed inside a pneumatic cell. THz radiation incident on the absorber heats up the gas inside the cell and as stated

by Charles's law the gas pressure increases and the gas expands, a flexible mirror fixed at the end of the cell gets deformed and the motion gets detected by an optical reflectivity measurement as can be seen in Fig 1.5 below

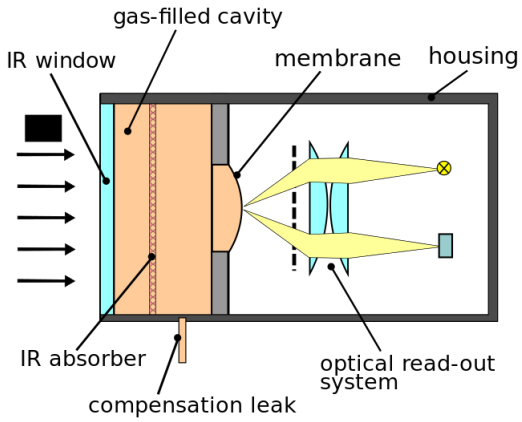

Figure 1.5: A schematic of a Golay cell detector[36]

Electro-Optic Sampling

Free space EO sampling can be used to measure the electric field of THz pulses in time domain while measuring both the amplitude and phase with high precision. The principle underpinning EO sampling is the Pockels effect which has the same nonlinear coefficients as optical rectification. The incident THz field induces birefringence in a nonlinear optical crystal that is proportional to the amplitude of the field. A weak optical probe is utilised in measuring the field induced birefringence as a function of the relative time delay between the THz and the optical probe pulse to obtain the waveform[7].

Photoconductive antenna

PCAs as used in this research work can also be utilised to measure broadband THz pulses in the time domain. A THz field incident on the PCA gap induces a current when an optical probe pulse injects photocarriers, the photocurrent induced is proportional to the amplitude of the THz field. Varying the time delay between the THz pulse and the optical probe pulse while measuring the

photocurrent allows for the THz pulse in the time domain to be outlined[7].

Lock-in detection

The THz signal detected for most sources is very small and surrounded by a noisy environment that necessitates a detection mechanism that will allow for low signal detection. The lock-in amplifier is used to detect and measure very small AC signals to the order of nano volts (nV) and slows for measurement even when the small signal is surrounded by noise thousands of times larger than the signal. The lock-in amplifier utilises a technique known as phase-sensitive detection to isolate a component of a signal at a specified reference frequency and phase. For the purpose of this experiment, an optical chopper was used to modulate the THz signal and optical laser pulse respectively to provide a reference signal for the Stanford SR830 amplifier for the detection of THz radiation. The noise signals at all other frequencies bar the reference frequency are rejected and don't interfere with the measurements[37, 38].

1.6 Terahertz Applications

1.6.1 Biomedical applications

Hu and Nuss were amongst the pioneers to first demonstrate the application of THz imaging for biomedical purposes by producing a THz image of porcine tissues that shows a contrast between muscle and fat [39], thereafter imaging of teeth and skin models using a pork skin was demonstrated by Arnone et al. The use of THz radiation for biomedical purposes has since been applied in disease diagnostics [40]. Teraview Ltd in Cambridge used THz imaging to show contrast between healthy skin and basal cell carcinoma (BCC) in both in-vitro [41] and in vivo [42] systems [43]. The low energy levels of (1-12meV) at 0.3THz to 3THz means THz waves have a favourable suitability to biomedical applications due to this non-ionising feature, consequently, damages to cells or tissue are only limited to thermal effects. Terahertz radiation causes Mie or Tyndall scattering when passing through tissues as opposed to Rayleigh scattering which dominates in IR and optical frequencies. Moreover, with respect to imaging a resolution of (70 dots/in) from diffraction-limitation is achieved at 1 THz which makes it viable for imaging[44]. Fig 1.6 [2] below shows an in-vivo images of cancer

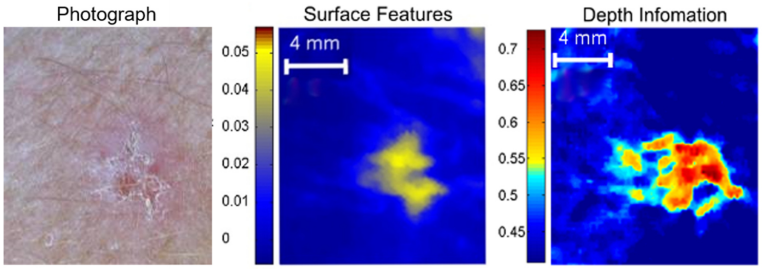

Figure 1.6: In-vivo cancer images from a TD-THz system by Teraview Ltd

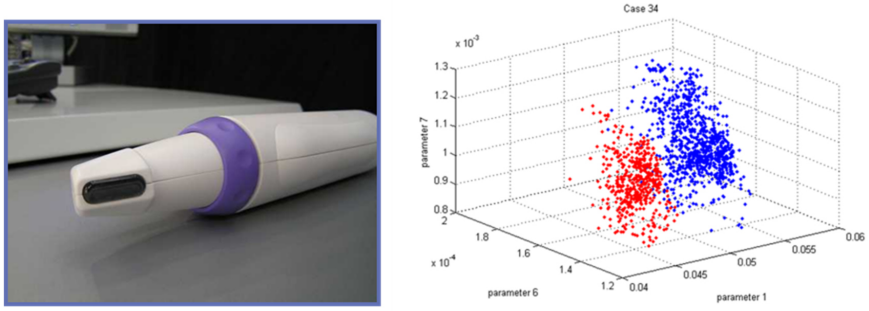

Figure 1.7: Prototype THz surgical probe for breast cancer surgery

with a clinical picture from the left, a terahertz image in the middle and a depth image obtained by plotting a point further along the THz reflected pulse, this reveals features that can't be seen with the naked eye as it penetrates beneath the surface. On the left of Fig 1.7 [2] is shown a prototype device built for usage in breast cancer surgical operation. On the right of the figure, the classification of the breast cancer data can be seen, where the tumour is represented in red and the normal tissue in blue [2].

1.6.2 Spectroscopy

The possession of a unique spectral fingerprint by many materials in the THz range makes it very desirable for spectroscopy. Many gaseous molecules have rotational transitions in this regime that allows for narrow absorption lines for identification of the molecular structure of a particular substance. Moreover, there is an interest for the detection and identification of explosives by utilising the THz region, the absorption consequent to the motion

of molecules can be monitored and used as a characterisation tool. Furthermore, many explosive materials have unique spectral signatures at the THz frequency range, and hence their strong absorption can be used to distinguish them from each other and any material used for concealment. The sensitivity of THz spectroscopy to both inter/intra molecular vibrations in chemical species such as DNA can be used in the investigation of the crystalline state of drugs, i.e., polymorphism. The rearrangement of the molecular structure of proteins occurs in picosecond timescale that allows for probing with THz. Significant studies have been done in the study of the carrier dynamics of semiconductors and superconductors using THz radiation. Terahertz conductivity spectroscopy has been used in the analysis of electrical properties of semiconductor nanowires; charge carrier lifetimes, carrier mobility, dopant concentrations and surface recombination velocities have been measured with high accuracy [45].

1.6.3 Communication

In recent years, the world has witnessed a substantial increase in data usage, this necessitated the need for higher bandwidth and data rates in wireless communication which can be achieved by relatively higher frequencies from the commercial microwave frequencies of 18-30 GHz (K band and Ka band) that are widely in use. According to Edholm's law data rates and bandwidth double every 18 months, this has led to numerous research work across the world to meet up to this significant demand [35]. THz communication bands (0.1-10THz) are being investigated due to the availability of large bandwidths in these bands that ranges from a few GHz to over 1THz. Communication links in W-band (75-95 GHZ) and for frequencies above 100GHz have been demonstrated. Shams et al. demonstrated a photonic generated multichannel THz wireless signal at a carrier frequency of 200GHz and data rate of up to 75Gbps in Quadrature Phase Shift Keying modulation format[46]. A 400 GHz carrier frequency THz wireless systems with bit rates of up to 46Gbps has been demonstrated at the University of Lille using a THz photomixer with a specific broadband antenna and a heterodyne electronic detection method [47]. Figure 1.8 shows a table of the reported THz wireless data links. In the Table Real-time denotes a system where the Bit Error rate BER is measured without offline data processing, Homodyne mode is where the same reference is used for the transmitter and receiver. [NB EVM= Error Vector magnitude; DSP = Digital Signal Processing] In 2020, while the world was

Freq. (GHz)	Data rate (Gbps)	BER / EVM	Type	Distance (m)
300	24	< 1e-10	Real time	0.5
120	10	< 1e-10	Real time	200
146	1	-	Coherent / Off-line D.S.P.	0.025
200	1	< 1e-9	Real time	2.6
625	2.5	< 1e-10	Real time	few meters
120	10	< 1e-10	Real time	5800
542	2	1e-8	Real time	0.01
300	0.096	EVM < 7 %	Real time	0.7
87.5	100	1e-3	Coherent / Off-line D.S.P.	1.2
237.5	100	3.4e-3	Coherent / Off-line D.S.P.	20
240	30	EVM < 16 %	Coherent / Off-line D.S.P.	40
196	0.1	EVM < 10 %	Homodyne (Same Tx/Rx)	0.5
220	30	1e-8	Homodyne (Same Tx/Rx)	20
300	24	< 1e-9	Real time	0.3
300	48	< 1e-10	Real time	1
237.5	100	1e-3	Coherent / Off-line D.S.P.	20
100	100	< 3.8e-3	Coherent / Off-line D.S.P.	0.7
400	40	1e-3	Coherent / Off-line	2

Figure 1.8: Details of reported THz Wireless Data links [47]

going through a global pandemic in amidst some pseudo-scientific concern from some public groups on the causality/correlation of the pandemic with 5G communication, the group of Prof Lu Chuan at University of Electronic Science and Technology of China worked in launching the world's first 6G test satellite into orbit to extend the 5G mm Wave frequency into the Terahertz range[48]. THz communications as compared to mm Wave frequency has higher bandwidth as a result of the higher carrier frequency, less susceptibility to scintillation effects than IR wireless links however due to the strong absorption of THz by water attenuation will be a significant drawback especially in certain weather conditions such as rain. The main challenges facing THz frequencies in communication are high path loss, and atmospheric absorption due to water vapour molecules. Also, the low source power and large down-conversion loss require the use of directional and line-of-sight systems instead of the omni-directional antennas used at lower frequencies [2].

Chapter 2

2.1 Photoconductive antenna

A biased Photoconductive antenna (PCA) excited by laser beams is widely implemented for the generation of terahertz radiation; the configuration of a PCA consists of two metal electrodes deposited on a semiconductor substrate. Illuminating the gap between the electrodes by an optical beam generates photo carriers, where a static bias field accelerates the free carries. This photo current varies in time, corresponding to the intensity of the incident laser beam. Consequently, femtosecond laser pulses produce broadband terahertz pulses. Mixing two laser beams with different frequencies forms an optical beat, which generates CW terahertz radiation at the beat frequency—This technique is called photomixing [7]

2.1.1 Photoconductive Antenna Materials

Since the early photoconductive switches, research has been done in selection of the most suitable photoconductive materials with the necessary electro-optic characteristics to enable more efficacy in their performance[49, 50, 51, 2]. F. J. Leonberger in 1981 identified InP photoconductive switches to have better than Si photoconductive switches. By 1991, S. Gupta et al. demonstrated the short carrier lifetime benefits of an epitaxially grown GaAs by MBE to have fast recombination lifetime and higher carrier mobility in the semiconductor to contribute to a better performance as a photoconductive switch [49, 52]. The earliest demonstrations of Photoconductive antennas used argon ion irradiated crystalline silicon epitaxially grown on sapphire by DH Auston and Peter R Smith at Bell labs using radiation damaged silicon

film with 2 MeV argon ions [53]. However, GaAs has long become a preferable choice for PCAs as would be shown in the latter section.

2.1.2 PCA Structure and efficiency

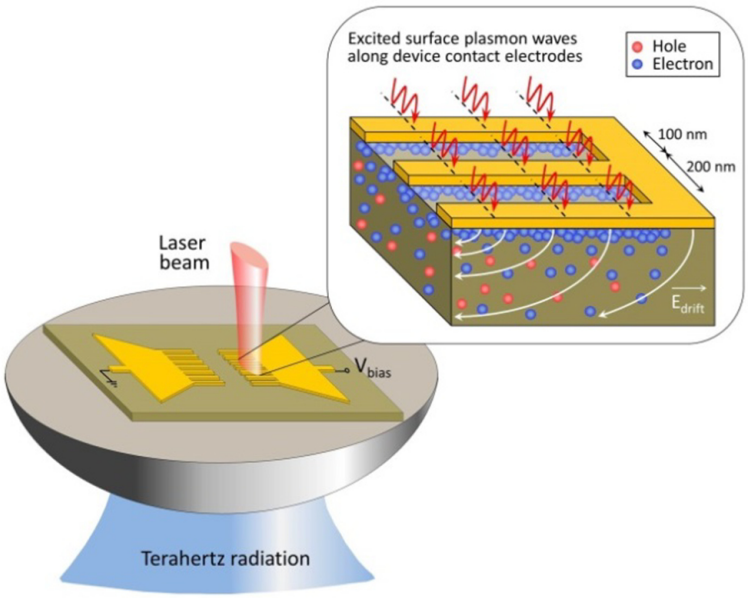

Figure 2.1: A schematic of a photoconductive Antenna showing optical pump illumination on a bow-tie antenna gap on the left and the generation of electron-hole pairs in the photo-absorbing substrate on the right [1]

Figure 2.2 shows a schematic of a photoconductive antenna, which consist of a metallic electrode, placed on a semiconductor substrate. The electrodes are biased and an intense sub picosecond laser pulses is incident on the photoconductive gap, which results in generation of THz signals on the other side of the PCA. The structure of the PCA is referred to as a dipole antenna by Tani M et al. and shown in Figure below [54].

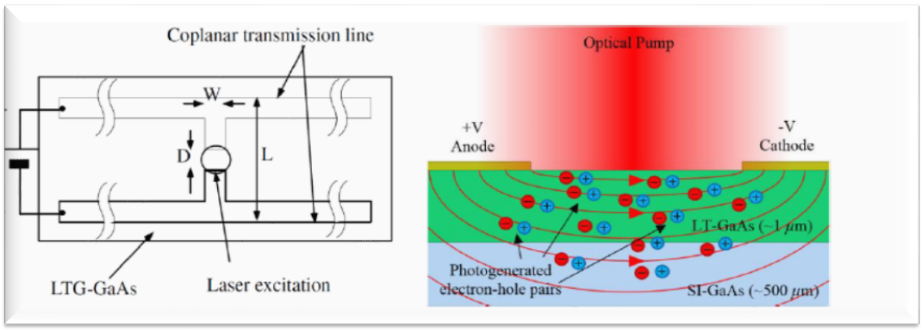

Figure 2.2: A schematic of a photoconductive Antenna [7]

The stripline antenna is printed on a Photoconductive substrate. The antenna has a gap at the center which is dc biased and irradiated by femtosecond laser pulses. Photo excited carriers are then accelerated under the bias field creating an ultra-short current pulse as can be seen in Fig 2.1[55], this decays with a time constant determined by the carrier lifetime of the Photoconductive substrate. The transient current J(t) generates ultra-short electromagnetic pulse radiation in Terahertz frequencies. The field amplitude of the radiation is proportional to the derivative of the photocurrent J(t) in the far field.The peak change of the photocurrent is proportional to the averaged photocurrent $\bar{J}$ divided by the duty ratio of the current pulse, this is approximately the ratio of the lifetime of the photo carriers τc and the interval of the pump laser pulses $T_{int.}$

$$\begin{cases} E_{THz} \propto \dfrac{\partial J(t)}{\partial t} \\ E_{THz}^{peak} \propto \Delta J \quad \overline{J}\dfrac{T_{int}}{\tau_c} = \overline{G}V_b\dfrac{T_{int}}{\tau_c} = \overline{\sigma}\dfrac{W\delta}{D}V_b\dfrac{T_{int}}{\tau_c} \\ = e\mu\overline{n}_e\dfrac{W\delta}{D}V_b\dfrac{T_{int}}{\tau_c} = e\mu\tau_c\dfrac{(1-R)}{h\nu}\dfrac{P_{in}}{DW\delta}\dfrac{W\delta}{D}V_b\dfrac{T_{int}}{\tau_c} \\ = e\mu T_{int}\dfrac{(1-R)}{h\nu}\dfrac{P_{in}}{D}\dfrac{V_b}{D} \qquad [54] \end{cases} \tag{2.1}$$

In equation (2.1) above ($\bar{G}$) is the time-averaged photoconductance of the PC gap, $\bar{\sigma}$ is the time-averaged conductivity, δ is the absorption depth of

the optical pump light, $\bar{n}_e$ is the averaged photo-carrier density, Vb is the bias voltage, μ is the mobility of the carriers, R is the reflectance of the PC substrate, hν is the photon energy of the pump laser, P_{in} is the averaged pump laser power, and D is the PC gap [54]. Figure 2.3[7] below shows an electric

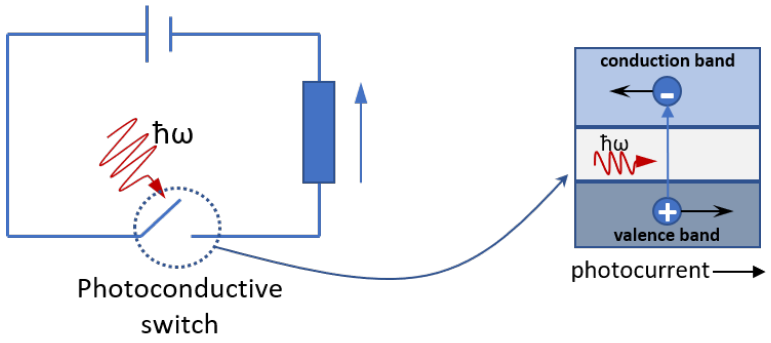

Figure 2.3: An electric circuit representation of a PC switch

circuit depicting the switching action that takes place in a photoconductive antenna upon optical excitation. A bias voltage source and a load resistor are connected in series with the semiconductor in the PCA substrate. When light is incident on the gap the switch closes and photocurrent flows through the circuit due to the generation of free electrons and holes in the semiconductor, the switching action is required to be in a sub-picosecond timescale for THz generation[7].

2.1.3 Semiconductor Materials for PCA

GaAs

Since the 1990s GaAs has been the photoconductive material of choice due to its mobility (∼200cm^2/V.s), high dark resistivity (∼10^7Ω.cm) and fast carrier lifetime (∼0.2ps)[9]. GaAs has a room temperature bandgap of 1.424eV (871nm wavelength), which makes it compatible with the commonly used Titanium sapphire laser for ultra-short pulse excitation of PCAs. It is widely used in the form of semi-insulating SI-GaAs [56], low-temperature LT-GaAs[57], and ion implanted GaAs respectively[58].

InP

F.J.Leonberger first identified the suitability of using InP for high speed photoconductive switching by obtaining a response time of ∼50psec. Over the years the short carrier average collision time, high bandgap energy, high carrier mobility, and low effective mass has made InP a very desirable material for the generation of THz using Photoconductive Antennas [52, 59].

InGaAs

Recently, the group III-V compound InGaAs has been investigated as a candidate for THz photoconductive material. The main benefit highlighted for using InGaAs is its potential to achieve 0.8eV bandgaps at room temperature, which allows the use of more compact fibre lasers for 1.55 µm optical pulse excitation[60].

InGa(Al)As

A terahertz PCA operating at 1.5 µm can benefit from compatibility to a wider variety of laser and fibre components for applications particularly desirable for telecommunications. For a long time, the PCA for 1.5 µm had been a bottleneck. Multiquantum wells and superlattices of InGa(Al)As have been proposed as potential materials for THz PCAs. Just like InGaAs PCAs, InGa(Al)As can achieve strong optical absorption under 1.55 µm wavelength excitation, due to its tunable bandwidth, the highly electro-optic properties of InGa(Al)As has been proposed as an avenue to achieve similar or more performance achieved by LT-GaAs at 800nm at 1.5 µm[58].

2.2 Contact Geometries of Photoconductive Antennas

The geometries of the contact electrodes on Photoconductive antennas has been shown to influence the emission properties of the Terahertz radiated by the PCA. Tani et al. compared the emission properties of a bow-tie, dipole and simple strip-line photoconductive antennas based on LTG GaAs and SI GaAs and reported a higher output powers in the bow tie antenna. R. Yano et al. also reported an almost 20 % larger peak to peak amplitudes

of detected THz waves in bow tie antennas than in dipole antennas, however the peak frequencies of terahertz emitted by the bow tie antenna is lower than that of the dipole antenna [61]. The radiation field E(r, t) as shown in equation 2.2 for an elementary Hertzian dipole antenna in free space, at a distance r (much greater than the wavelength of the radiation) and time t are described as

$$\begin{cases} E(r,t) = \dfrac{l_e}{4\pi\epsilon c^2 r}\dfrac{\delta i(t)}{\delta t} sin\theta & [54] \end{cases} \tag{2.2}$$

In the equation (2.2) above i(t) is the current in the dipole, l_e the effective length of the dipole, ε the dielectric constant of the radiation medium, c the velocity of light in the vacuum, and ϑ the angle from the direction of the dipole. Equation (2.2) indicates that the radiation amplitude is proportional to the time derivative of the transient photocurrent δi(t)/δt and the effective antenna length le

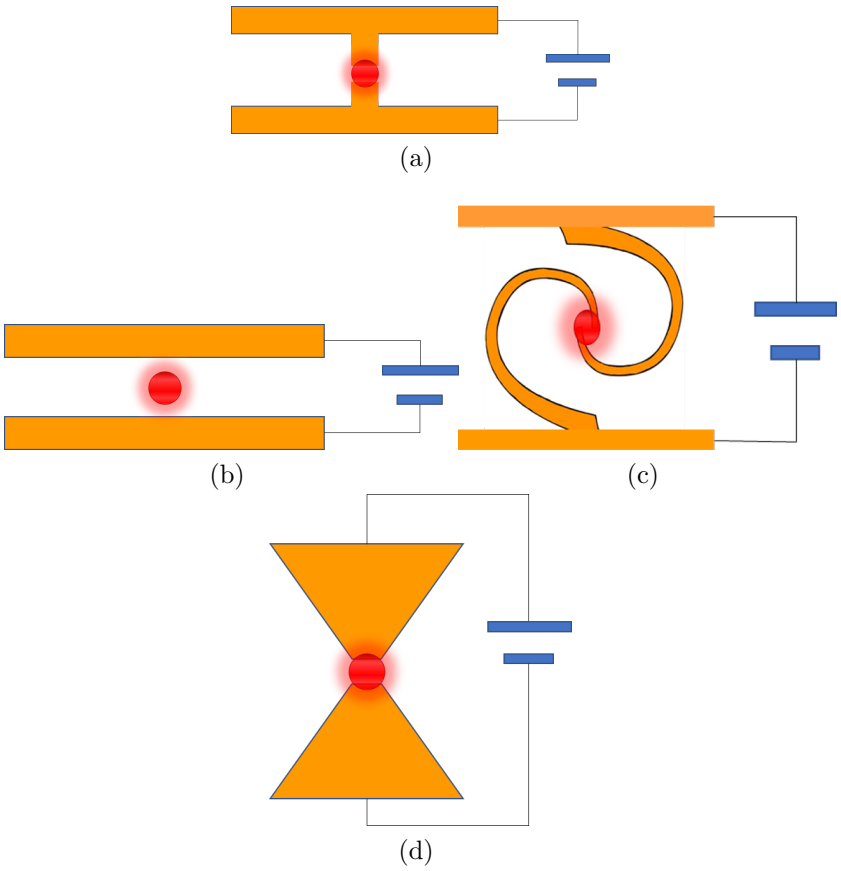

Figure 2.4: From top left (a) dipole, (b) Stripline, (c)Spiral, (d) bow-tie photoconductive antenna geometries

Tani et al. showed a comprehensive comparison of the dipole bowtie and stripline antenna designs, all with relatively small gap widths of 5-30um. All of the electrode designs were tested on both a LT-GaAs and SI-GaAs substrates. The results showed that the amplitude of the emitted THz signal is proportional to the length of the dipole antenna, which is due to a rise in the resonant frequency with the decreasing electrode length. Furthermore, the spectral bandwidth and peak signal were found out to be design dependent, with the stripline antenna producing a THz bandwidth of up to 4 THz with a peak around 1THz compared to the values of 3/0.6 TH and 1/0.1THz bandwidth and peak signal of the dipole and bowtie designs respectively. The bow-tie design although having the smallest spectral width had six times more THz output power than the dipole design under the same excitation

conditions. The result also showed that output saturation due to screening of the bias field by excited carriers was more influential in the dipole design due to the higher optical fluence within the small gap

In addition to the advances in the material of choice in photoconductive antenna substrates, the contact geometry has evolved from simple strip-line, dipole or bow-tie structures to more sophisticate geometries that act as antennas and mediate coupling of the THz in and out of the device[2]. The spiral antenna is also widely used in THz PCA as demonstrated by, and moreover in the generation of high power THz by Yang et al. that will be discussed later in the paper [62].The log spiral antenna has been demonstrated by Han et al. to have superior characteristics that include less influence on polarisation state of the THz source, low divergence angle and a small size [63]. Some designs have utilised nanoscale plasmonic contact electrodes that significantly mitigate the lo-quantum efficiency performance of photoconductive antennas, demonstrating up to 50 times higher terahertz radiation than non-plasmonic contact electrodes. Berry et al. used a plasmonic grating incorporated on a bow-tie where the plasmonic grating maximises the concentration of photocarriers near the electrodes and hence provides more photocarriers that contribute towards terahertz generation[64].

2.2.1 Metallisation of PCA Electrodes and Hybrid Antennas

The material choice for the contacts on the PCA has been shown by N. Vieweg et al. to have a considerable effect on the characteristics of the THz output from the PCA. While both AuGe based alloys and Ti/Au metal layer stacks are widely implemented as contacts for THz PCAs. The suitability strongly depends on the semiconductor material. Both AuGe alloy and Ti/Au layers have been found to be suitable for n-doped III-V semiconductors, which is appropriate for LT- GaAs – widely used PCA material. N Vieweg et al demonstrated that the power emitted from PCAs with AuGe metallisation is almost 50% higher than that emitted by the Ti/Au metal layer due to lower contact resistance of the AuGe contacts. However, in a system requiring high stability, the Ti/Au metal layer is more advantageous due to having higher thermal stability [65].
More recently, the use of hybrid antennas with plasmonic nano islands and nano-antennas is being implemented towards a more efficient terahertz gen-

eration. S.I. Lepeshov et al. utilised an antenna with log-periodic electrodes that provides broadband radiative spectrum. The antenna has its gap filled with nano-silver particles around 280nm apart that are fabricated by thermal dewetting process caused by heating a 20nm silver film on the substrate of the antenna. Upon comparison of the log periodic antenna with and without silver nano-antennas. An increase of up to 5 times was recorded at certain frequencies in the antennas with silver nano antenna as compared to that without. Christopher W Berry et al. credited the enhancement in PCAs using plasmonic materials as due to the reduction of the average transport for the photo-generated carriers to reach the plasmonic electrodes, thereby increasing the number of photocarriers that contributes to the generation of terahertz[66] [67]. The incorporation of a plasmonic photoconductor contact electrode configuration leads to photocarrier concentration near the contact electrode which significantly reduces the average photo-generated carrier transport path to the photoconductor contact electrodes as compared to conventional antennas [55].

2.2.2 Interdigitated Electrodes for Terahertz PCA Optimisation

Recently, the use of interdigitated electrode structures (which were originally used in metal-semiconductor-metal structures MSM photodetectors) has been widely applied in photo mixers to optimise the efficiency of photon-current conversion, studies have also been carried out in the use of interdigitated electrodes for pulsed THz generation. Park et al. have previously shown that gold grating lines of sub wavelength width can couple incident IR light more efficiently into the substrate, the grating lines when attached to the electrodes lead to a greater number of photo generated carriers reaching the electrodes in subpicosecond time which in effect results to the enhancement of the generated THz [68].

The use of interdigitated electrodes on PCAs has shown significant improvement in the PCA performance such as in the work of Hale et al. where they used interdigitated electrodes SI GaAs for achieving broadband THz radiation; they deployed the interdigitated PCA structure to achieve large spectral bandwidths and higher SNR of the PCA. The finger-like structure of the antenna electrodes interweaves together to create a large THz antenna array that is constructively interfering in the far-field, the structure also has

a large aperture that allows illumination by a higher power and lower repetition rate optical sources. It reduces the diffraction of the generated THz pulse and hence negates the need for using a silicon lens. Moreover, the small electrode spacing leads to a faster screening of the applied E-field by the depleted photo carriers which hence allows for a broader bandwidth THz emitter[69].

Matthäus et al. deployed interdigitated electrodes to achieve approximately 75% IR light that contributed to the generation of THz radiation. They deployed two interdigitated Ti/Pt/Au electrodes that were processed on the surface of a 3 um LT GaAS layer grown on SI GaAS substrate using optical lithography. Using a conventional Ti:Sa that delivers 150 fs pulses on the antenna gap, and a max IR power of 540mW and laser spot of 150um diameter focused on the Antenna they achieved a 6.5 uW THz power [70]

Singh and Prabhu compared two PCA designs on SI GaAs, the antennas were pumped with 100 fs, 800nm laser pulses of 76 MHz repetition rate. The conventional antenna had an incident optical pulse focused on a spot of 10µm diameter and gets saturated after 200mW of incident power, while the interdigitated electrode Antenna with large area was excited with an optical pulse of 350µm and was emitting THZ up until a 750mW of incident power and recorded 12.5 times higher THz power in the interdigitated electrode PCA than the conventional PCA as shown in Fig 2.5 below [71, 72].

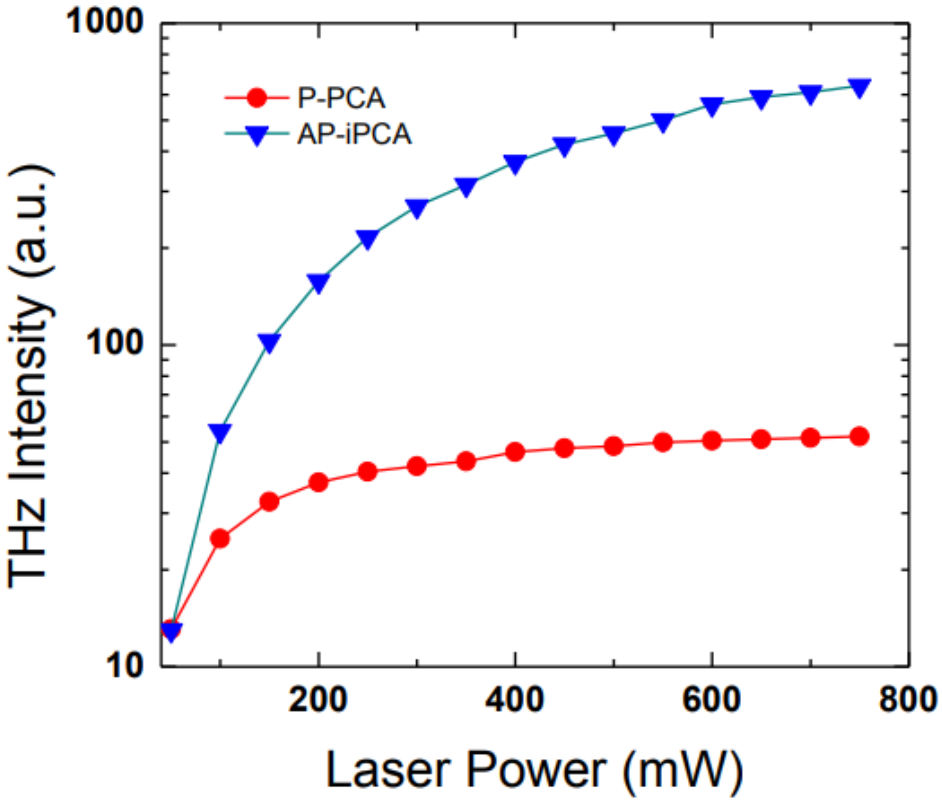

Figure 2.5: THz intensity detected with a bolometer with a variation of the incident optical pulse power for the conventional antenna (P-PCA) and the interdigitated electrode antenna (AP –iPCA) as reported by Singh and Prabhu [71]

2.2.3 High Power PCAs

A plasmonic contact photomixer integrated with a log spiral antenna was implemented by Shang et al to record an unprecedented THz output power of 17 µW at 1 THz and a tuning range of more than 2 THz. Metallic gratings of Ti/Au covered by a SiO_2 anti reflection coating were utilised as the plasmonic contact electrodes [62, 73]. Yardimic et al. recorded a 3.8mW THz radiation over 5THz in response to a 240mW optical power, utilising a

large area plasmonic photoconductive antenna, arrays of plasmonic antennas were connected to the anode bias line of the large area PCA. The plasmonic antennas were in the form of Au gratings and offered a high concentration of photocarriers around the plasmonic antennas. The incorporation of plasmonic antennas have been shown to increase the optical-terahertz conversion of Photoconductive antennas significantly as compared to other designs[74]

2.3 Quantum dots in PCAs

2.3.1 Implementation of QDs for PCA Optimisation

The principle of operation of Photoconductive antennas relies on the generation of photocurrent and the movement of charge carriers. The THz signal generation layout in the experimental set-up as shown in Figure 3.5; the two beams from the pump external cavity diode laser are focused on the gap of the photoconductive antenna placed between biased electrodes and is absorbed by the semiconductor, optical to terahertz conversion occurs from a generation of photocurrent that is modulated by the beat frequency from the two beams and radiated from the antenna as THz [75]. E.U.Rafailov et al. demonstrated an active layer of InAs quantum dot on GaAs, efficient emission of both pulsed and continuous wave THz signals with significant optical to THz conversion at $\leq$850nm and $\leq$1300nm [76].

Quantum dot materials properties and growth

Quantum dots are three-dimensionally confined quantum structures that possess the ability to have tailored electronic structure with discrete energy levels and highly configurable properties that earned them the name ″designer atoms″ [77].They have been identified and investigated as potential candidates for lasers [78], detectors [79], single electron transistors, quantum computers [80], and for the interest of this research as PCA material for THz generation. [81, 76, 9, 82, 83].Quantum dots have been grown from both group IV elemental material (i.e., silicon and germanium) and compound group III-V materials such as (I.e. Gallium, indium; arsenic, phosphorus) and group II-VI materials (i.e. zinc, cadmium ; tellurium and selenium).

Quantum dot growth-Epitaxial Methods

Achieving high quality dislocation-free Quantum dots has been primarily implemented by Molecular beam epitaxy, which is a thin film epitaxial growth technique invented by Arthur Cho from Bell laboratories in 1968. Under high vacuum with different groups of atoms supplied, a high thermal velocity molecular beam is formed which is made incident on a heated substrate surface to carry out MBE [76].The QD laser and the QD material in the Photoconductive antenna for the purpose of this research was grown by MBE in the Strantski-Krastanow mode. Frank-van der Merwe Growth – The FM growth mode utilises a layer-by-layer growth mode routinely used for growth of Quantum well structures. Strantski-Krastanow Growth is a hybrid of FM and Volmer weber growth modes. For moderate lattice mismatch, the growth is initiated layer by layer and the increase in the thickness of the epilayer accumulates strain due to lattice mismatch. At a critical thickness of the 2D layer, the strain is release to form small islands with the addition of epitaxial material the small islands will grow until desired [84]. QDs typically form with pyrmidal physical profiles with dimensions on the order of (15-25) x (15-25) x (5-15) nm (base width x base length x height), however, this can be controlled by deposition conditions [81].

Table 2.1: A comparison between quantum dot properties and LT-GaAs for PCA material [6]

Desired Parameters	Quantum Dots PCA substrate	Low-temperature grown GaAs substrate
Short Carriers lifetime	Yes	Yes
High carriers mobility	Yes	No
Optoelectronic efficiency	Yes	Yes
Thermal tolerance	Yes	No
Pump wavelength	<1.27 µm	<0.85 µm

2.4 Quantum Dot Photoconductive Antennas

Owing to the aforementioned benefits of quantum dots in this chapter, the PCas for this research were integrated with QD structures for the optimisation of THz radiation from PCAs and also for the realisation of optical pumping with compact semiconductor lasers towards a compact THz system. Three designs of antennas show in Figure 2.6 (a), (b) and (d) were designed and built with the following parameters.

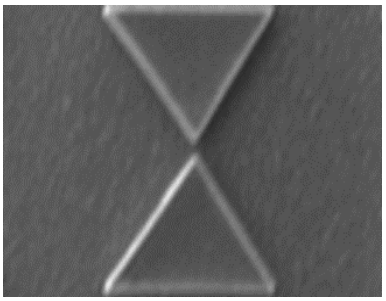

(a) QD_Bt1 and QD_Bt2 geometry

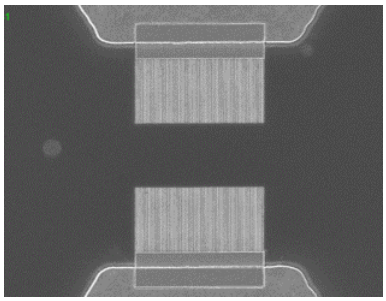

(b) QD_Pl geometry

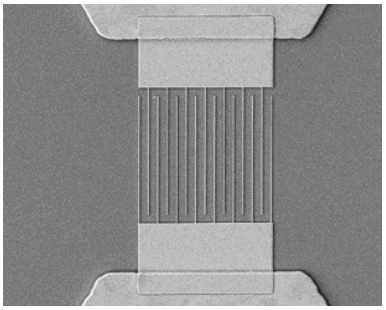

(c) QD_id geometry

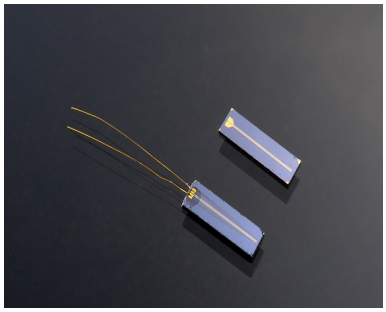

(d) Teravil geometry

Figure 2.6: Antenna Electrode Geometries

QD_Bt1 and QD_Bt2 bow tie BT60 (bow-tie with 60^o flare, 10 µm width $\times$10 µm gap)
QD_Pl plasmonic gratings BT60P10 (bow-tie with 60^o flare and plasmonic gratings 10 µm length, 10µm width $\times$10 µm gap). The plasmonic grating dimensions are: 150 nm height, 100 nm width, 130 nm gap

QD_id interdigitated fingers BT60ID 20µm (bow-tie with 60° flare and interdigitated fingers 200 nm width ×1.2 µm gap, 20 µm width) The QD_Bt1

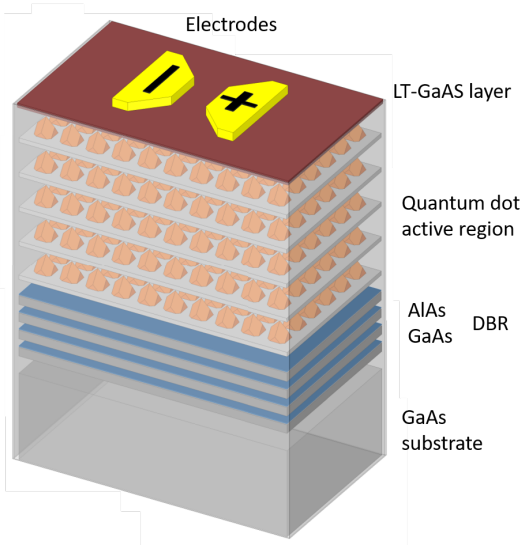

Figure 2.7: Quantum dots Antennas substrate structure

and QD_Bt2 antennas used for this experiment comprises a Ti/Au bow tie electrodes of 10µm gap deposited on a heterostructure wafer via standard UV photolithographic process and further wet etching; the heterostructure wafer is made up of a grown 40nm low-temperature GaAs layer covering an active region of 30 layers of InAs QD of 1789nm thickness grown via MBE. The LT-GaAs layer is implemented to enhance the ohmic contact between the wafer and the antenna electrodes and to reduce dark current. Underneath the active region of QD structures is a grown layer of AlAs/GaAs distributed bragg reflector of 4890nm thickness which is also deposited on a semi insulating GaAs substrate, the dbr's function is to reflect the pump wavelength corresponding to the QD excited state, the antennas were grown with the help of Innolume and Dr Andrei Gorodetsky.

2.5 Antenna Photocurrent measurements

For the photocurrent measurements and IV characterisation of the antennas, a Keithley Semiconductor characterisation system was used, the antennas were mounted as stated in the detection set-up in section 4.2 and the power and wavelength were adjusted from the titanium sapphire laser. A sweep from –20v to +20V was carried out for all antennas as shown in Fig 2.8- Fig 2.15 with photocurrent for the antennas and the IV characteristics.

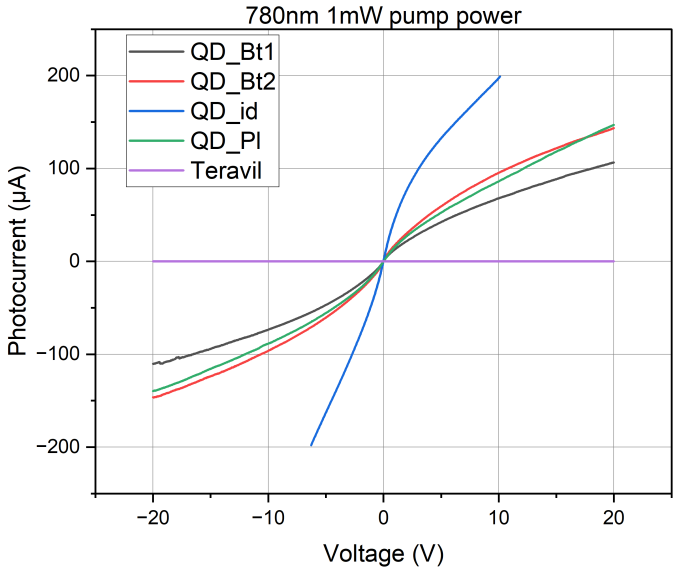

Figure 2.8: Photocurrent of the PCAs at 1mW optical pump power

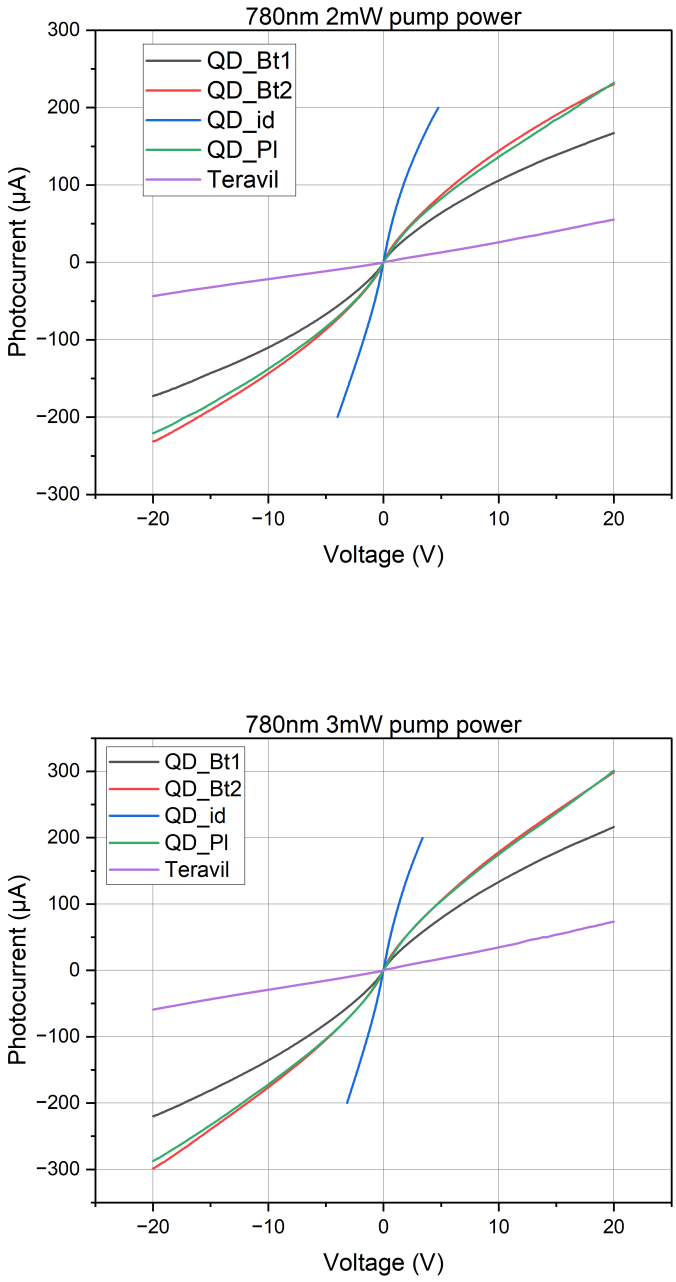

Figure 2.9: Photocurrent of the PCAs at 2mW (top) and 3mW (bottom) optical pump power

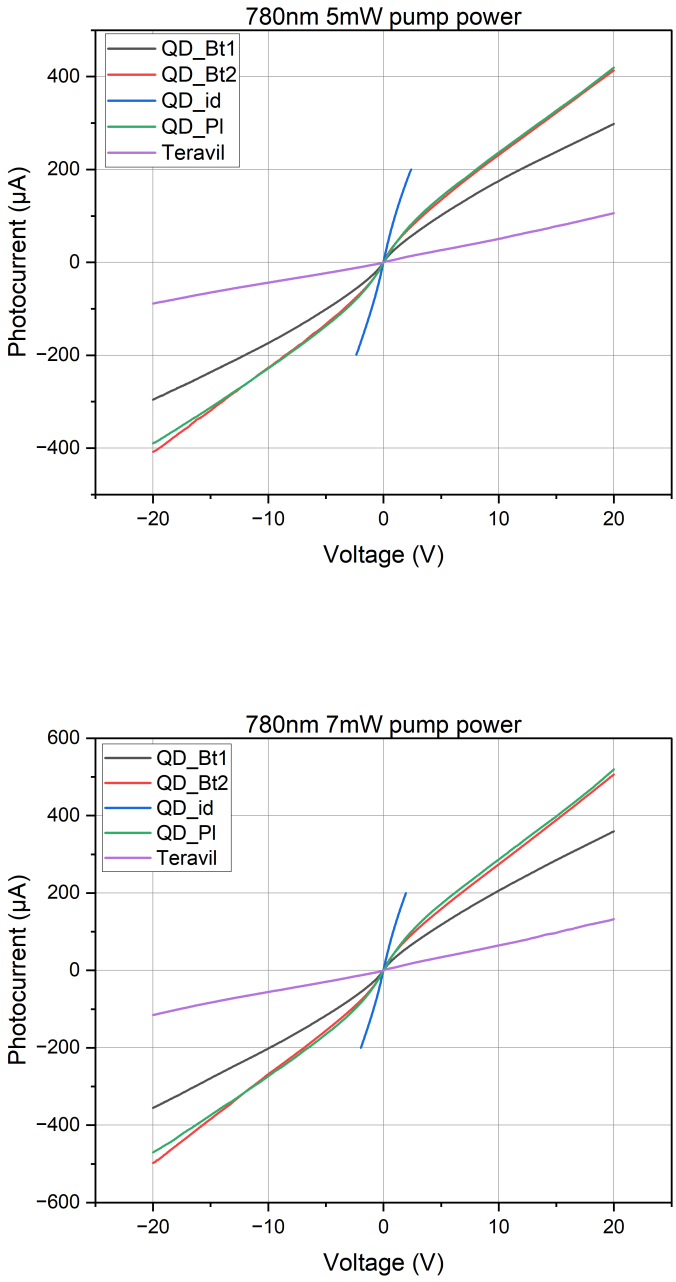

Figure 2.10: Photocurrent of the PCAs at 5mW (top) and 7mW (bottom) optical pump power

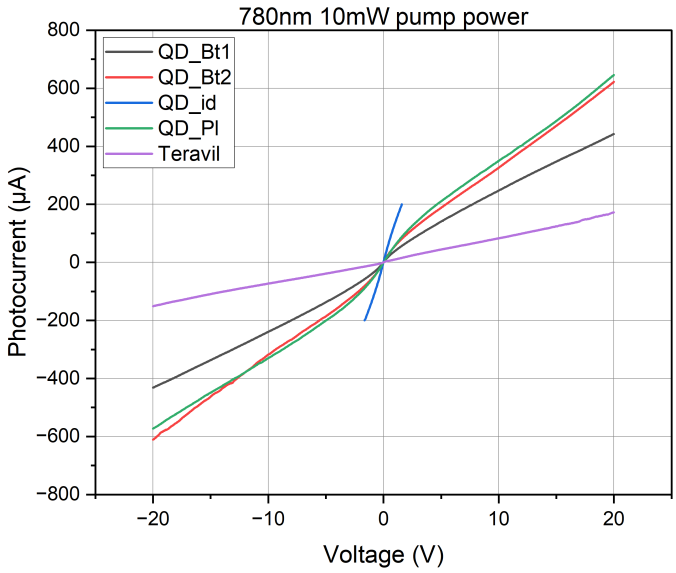

Figure 2.11: Photocurrent of the PCAs at 10mW optical pump power

Photocurrent measurements at 780nm

The antennas were measured using the same set up in chapter 4 and optimising the positing for lowest resistance before measurements were taken.

For 1mW, the QD_id antenna with interdigitated electrodes has the highest generation of photocarriers and hence the highest photocurrent, however it is responsive with increase in photocurrent only till ≈ 10V so wouldn't withstand high bias voltages as will be elaborated more for the THz generation section. The two bow tie antennas QD_Bt1 and QD_Bt2 and the plasmonic QD_Pl antenna have nearly identical photocurrent readings for all voltages with the QD_BT1 having slightly lesser photocurrent, the teravil antenna had a very low photocarrier generation at 1mW and even more significant at lower voltages. This trend remained consistent as shown in from Figure 2.8 to Figure 2.11 for measured pump powers till 10mW with the QD_id having responsive voltage limit of 5V,3V and 2V for powers of 2mW, 3mW and 5mW-10mW respectively. For 1mW at ≈10V the QD_id antenna had the highest photocurrent of ≈200µA while at 10mW and 20V the QD_Bt2 and the QD_Pl had the max photocurrent of 620 µA respectively.

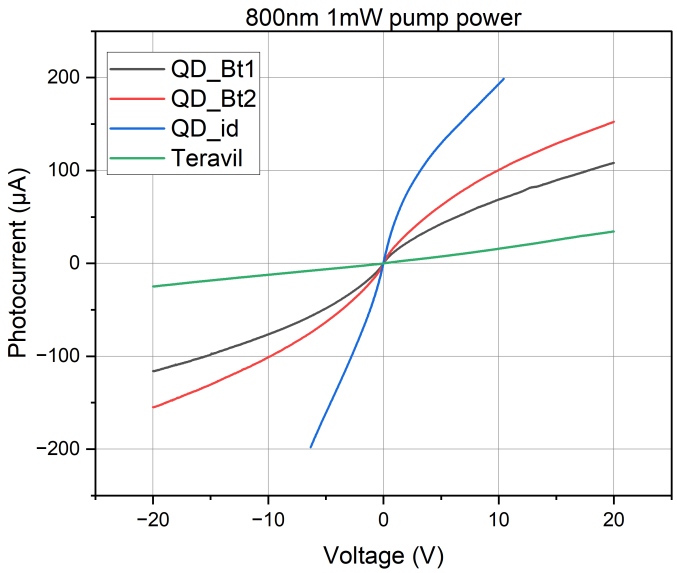

Figure 2.12: Photocurrent of the PCAs at 1mW optical pump power

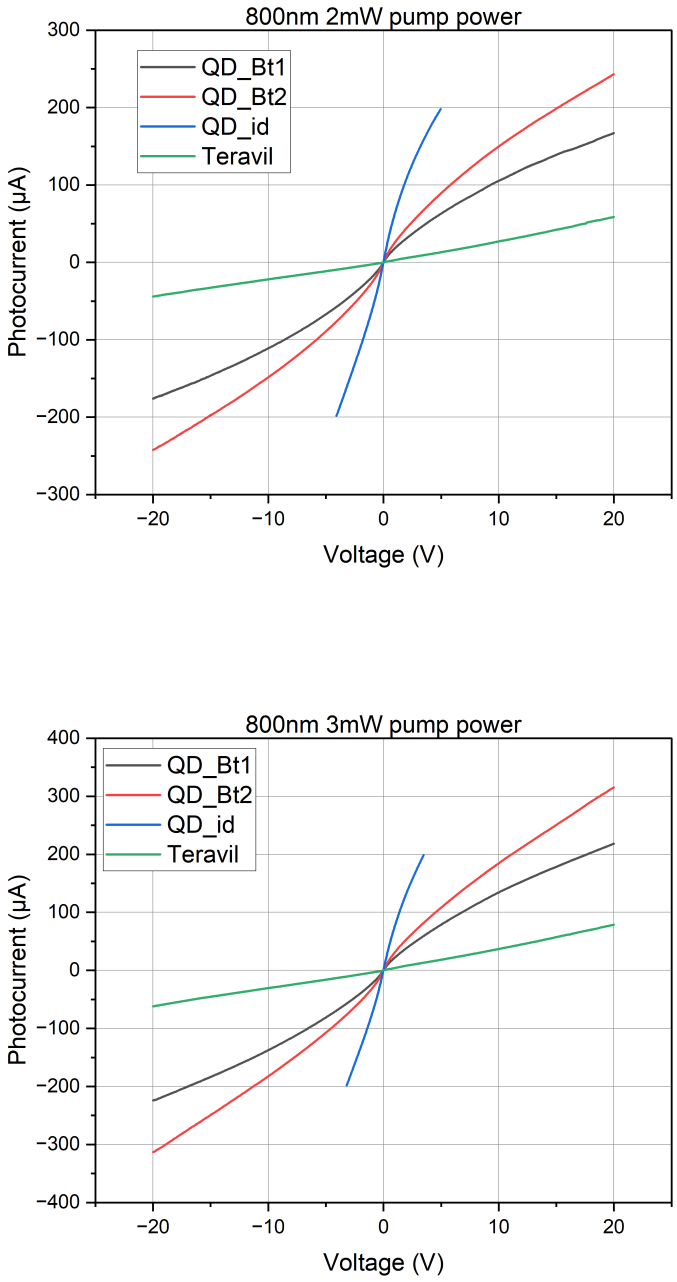

Figure 2.13: Photocurrent of the PCAs at 2mW (top) and 3mW (bottom) optical pump power

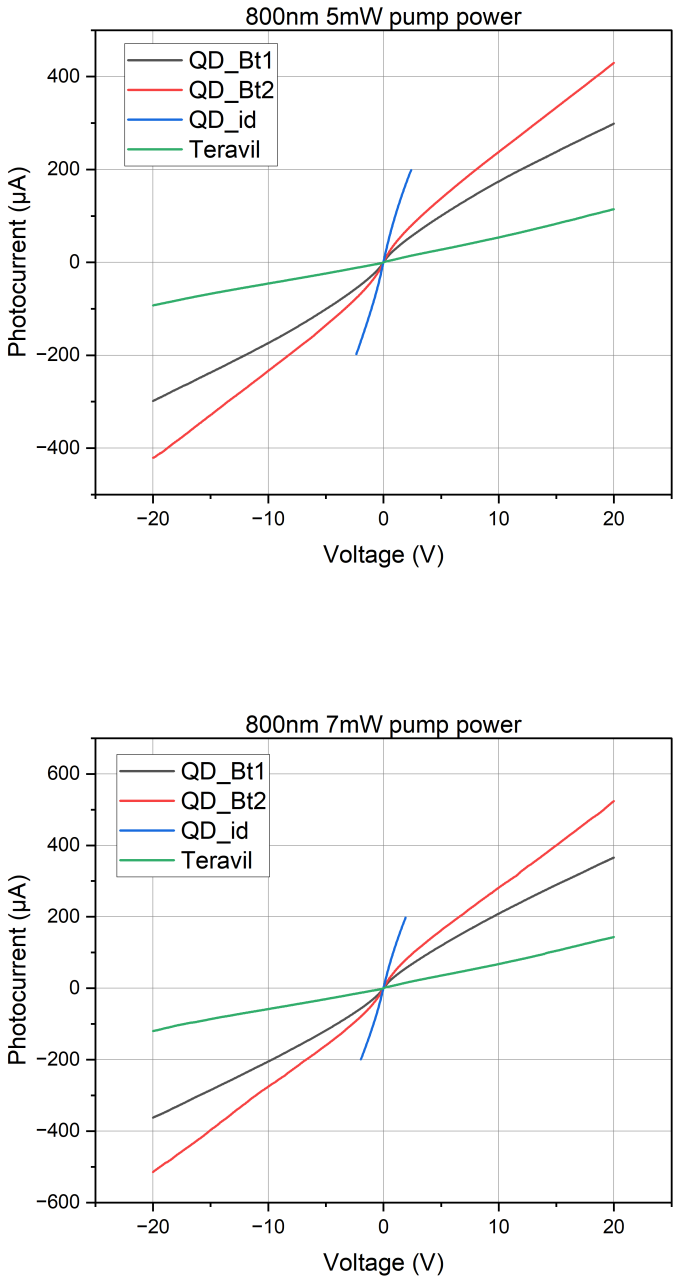

Figure 2.14: Photocurrent of the PCAs at 5mW (top) and 7mW (bottom) optical pump power

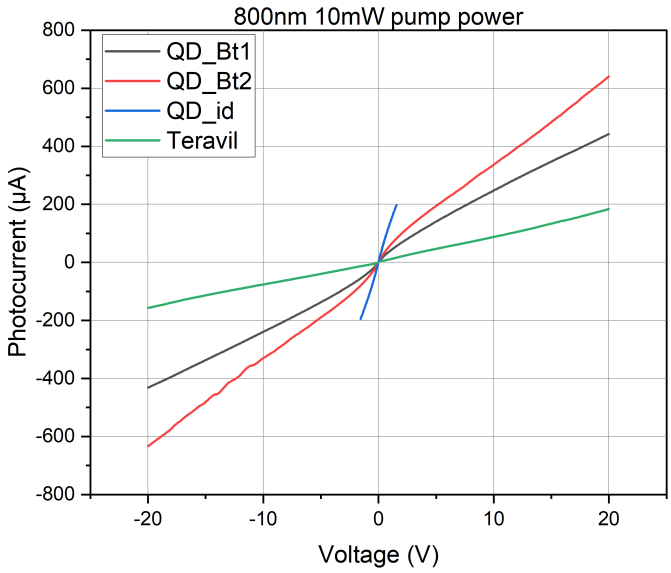

Figure 2.15: Photocurrent of the PCAs at 10mW optical pump power

Photocurrent measurements at 800nm

With the wavelength tuned to 800nm the same set of measurements were taken and for the obtained results, as shown in Figure 2.12 at 1mW , the QD_id antenna with interdigitated electrodes has the highest generation of photocarriers just as at 780nm and being responsive till ≈ 10V of forward bias , however, in reverse bias the antenna is responsive only till 6V. The two bow tie antennas QD_Bt1 and QD_Bt2 have the higher photocurrent readings for all voltages with the QD_BT1 having slightly lesser photocurrent, the teravil antenna just as in at 780nm had lower photocarrier generation at the lower pump wavelength and voltages. The same trend remained was consistently recorded in Figure 2.13-2.15 for measurements pump powers from 2mW-10mW. The QD_id has a responsive voltage limit of 5V,3V and 2V for powers of 2mW, 3mW and 5mW-10mW respectively with lower voltages observed for reverse bias at the lower pump powers. For 1mW at≈10V the QD_id antenna had the highest photocurrent of ≈200µA while at 10mW and 20V the QD_Bt1 and the QD_Bt2 had a photocurrent of ≈ 620µA and ≈ 420

In this chapter, the PCA has been identified as the method of choice

for generating THz radiation for this research project. The use of Quantum dots to improve the optical to terahertz conversion efficiency of PCAs has been established. PCA samples based on Quantum dot devices have been designed and tested for THz radiation as will be seen in chapter 4 of this thesis.

Chapter 3

3.1 Continuous Wave Terahertz System

This chapter will present the research that was taken towards realising a compact tunable continuous wave THz source. This will encompass background literature on continuous wave terahertz generation and principles, lasers for CW THz generation and experimentation and results on QD laser for continuous wave THz generation. In Chapter 1, various methods of generating THz radiation have been outlined including broadband and continuous wave sources, this chapter will focus on continuous wave sources based on Photomixing and difference frequency generation. A tunable compact continuous wave terahertz source is immensely desirable for various applications such as spectroscopy due to its high spectral resolution and for the realisation of compact and low-cost systems over pulsed terahertz systems. The implementation of optical heterodyne down conversion in a photoconductive antenna and Terahertz quantum cascade lasers are the most widely used methods of generating continuous wave terahertz radiation. However, the required cryogenic cooling in THz quantum cascade lasers makes achieving a compact room temperature terahertz source difficult to achieve. The use of dual wavelengths at a terahertz difference frequency in a Photoconductive antenna has been long used for generating continuous wave terahertz radiation [33, 61, 85, 9]. The rise of semiconductor lasers and the appreciable properties of quantum dot gain media in semiconductor lasers has paved the way for widely tunable high power semiconductor lasers, moreover, the external cavity diode lasers provide narrow-linewidth that is suitable for CW terahertz emission

3.2 Literature Review

3.2.1 Photomixing

D.H Auston first demonstrated the use of a Photoconductive switch also called auston switch for the generation of pulsed THz radiation in the 1980s, nearly a decade later, E.R. Brown's group at MIT reported a continuous wave THz generation from an optical beat of two CW laser sources in place of the ultrashort laser pulses as pump. This technique now known as photomixing or optical heterodyne down frequency conversion poses several advantages such as wide tunabilty of the THz output frequency due to the ability of determining the difference frequency by tuning the frequency of the two pump lasers, however it comes with lower conversion as compared to the pulsed system[35].

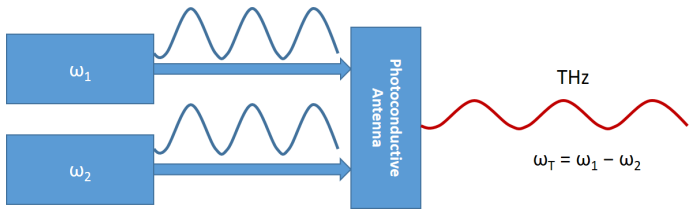

Figure 3.1: A simplified depiction of photomixing

3.2.2 Difference frequency Generation

This technique is analogous to photomixing as it utilises two beams of frequencies ω1 and ω2 at a difference frequency in the THz regime interacting in a medium with second-order nonlinear susceptibility to generate THz at the difference frequency ω3= ω1- ω2. The input frequencies are chosen so that an output THz radiation field is produced by the time-varying second-order polarization [7, 3].

3.2.3 Continuous wave lasers for THz generation

Distributed feedback diode lasers are widely used as the laser sources, they employ a grating structure within the active section of the semiconductor to restrict the laser emission to a single longitudinal mode and a specific tuning process such as thermal tuning of the grating pitch which allows

for wide continuous frequency scans. These two diode lasers can then be tuned to the appropriate frequency difference and combined in a photomixer or a non-linear crystal for THz generation. Commercially available lasers from Toptica photonics utilises this technology of deploying two DFB lasers. Two distributed feedback laser diodes with a nominal wavelength of 783nm at 25°C with a temperature dependant tuning range of 2.5nm were used at a difference frequency of 2.5THz for achieving CW THz generation in a photomixer by Demers et al.[86]. Two distributed bragg reflector laser diodes with a combined NIR light of 850nm werr implemented by Verghese et al. for optically pumping a photomixer for CW Terahertz generation. In the same research publication, Verghese et al. utilised two CW Ti:Sapphire lasers as the optical pump lasers to achieve a wider tuning range than the diode lasers[87].

3.2.4 Two-Colour Lasers for Continuous wave Terahertz

Two-colour titanium-sapphire lasers have been explored due to their high spectral purity and tunability. Brown et al. in 1993 incorporated 2 etalons in Ti:Sa lasers to realise a 2 colour laser [33]. However, Ti:Sa Lasers are expensive, complex and have a large footprint that makes them impractical for realisation of compact terahertz source [88]. Shortly after the first demonstration of THz photomixing; diode lasers have been discussed as an alternative pumping source for the photomixers [88]. However, they had power and linewidth limitations; however, the advancement in fabrication techniques has allowed for high power narrow linewidth diode lasers that are suitable for THz generation in PCAs. In 1997, Tani Masahiko's group used a multimode diode laser to demonstrate photomixing in a LTGaAs Antenna, further works by the same group using multimode laser diodes have been previously demonstrated. As demonstrated by E.U. Rafailov et al. the use of QDs as the gain medium of the laser has enabled stable low threshold high power, stable laser system for THz generation [84]. Additionally, the deployment of an External Cavity Diode Laser (ECDL) allows for wide tunability and narrow linewidth for tunable broad range THz emission.

Quantum dot dual mode lasers

The dual-mode laser excitation for photomixing is preferable to that by two independent lasers since the system can be more compact and the difference frequency stability is improved by the common-mode rejection effect. The first realisation of semiconductor laser was in 1962 by groups in the United States and the then Soviet Union [89] through the works of R.N. Hall et al. Over the years advances in epitaxial growth methods such as MBE has paved the way for sophisticated and highly controllable semiconductor lasers with many desirable properties as in Quantum dots [82]. The earliest demonstration of LDs that utilises a QD-based gain medium was in 1994 by Ledentsov et al. [90] and Kirstaedter et al. [91] with properties superior to quantum well lasers and reduced temperature sensitivity. A major design goal at the time was to improve the gain and lasing threshold, alongside the reduction of the limiting thermal rollover effects reported in LDs by [90]. Nader et al. a two colour emission Quantum dot laser with an 8 THz difference frequency as potential compact CW THz source [92]. Naftaly et al. demonstrated a two-colour Ti:Sapphire laser with Fabry-perot etalon for CW terahertz generation and hence reducing the footprint of the THz source[93]. A quantum dot laser with smaller footprint than the Ti;sapphire enables a more compact THz source. InAs/GaAs. A tunable terahertz beat signal from 1 to 2.21 THz was demonstrated by Jiao et al. from an InAs/InP Quantum dot modelocked laser combined with external cavity of two fibre bragg gratings, the dual modes are phase correlated and the generated THz have less phase noise[94]. Ksenia et al. , Leyman et al. , demonstrated an external cavity Quantum dot laser for an ultra-compact, room temperature, tunable terahertz generation that is of immense interest to this research [9, 81].

3.2.5 External Cavity diode Lasers

External Cavity diode lasers (ECDL) are of great interest to continuous wave Terahertz generation owing to their highly controllable wavelength tunability using a frequency selective element. The ECDLS capitalise on low cost and efficient laser diodes and by using a frequency selective feedback mechanism in the form of usually a diffraction grating or mirror they achieve narrow linewidth and tunability. Many methods have been used in the realisaion of external cavity dual mode semiconductor lasers such as those that utilise double grating[95, 96], grating lens[97], grating double-slit[98], double stripe

mirror[99, 100]. The most widely used configuration for setting up an external cavity laser are the Littrow and Littman-Metcalf configurations.

Configuration

Littrow

The littrow configuration utilises first-order diffraction from a diffraction grating coupled back into the laser diode, and the output beam forms from the directly reflected light. The littrow configuration is simple and effective and can be used with gratings to reduce the feedback and increase the power output, thereby increasing the overall efficiency. The lasing wavelength is dependent on the littrow angle, which is the angle of incidence of the laser beam with respect to the grating. Precise wavelength tuning can be achieved by changing the littrow angle. This configuration has been utilised and demonstrated earlier by works such as that of L.Ricci et al. [101] and Arnold et al.[102].

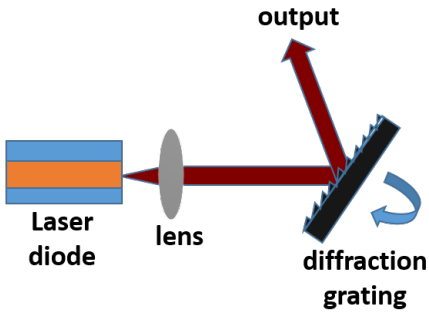

Figure 3.2: Littrow configuration

Littman Metcalf

In the Littman Metcalf configuration a grating at near grazing incidence is used, the first order diffracted beam gets reflected back to the grating and the diode laser by an additional mirror. In this configuration, the wavelength is selected by the mirror angle in such a way that the grating and

the zeroth-order reflected output beam remains fixed in respect to the wavelength. The Littman Metcalf configuration adds a layer of complexity by requiring a larger grating and an additional mirror, moreover the loss of the zero-order reflection of the beam reflected by the tuning mirror leads to output powers that are less than that for a Littrow configuration hence has less output efficiency. With respect to the aforementioned reasons, the littrow configuration was implemented in the design of the ECDl for this research, as further elaborated in the latter section.

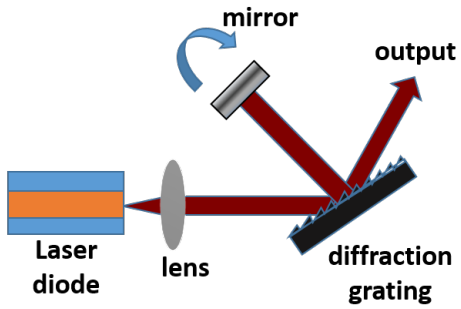

Figure 3.3: Littman Metcalf configuration

3.3 Characterisation of Dual-wavelength Quantum Dot External Cavity laser for CW THz Generation

3.3.1 Experimental Set-up

The design adopted for this research is a modification of the littrow configuration with dual arms, Figure 3 shows the experimental layout of the system, The QD structure active region used for the laser was grown on GaAs substrate and consists of 10 non-identical layers of InAs Quantum dots grown by molecular beam epitaxy in the Strantski-Krastanow mode. The laser has a 5µm wide and 4mm long waveguide angled at 5^{o} with respect to the normal of the back facet to prevent unwanted reflections going back to the laser cavity. Both laser facets have conventional anti-reflective (AR) coatings, with total estimated reflectivity of 10^{-2} for the front facet and less than 10^{-5} for

the angled facet.

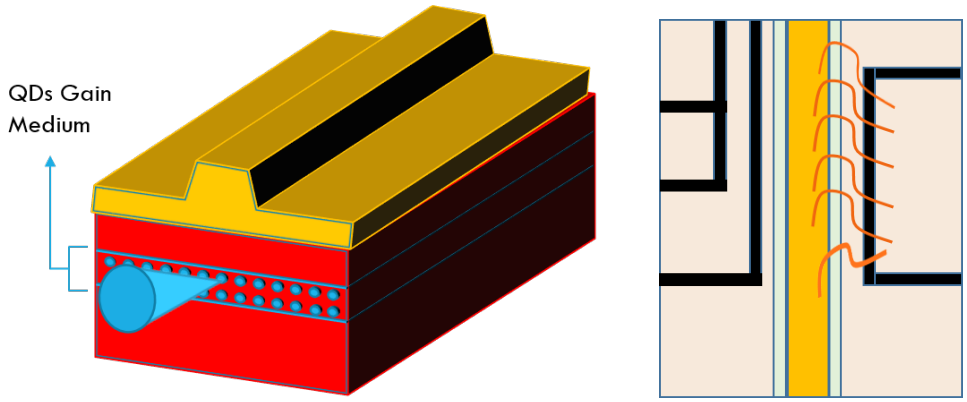

(a) QD_laser (b) QD_laser top

Figure 3.4: Quantum dot Laser

The experimental set-up is based on an external cavity diode laser with simultaneous two-wavelength operation achieved using a beam splitter and two littrow gratings in each arm, wavelength scanning is achieved by rotating the diffraction gratings to be diffracted back along the incident beam. The laser was tested in single-arm operation as shown in Figure 3.8 with a tunability of 152nm achieved under an operation current of 800mA and temperature controlled at 20° by a Thermoelectric cooler. Thereafter, the laser was tested in the double grating quasi-littrow configuration, the tunability was made possible across the 152nm tunable bandwidth of the laser by changing the incidence angle of both gratings shown in Fig 3.5. The design is to be implemented such that the optical beat of the two beams will be made incident on a photoconductive gap of a Photoconductive antenna and terahertz radiation is obtained from optical heterodyne down conversion (Photomixing). The laser was electrically pumped by a Thorlabs ITC4005 Laser diode/TEC controller; the radiation emitted was split then into two by a non-polarising beam splitter and coupled into a diffraction grating of 1200 grooves/mm respectively. The DG reflects the first-order diffraction beams back to the laser chip allowing the simultaneous generation of two wavelengths. The dispersion of light by the grating is governed by the equation $2\alpha(\sin\vartheta_L) = m\lambda_D$ [103], where the littrow angle ϑ_L is dependant on the most intense order (m=1), the design wavelength, λ_D, and the grating spacing

α[103]. Stable laser operation and characteristics demand a precise temperature stabilisation of the QD laser diode, which was implemented in this setup by a peltier (Thermo-electric controller) element controlled by a Thorlabs ITC4005 Laser diode./TEC controller. The temperature was monitored and stabilised at 20° degrees Celsius

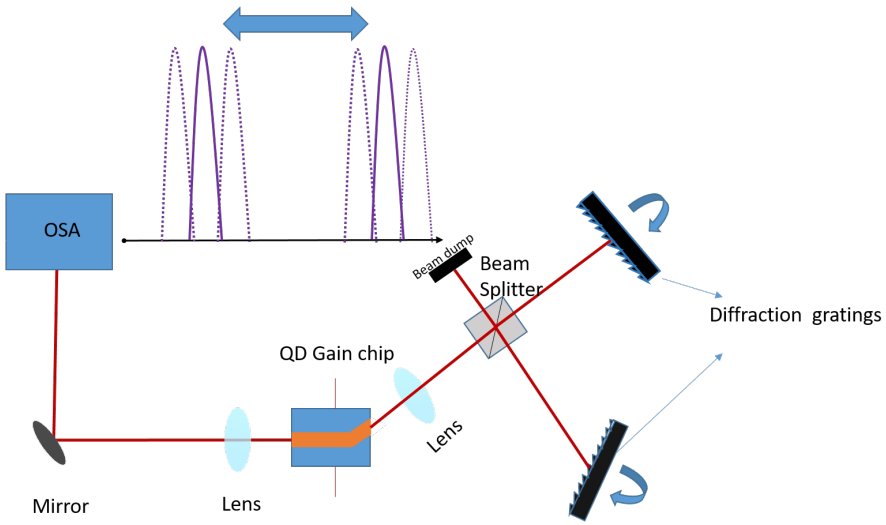

Figure 3.5: shows the set-up configuration for the generation of tunable continuous wave terahertz generation

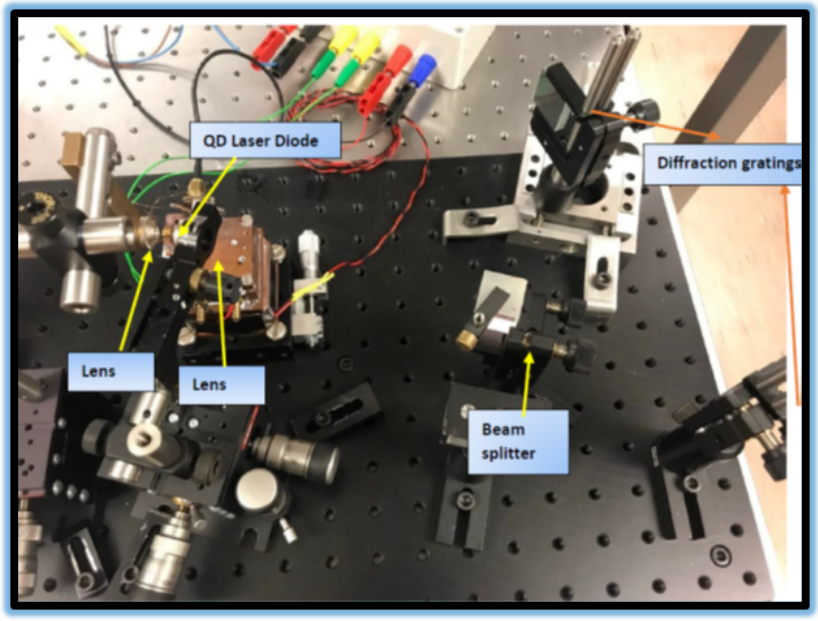

Figure 3.6: The designed external cavity dual wavelength Quantum dot laser set-up

3.3.2 Results and discussion

Fig 3.7 shows the IV characteristics of the QD laser for a forward drive current of up to 1.2A, the laser has a maximum output power of $\leq$420mW and a low threshold current of $\leq$ 120mA, the laser shows a healthy IV curve without any presence of kinks and has a stable operation. The laser has been characterized for potential integration with resonant QD antennas for the realisation of a compact THz system.

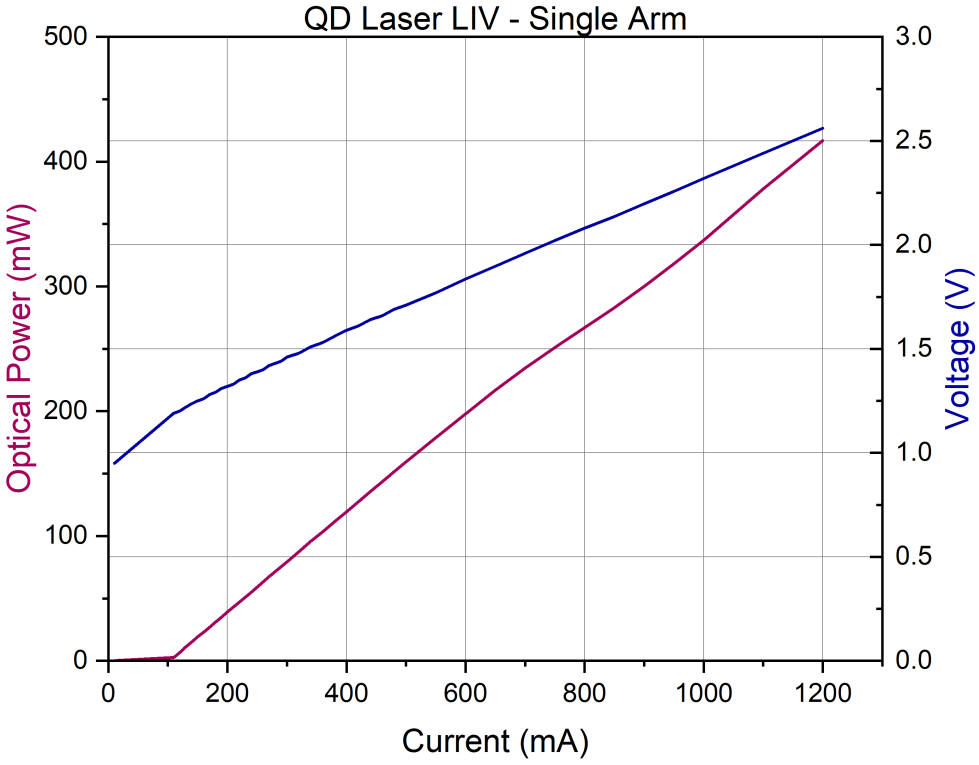

Figure 3.7: LIV Characteristics of the External Cavity Quantum Dot Laser

Single Arm Tunability

The optical spectrum and power at each laser operating wavelength was measured while using only a single diffraction grating and allowing lasing at single wavelength; the optical spectrum was measure by the aid of a fiber coupled optical spectrum analyser. The power was measured by an optical power meter. The laser drive current was set at 800mA and temperature was maintained at T = 20°C. The Fig 3.8 below shows the tunability of the ECDL which lies within the THz frequency range for the generation of tunable continuous wave THz radiation. Stable dual-wavelength operation from the two laser arms was achieved across the range of 1143nm - 1295nm obtained wavelengths. The stable operation of the laser is significant for the

efficient generation of terahertz radiation. The peak power of the laser is obtained at 1220nm as 247mW.

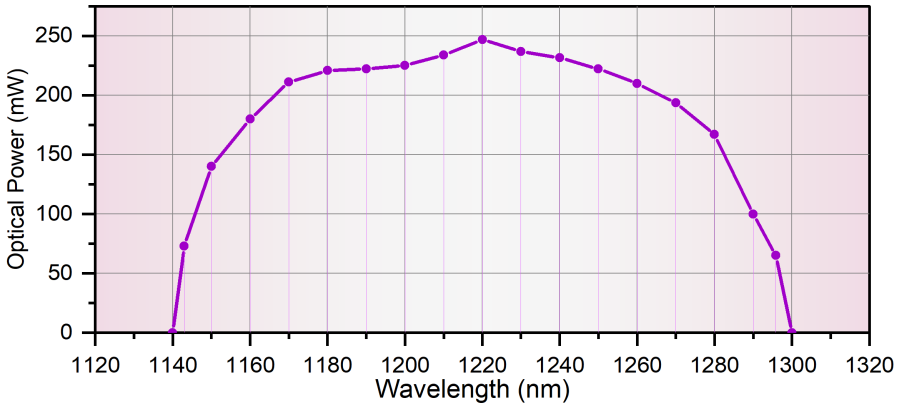

Figure 3.8: shows the tunability and output power operation of the laser in single arm operation

Dual Arm Operation

For this measurement, both diffraction gratings were used to couple back into the QD laser gain medium to enable dual-wavelength operation. The power of the independent wavelengths were obtained using a Newport hand-held optical power meter model 1916-r alongside an APE wavescan optical spectrum analyser that displays the wavelength-dependent intensity of the input light. The diffraction gratings were rotated to deflect lights of different wavelengths at different angles to determine the intensity of the wavelengths.

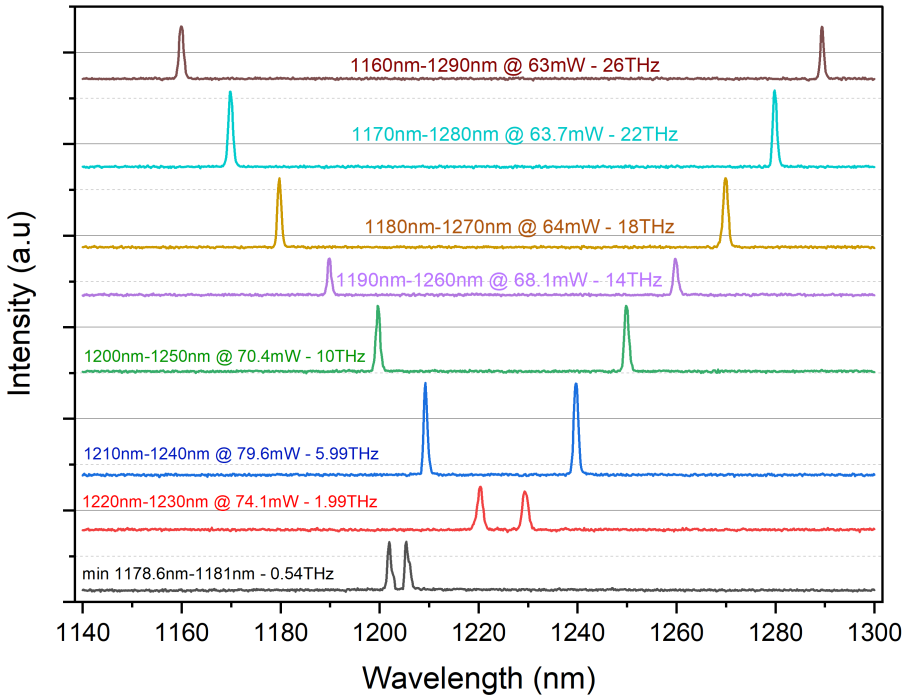

Figure 3.9: Dual mode operation of the laser at multiple THz difference frequencies

Fig 3.9 shows the optical spectrum and tunability of the ECDL QD laser, the laser operation was established with dual stable modes without mode interplay and the optical spectrum recorded with the optical spectrum analyser while the power is recorded by the optical power meter. A maximum stable dual wavelength operation was obtained at 1160nm - 1290nm, which corresponds to 26 THz difference frequency with power measured at 63mW. Thereafter, difference frequency at 22THz, 18THz, 14THz, 10THz, 5.99 TH and 1.99 THz were measured successfully all possessing a stable operation at optical powers of 63.7mW, 64mW, 68.1mW, 70.4mW, 79.6mW and 74.1mW respectively. Finally, on the bottom row in Fig 3.9 coloured in black is the minimum dual wavelength separation of the laser without any mode interplay at 0.54THz difference frequency. To obtain continuous wave THz the two frequencies from the laser diode will be irradiated on a PCA at

a beat frequency $\omega_T = \omega_1 - \omega_2$. The optical field of the antenna is expressed by equation (3.1)

$$\left\{ E_{opt}(t) = \ E_1 e^{-i\omega_1 t} + E_2 e^{-i\omega_2 t} \qquad [7] \right. \tag{3.1}$$

Where E_1 and E_2 are the electric field amplitudes and ω_1,ω_2 are the frequencies of the 2 waves, respectively. The induced photocurrent oscillates with the beat frequency and THz radiation is obtained when the difference frequency ω_T is tuned to the THz range.
The external cavity QD Laser has been characterised with a tunability of 152nm and a tuning range from 1143nm-1295.8nm that lies within the THz difference frequency of 26THz - 0.54THz in stable dual mode operation. The implementation of such ECDL as an optical pump source in a THz generation system will provide for a much compact THz system, consequent to the lack of requirement of femtosecond lasers for pulsed optical pumping as in chapter 4.

Chapter 4

4.1 Pulsed Terahertz System

This chapter will introduce ultrashort pulse lasers that are required as an optical pump source for use with non-linear crystals and photoconductive antennas for Terahertz generation. The spectral bandwidth of dyes paved the way for ultrafast pulse generation as well as tunability. As early as 1964, Wills lamb demonstrated that mode-locking a laser could generate a short pulse limited in duration by the fourier transform of the bandwidth[104]. Ultrafast lasers generating ultrafast pulsed optical output signals are achieved using several techniques including gain switching, Q switching and mode locking in predominantly femtosecond lasers [105]. The most widely gain medium for femtosecond lasers is Titanium-doped aluminium oxide (Ti:Sapphire)

4.2 Literature Review

4.2.1 Mode-locking

Mode-locking is a term that is used to describe in the frequency domain the oscillation of several resonator modes with a relatively locked phase, it is the most widely used technique for generating pulses of picoseconds and femtosecond durations that are required for pulsed THz generation. Several pulses are circulating in a laser cavity when the laser is mode-locked, a part of its energy is emitted every time the pulse hits the output coupler mirror so that the laser output is a regular pulse train. The pulse energy is replenished by the gain medium during each round trip[8]. The optical cavity's round trip time and the number of pulses determines the pulse repetition rate of the

mode-locked laser, with longer round trip times leading to lower repetition rate and vice-versa. Two types of mode-locked lasers will be discussed in the next section for the generation of THz radiation

4.2.2 Lasers for Pulsed THz Generation

Ti:Sapphire Laser

Ti:Sapphire laser is a solid state vibronic laser that was first confirmed to oscillate in 1982 by the work of Peter Moulton[106]; (Ti: Al_2O_3:Ti:Sapphire) crystal is a sapphire crystal (Al_2O_3) material in similitude with the earlier ruby laser base material (Cr: Al_2O_3 laser) that is doped with Ti^{3+}. It has a broad tuning range of 660 to 1180nm and high repetition rate, however, required pumping by another laser. It has so many advantages, that includes high optical pumping power ($\leq 20W$ owing to it's high thermal conductivity and relatively short carrier lifetime of (3.2ms). Ultrashort pulses can be generated from Titanium sapphire laser through passive mode-locking usually by utilizing a non-linear optical phenomenon referred to as Kerr-lens Mode locking or self-mode synchronization. Ti:Sapphire laser's lasing mechanism can be simplified as a four level system where electrons are excited by a green pump laser and then relax into lower and more stable energy states to achieve population inversion in order to realise stimulated emission[7]. The figure 4.1 below shows a schematic diagram of a mode locked Ti:Sa laser, an optical pump laser in the form of a diode-pumped solid state laser and argon ion laser with peak wavelength at around 500nm is utilised, the dispersion induced by the gain medium and other optical components is compensated for by the introduction of a prism pair. Kerr lens mode-locking is achieved through the adjustable slits by suppressing all the continuous wave modes while allowing the short pulses to pass through the aperture as shown in the schematic below.

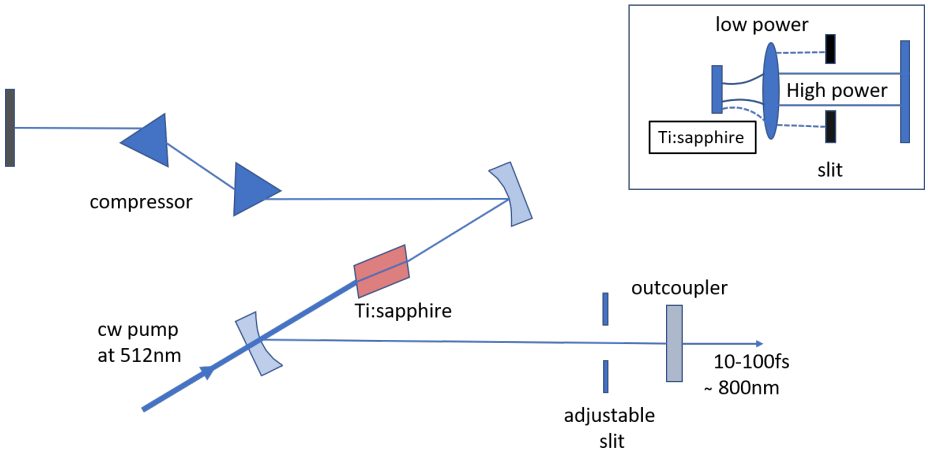

Figure 4.1: A schematic of a Ti:sapphire laser

The titanium sapphire laser has become ubiquitous in applications of generating both pulsed and continuous terahertz radiation due to its tunability, femtosecond pulses, stability and high power output. Since the work of E. R Brown et al., numerous researchers have employed the Ti:Sa for THz generation in continuous wave [107] and broadband THz generation [108, 109]; as well as using various THz generation techniques such as photomixing[107], difference frequency generation[110] and other methods [109, 111, 112, 113, 114, 115].

Table 4.1: Commercially Available Tunable Pulsed Titanium Sapphire lasers

Lasers	Lasers	Tuning range	Output Power	Pulse repetition rate
M2 Sprite	<180fs	720nm-940nm	>1.3 W	80MHz
M2 Sprite XT	< 150 fs	720nm-980nm	> 1.5 W	80 MHz
Thorlabs Tiberius	140fs	720nm-1060nm	>2.3W	80 MHz
Km Labs Griffin	<12fs	∼680nm - ∼910nm	>2.3W	75-102 MHz
Spectra Physics Mai Tai SP	<25fs	780nm-820nm	750mW	84 MHz

Mode-locked Fiber Lasers

Femtosecond fiber laser are of growing interest in generation of terahertz due to their compactness compared to Ti: Sapphire lasers and non-requirement for cooling among other benefits, however their major drawbacks are longer wavelength and lower peak power than the Ti: Sapphire laser[23]. Moreover, significant research is currently undertaken in terahertz materials that will enable integration with 1.5 µm wavelength of most fiber lasers. Erbium doped fibre lasers producing 1550nm wavelength are of benefit for terahertz generation for their low cost, compactness and integration with telecommunications components.

Fiber lasers have a number of qualities that make them attractive for the generation of ultrashort pulses via active or passive mode locking due to the large gain bandwidth of rare-earth-doped fibers which will allow for the generation of femtosecond pulses. Active fibers have high gain efficiency that allows for low pump power operation of the lasers and tolerance for optical cavity elements with relative high losses. Roman J et al. implemented two erbium-doped fiber lasers in demonstrating an all fiber-coupled THz Time-domain-spectroscopy system. The lasers were passively mode locked by a saturable absorber and emitting at 1560nm with <100fs optical pulse duration and 80mW average power at 100MHz repetition rate. An InGaAs./InAlAs heterostructure PCA was used to achieve output powers of up to 64µW [116].

4.3 Experimental Set-up

Not only resonant optical pumps at the ground state and excited state photon energy of the QDs excite the photocarriers in the QD substrates moreover photons with energy above the bandgap of GaAs due to the carrier excitation in the bulk GaAs containing the QDs. The QD's pivotal role is serving as a carrier capture site and hence shortening the carrier lifetimes of the free carriers.

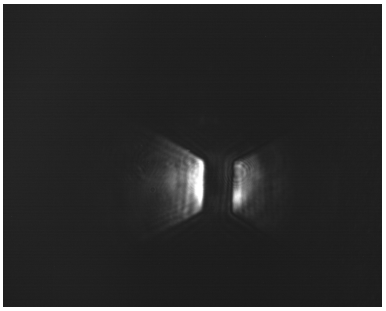

(a) QD_Bt1 optical pump image

(b) QD_Pl optical pump image

(c) QD_id optical pump image

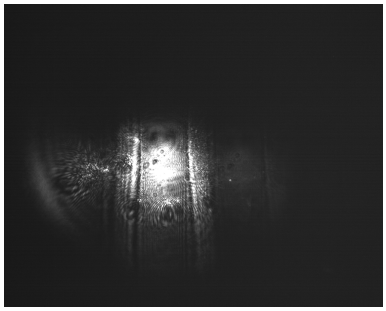

(d) Teravil optical pump image

Figure 4.2: Camera Image of the optical pump source focused on Antenna gaps

4.3.1 Golay Cell Detection

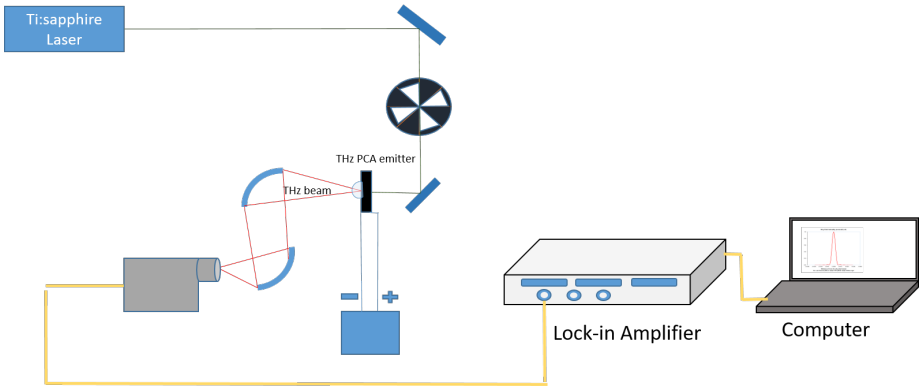

Figure 4.3: THz power detection with golay cell

For the detection of the generated THz power from the PCAs, a Tydex Golay cell detector was implemented as shown in Fig 4.3 above, the golay cell was calibrated prior by the work of Dr Ross Leyman with a bolometer to ensure the accuracy of the obtained results. An Msquared Sprite XT ultrafast tunable Ti:sapphire laser was used as the optical pump source owing to its relative compatibility and stable operation without frequent re-alignment. The temperature of the Ti:sapphire was maintained at 25°C, a pulse duration of 130fs at 78MHz repetition rate was obtained from the laser for the experiment. The laser beam from the Ti:Sapphire laser was focused on the antenna gap as shown in Fig 4.2; by the aid of mirrors, the antenna position was adjusted to the point with least resistance; a power supply was used to provide bias voltages of 2V to 20V at 2V increments to the antennas for the experiment. A hyper hemispherical silicon lens was used to focus the generated THz beam onto two parabolic mirrors and onto the golay cell for detection. For detection of the THz radiation, the laser beam was modulated by an optical chopper at a frequency of 16 Hz due to the low time response of the golay cell detector. This was fed into the Stanford Instruments SRS 800 lock-in amplifier to isolate only the generated THz signal at this reference frequency and suppress the surrounding noisy signal from the ambient environment. As the golay cell is a thermal detector, the laboratory temperature was maintained all through the experiments for consistency and also other sources of IR such as body heat were mitigated as much as possible to not interfere with the reading. The chopper frequency was chosen away from the mains AC frequency and it's harmonics to avoid cross talk or interference. The obtained data from the lock-in amplifier were recorded on a computer by the aid of a Labview programme designed with the help of Dr Semyon Smirnov for data analysis. The measurements were taken at 780nm and 800nm wavelengths, optical pump power of 1mW, 2mW, 3mW, 5mW, 7mW and 10 mW and bias voltages of 2V-20V as shown in figs 1-3

Golay Cell Results

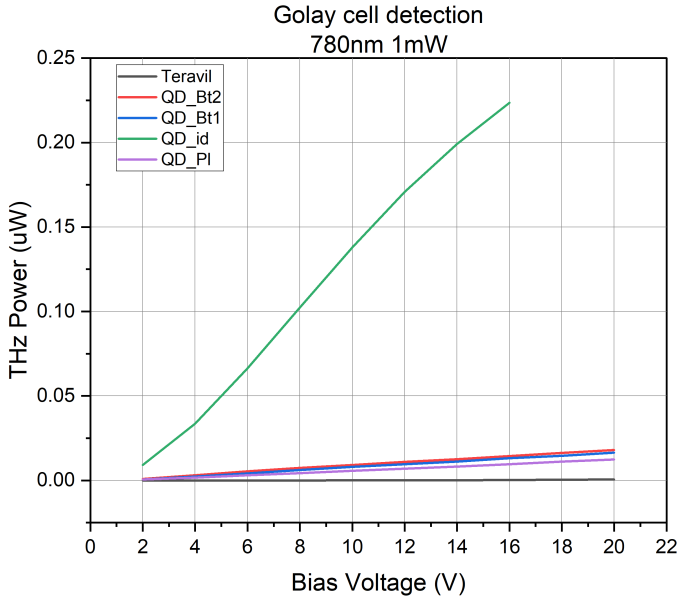

Figure 4.4: THz signal output power detected by Golay cell at 1mW optical pump power

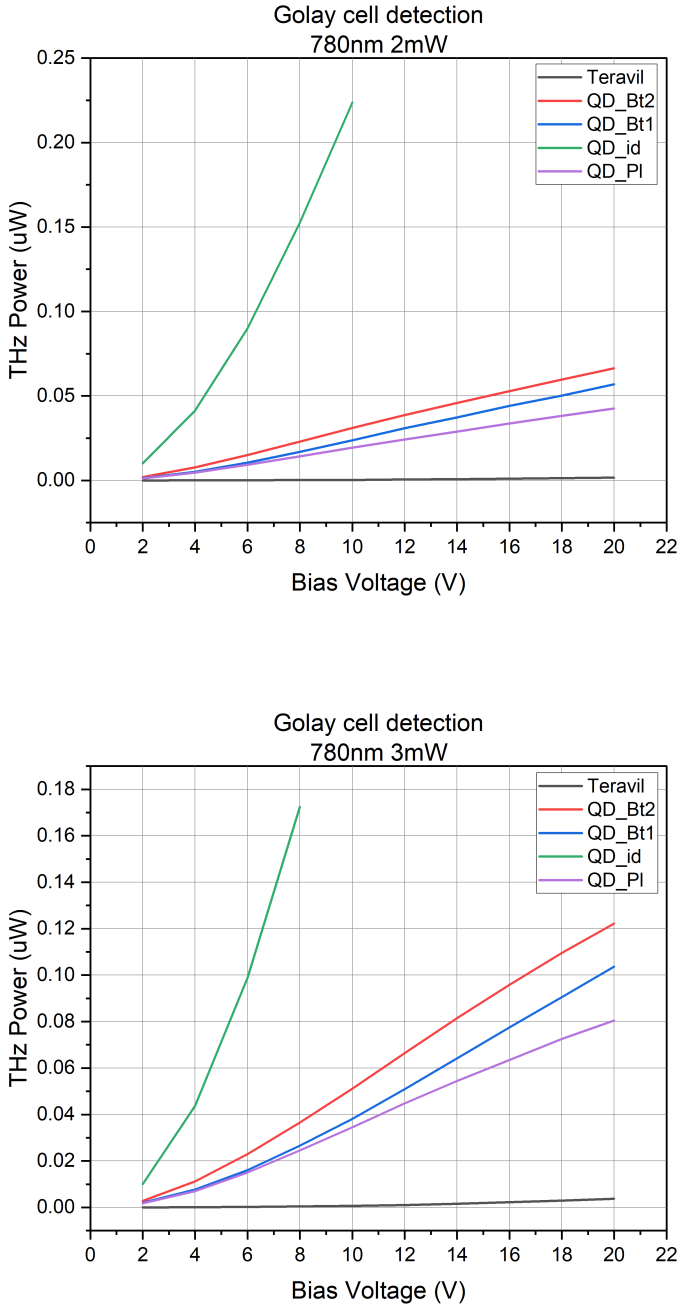

Figure 4.5: THz signal output power detected by Golay cell at 2mW(top) and 3mW (bottom) optical pump power

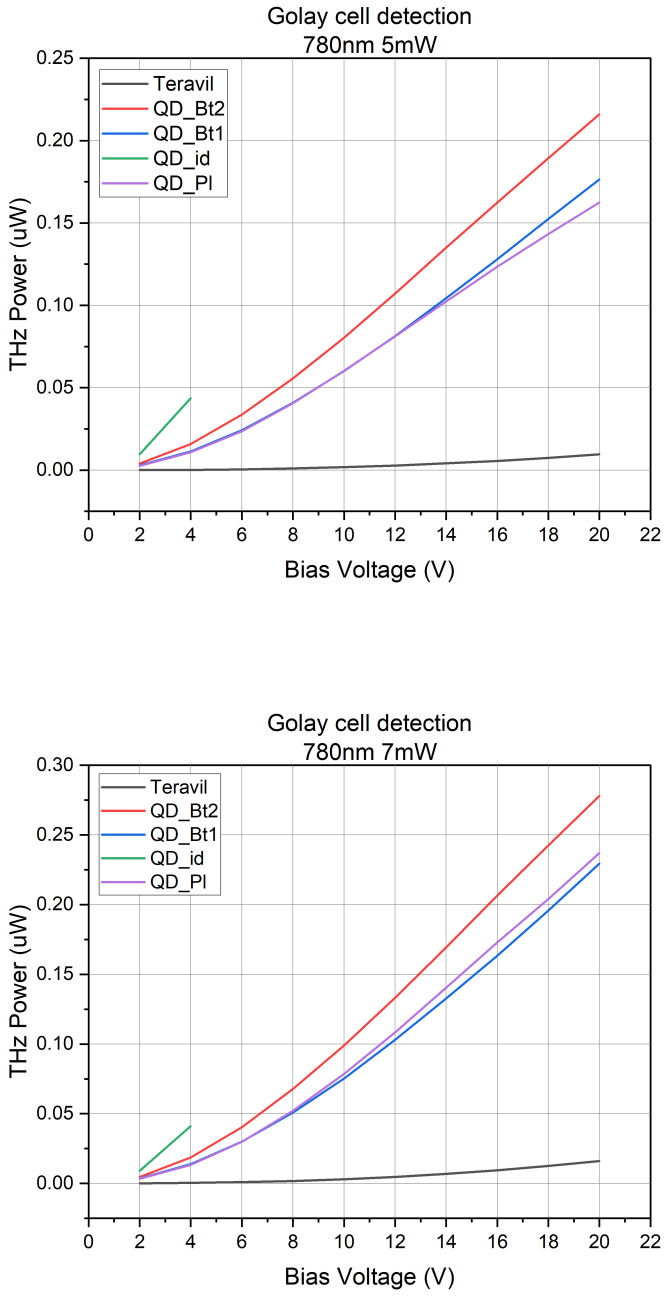

Figure 4.6: THz signal output power detected by Golay cell at 5mW(top) and 7mW(bottom) optical pump power

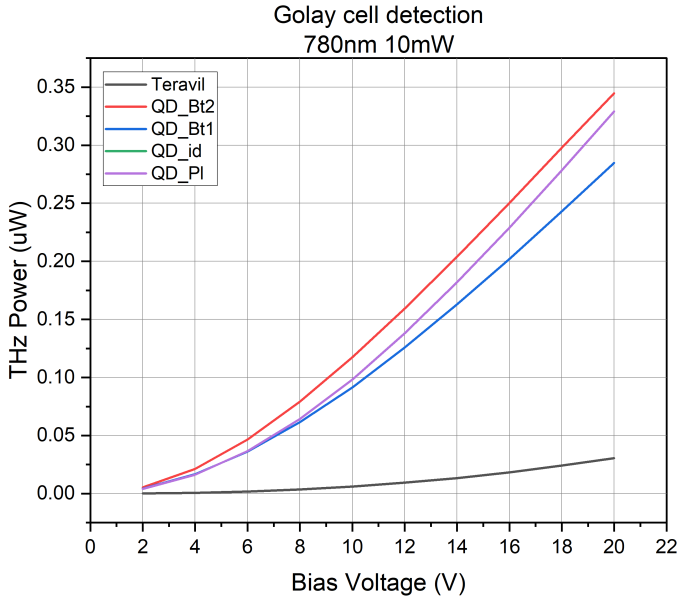

Figure 4.7: THz signal output power detected by Golay cell at 10mW optical pump power

4.3.2 Golay Cell Results Discussion at 780nm

Figs 4.4-4.6 shows the golay cell detection of THz radiation output power at 780nm and 2V-20V bias voltages. The QD_id antenna had the highest THz output power in respect to the applied voltage and pump power, however, as discussed earlier in Chapter 2, its IV characteristics shows a lower voltage limit than the rest of the antennas and hence it was limited to only lower bias voltages. At 2mW pump power the interdigitated electrode antenna QD_id has the highest power output of ∼0.22µW but due to the lower voltage limitation that was identified as stated earlier the bias voltage for the QD_id was limited at 10V. At this parameter of 2mW and 10V bias voltage the THz power of the QD_id antenna is more than 20 times higher than that of the teravil antenna. At 3mW the QD_id still had the highest power output of ∼0.17µW amongst all antennas however higher bias voltages can be applied to the other antennas and an almost linear increase is seen from 6V bias voltage to 20V bias voltage. At the relatively higher pump powers of 7mW and 10mW bias voltage the THz output powers of the QD_Bt2 and QD_Pl

were the highest. At 10mW and 20V bias voltage the QD_Bt2 and QD_Pl had a THz output power of ∼0.325µW and the QD_Bt1 coming next at ∼0.28 µW. The Teravil antenna had THz power of ∼0.028 µW. It can be seen from this that the Quantum dot antennas shows over 10 times more THz power than the commercial THz antenna from Teravil antenna at the aforementioned conditions.

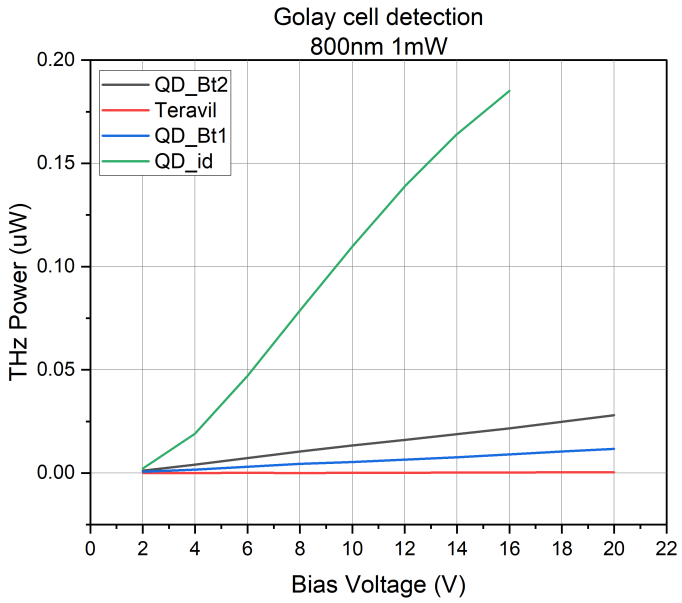

Figure 4.8: THz signal output power detected by Golay cell at 1mW optical pump power

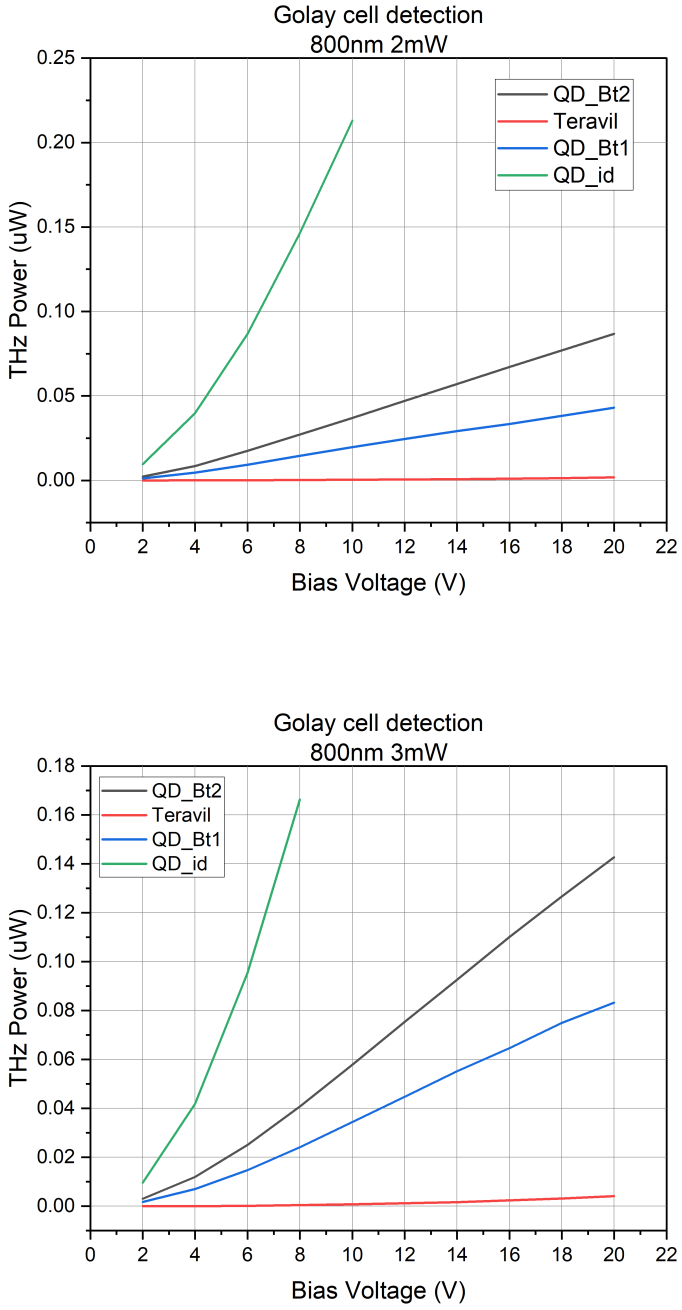

Figure 4.9: THz signal output power detected by Golay cell at 2mW(top) and 3mW(bottom) optical pump power

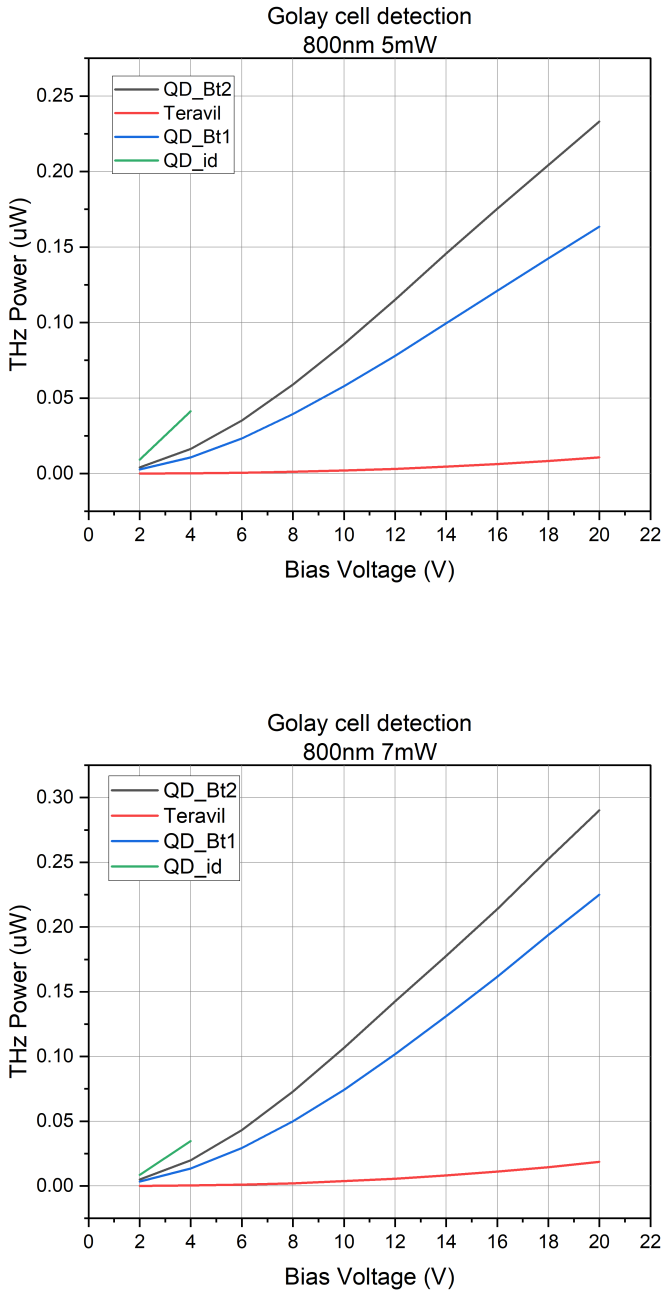

Figure 4.10: THz signal output power detected by Golay cell at 5mW(top) and 7mW(bottom) optical pump power

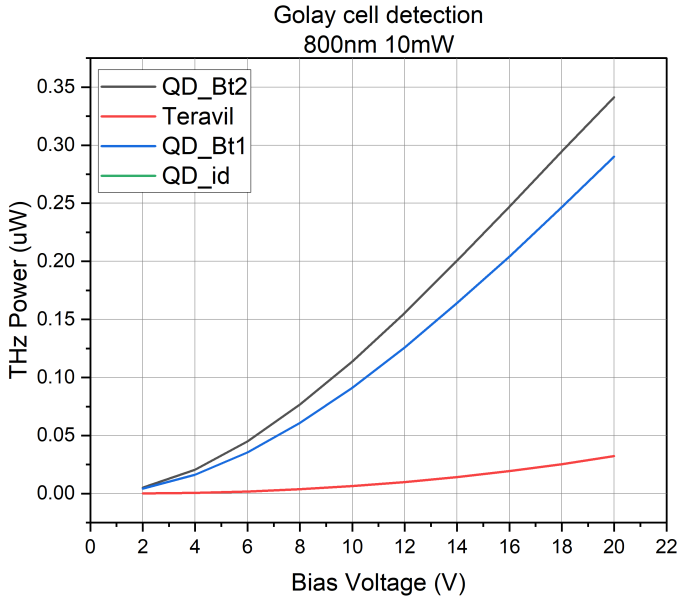

Figure 4.11: THz signal output power detected by Golay cell at 10mW optical pump power

4.3.3 Golay Cell Results Discussion at 800nm

The antennas were further optically pumped at 800nm with the same set of parameters as was carried out for 780nm. It can be seen Fig 4.7 - Fig 4.9 that at 1mW all the Quantum dot antennas show slightly increased THz output powers at 800nm. For comparison, the QD_id antenna at 1mW and 16V bias voltage recorded a power of ∼0.17 µW and ∼0.14µW at 800nm and 780nm respectively and hence higher absorption of the 800nm pump than the 780nm pump wavelength. A similar trend in respect to the quantum dot antennas powers and the teravil antennas was recorded at 800nm just as previously highlighted for the 780nm. In Fig 4.8 at 3mW and 8V bias voltage the QD_id antenna had a power output of ∼0.17 µW the QD_Bt1 recorded ∼0.021 , QD_Bt2 records ∼0.04 µW while the Teravil records ∼ 0 W THz power which shows that at these conditions there is very minimal photocarrier generation in the Teravil antenna as suggested by the ∼ 20µA photocurrent measured as shown in Figure 2.12. The antennas shows an increase in output power response with an increase in optical pump power

and bias voltage as expected, however saturation points and antenna limits were not recorded due to sample limitations.

4.3.4 PCA Detection

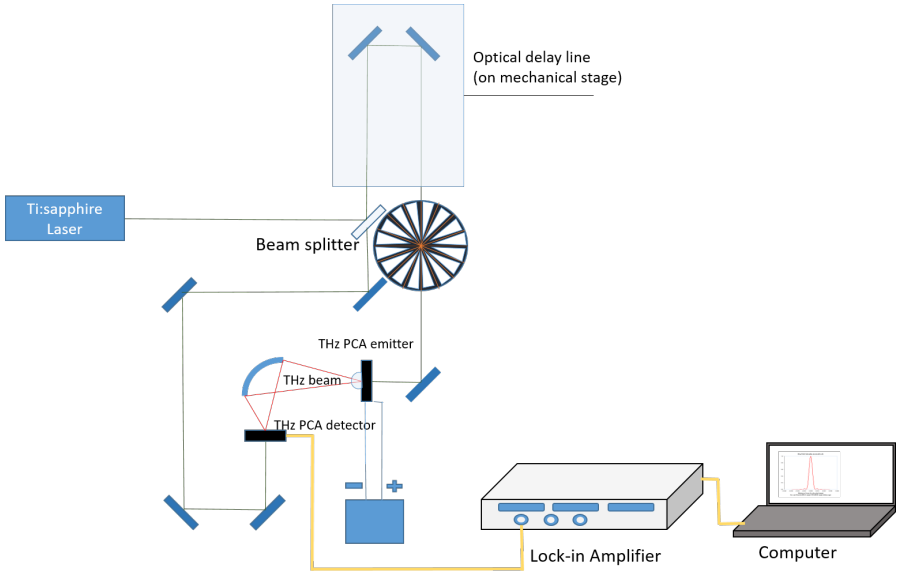

Figure 4.12: THz Pulse detection with Photoconductive Antenna

The system was tested with a THz optical-pump-probe set-up, a Ti:Sa laser by m squared was used to provide the ultrafast laser pulses to pump the emission antenna and probe the detector antenna. The pulses were split into two paths, with one going through an optical delay stage by aid of mirrors mounted on a translational stage. The other was focused on the detector antenna, the spot size and pump position on the emitter PCA was monitored by using a camera. The main parameters for the laser are stated as follows: 800nm wavelength, pulse width is 130 fs, repetition rate of 80MHz and the power at the probe path was maintained at 45mW while the pump power was controlled by an attenuator to provide the required power levels as will be stated.

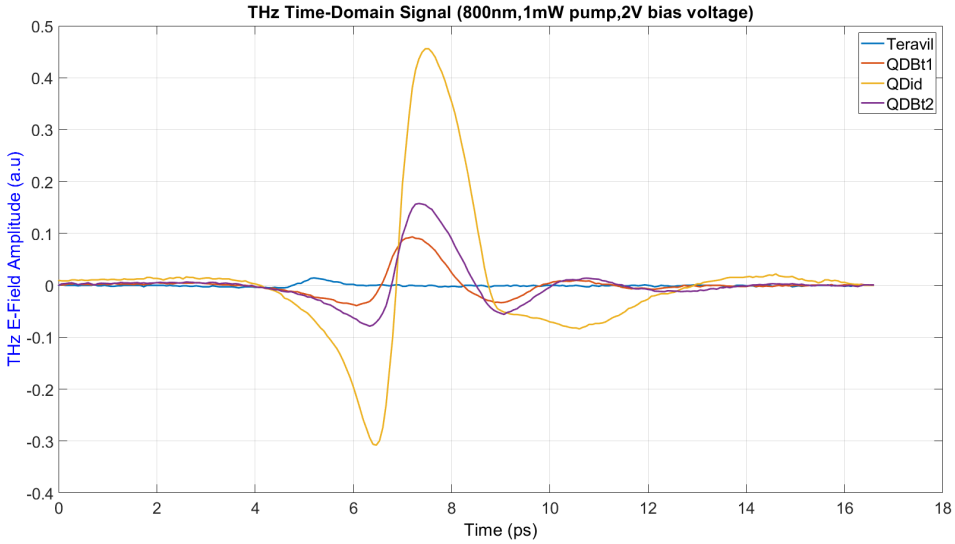
THz Time-Domain Signal (800nm,1mW pump,2V bias voltage)
THz E-Field Amplitude (a.u)
Time (ps)
Teravil
QDBt1
QDid
QDBt2

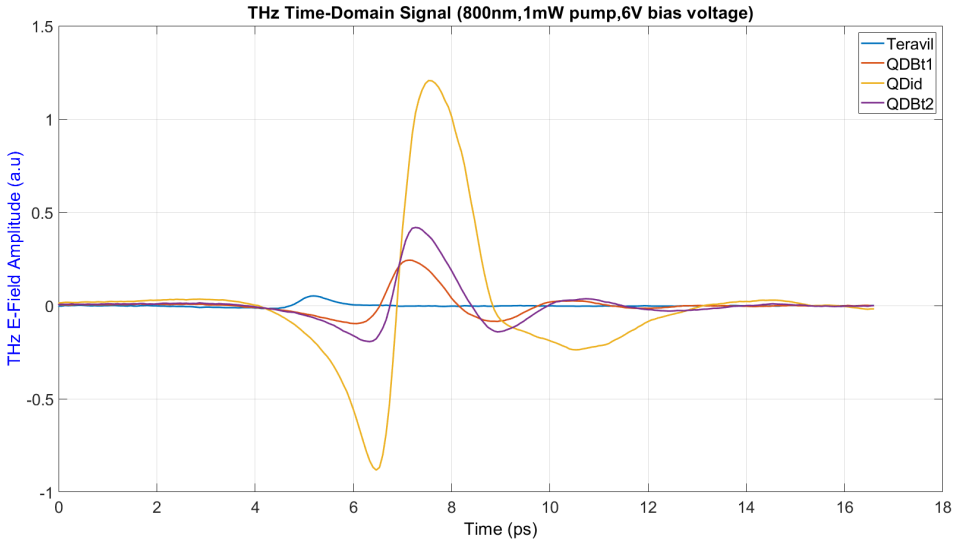
THz Time-Domain Signal (800nm,1mW pump,6V bias voltage)
THz E-Field Amplitude (a.u)
Time (ps)
Teravil
QDBt1
QDid
QDBt2

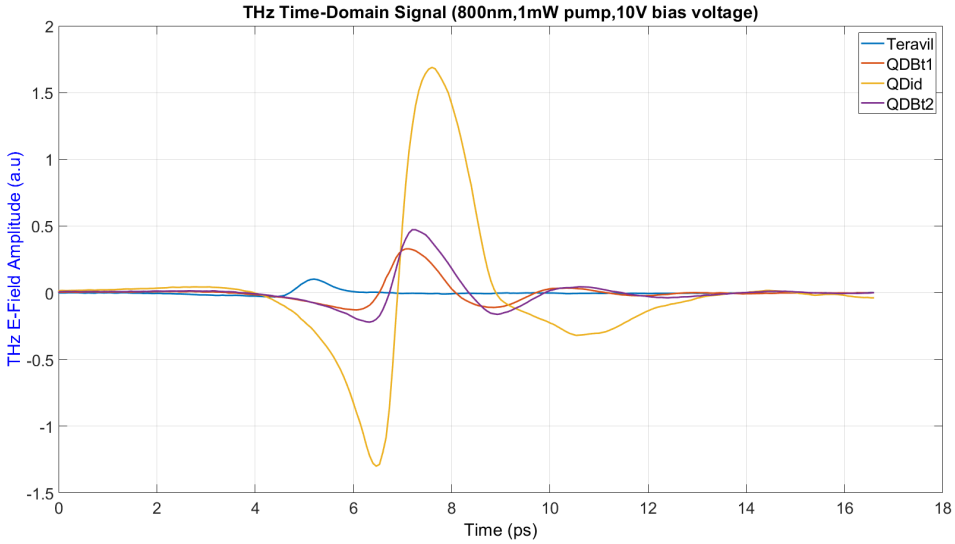

Figure 4.13: THz Time domain pulse at 1mW for 2v, 6V and 10V bias voltage

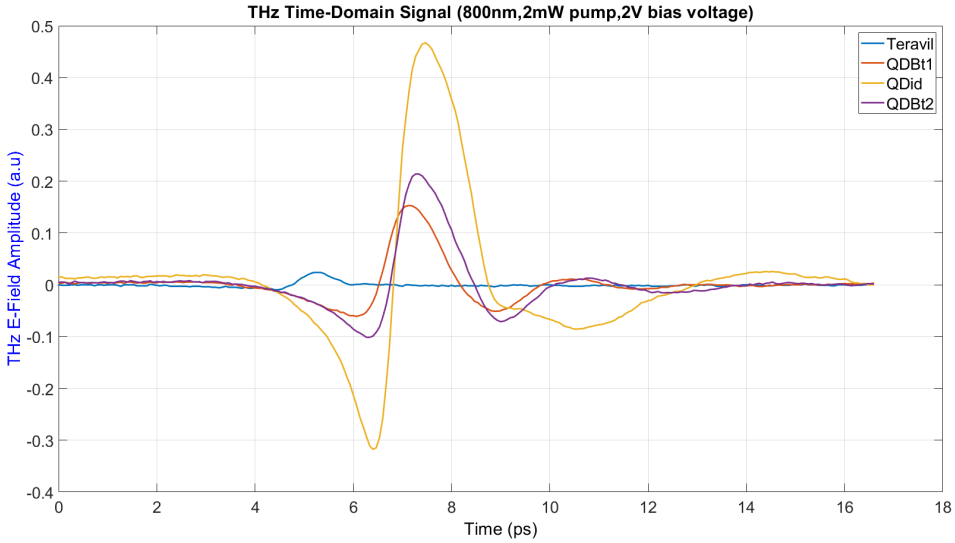

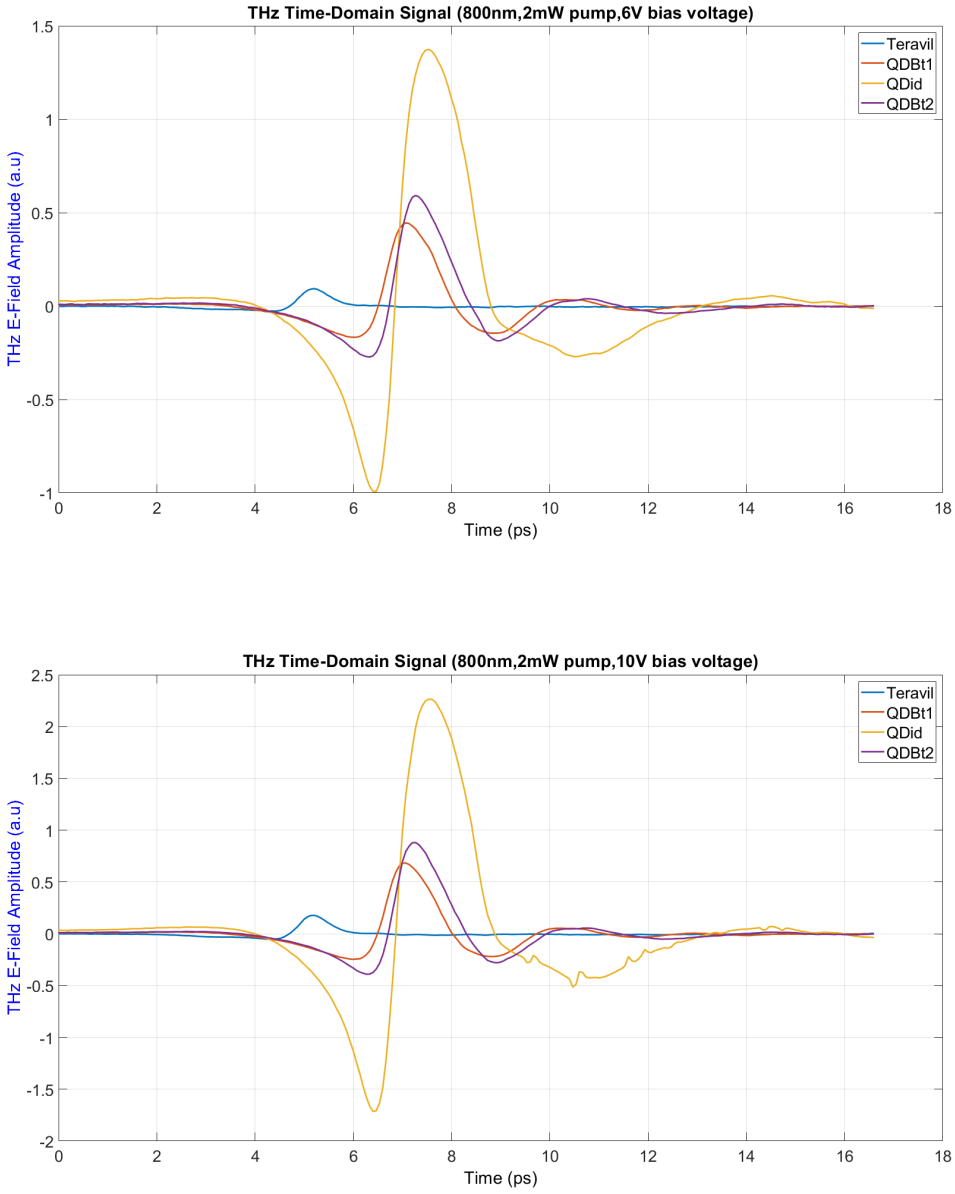

Figure 4.14: THz Time domain pulse at 2mW for 2v, 6V and 10V bias voltage

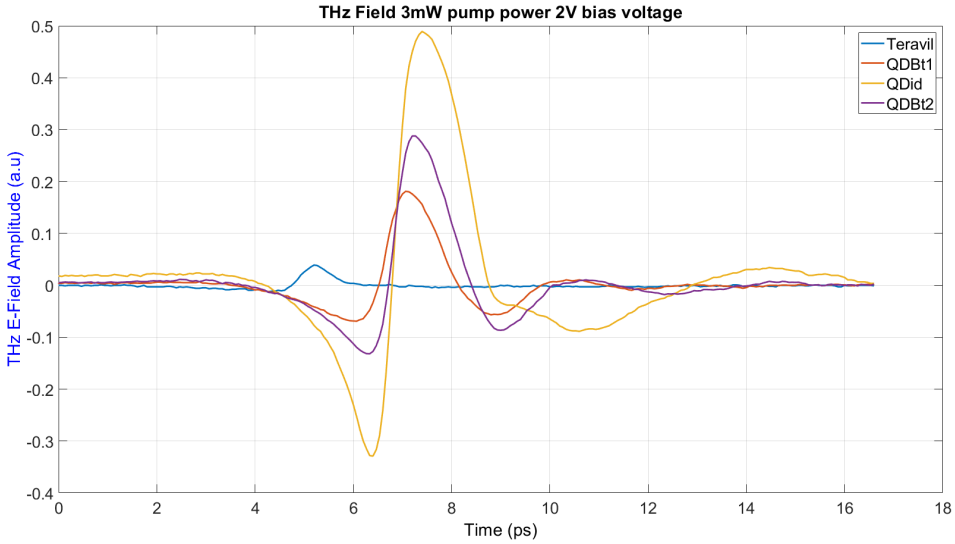
THz Field 3mW pump power 2V bias voltage
THz E-Field Amplitude (a.u)
Time (ps)
Teravil
QDBt1
QDid
QDBt2

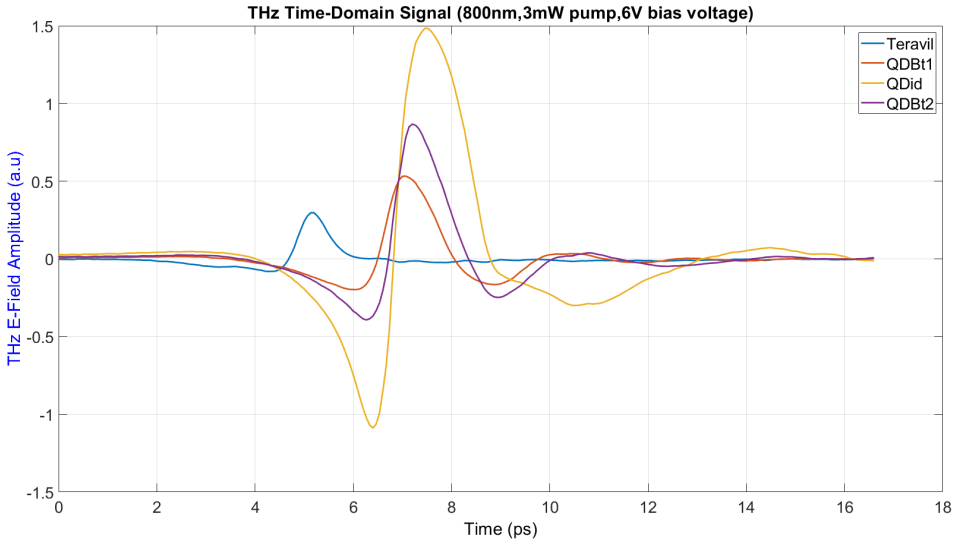
THz Time-Domain Signal (800nm,3mW pump,6V bias voltage)
THz E-Field Amplitude (a.u)
Time (ps)
Teravil
QDBt1
QDid
QDBt2

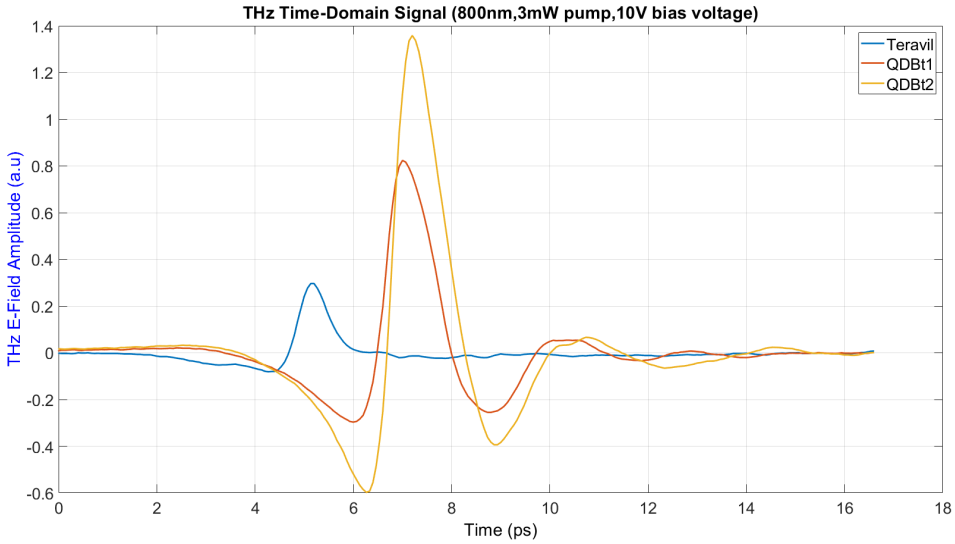

Figure 4.15: THz Time domain pulse at 3mW for 2v, 6V and 10V bias voltage

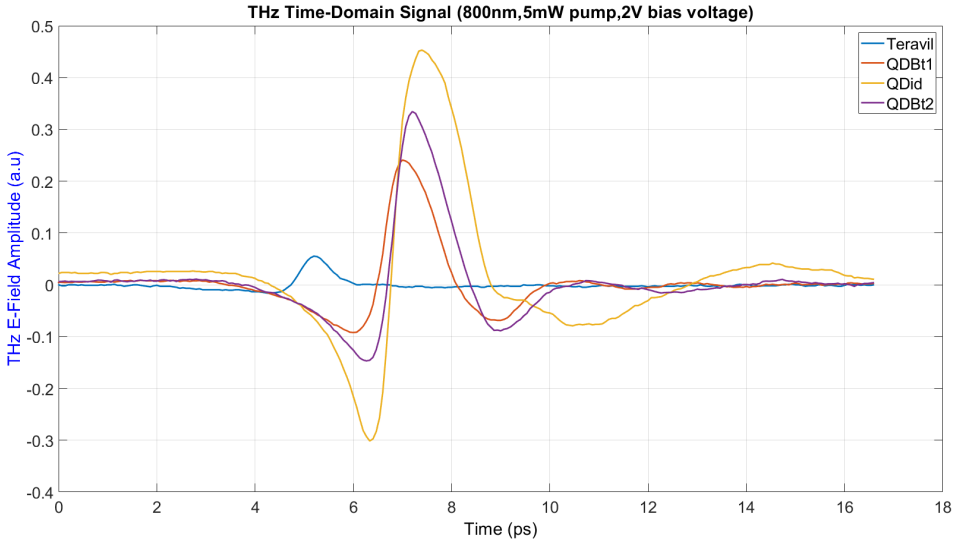

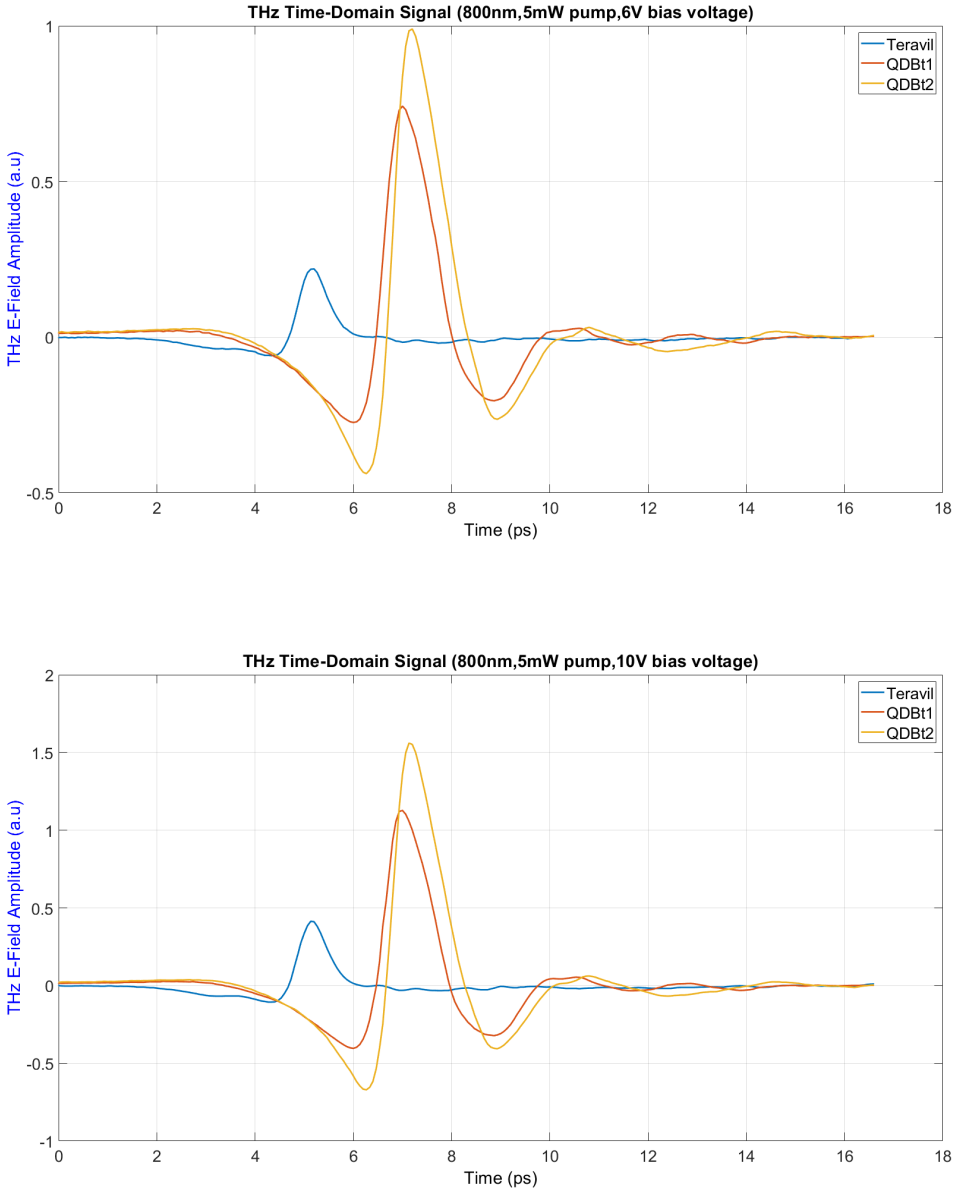

Figure 4.16: THz Time domain pulse at 5mW for 2v, 6V and 10V bias voltage

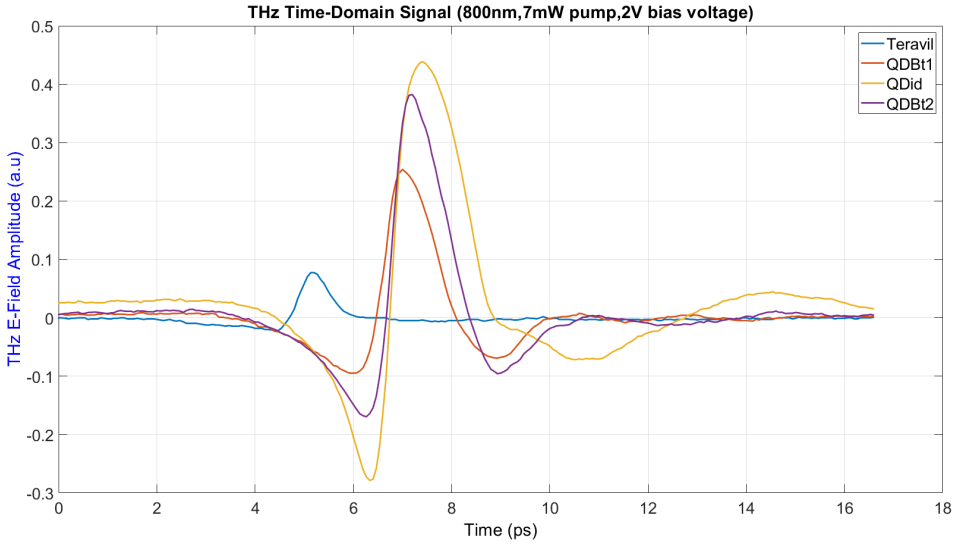
THz Time-Domain Signal (800nm,7mW pump,2V bias voltage)
THz E-Field Amplitude (a.u)
Time (ps)
Teravil
QDBt1
QDid
QDBt2

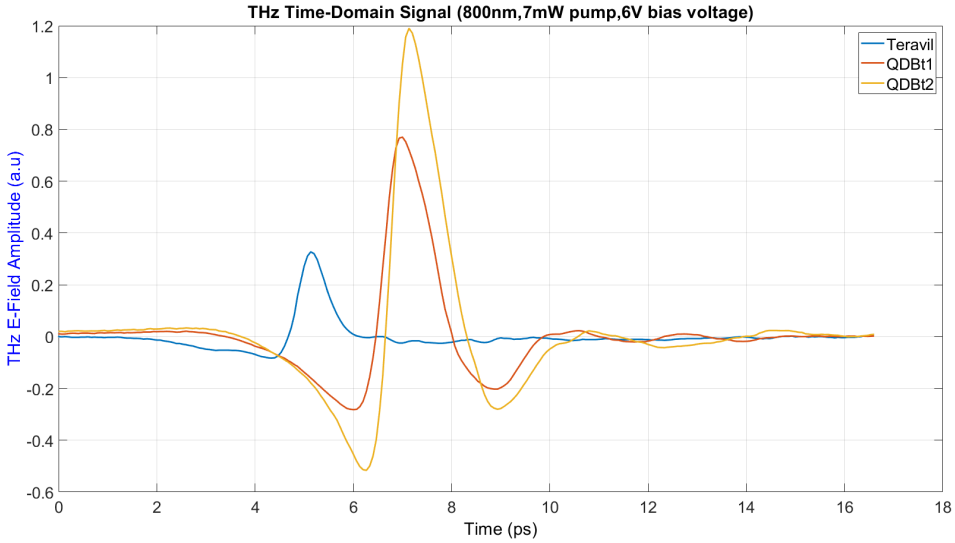
THz Time-Domain Signal (800nm,7mW pump,6V bias voltage)
THz E-Field Amplitude (a.u)
Time (ps)
Teravil
QDBt1
QDBt2

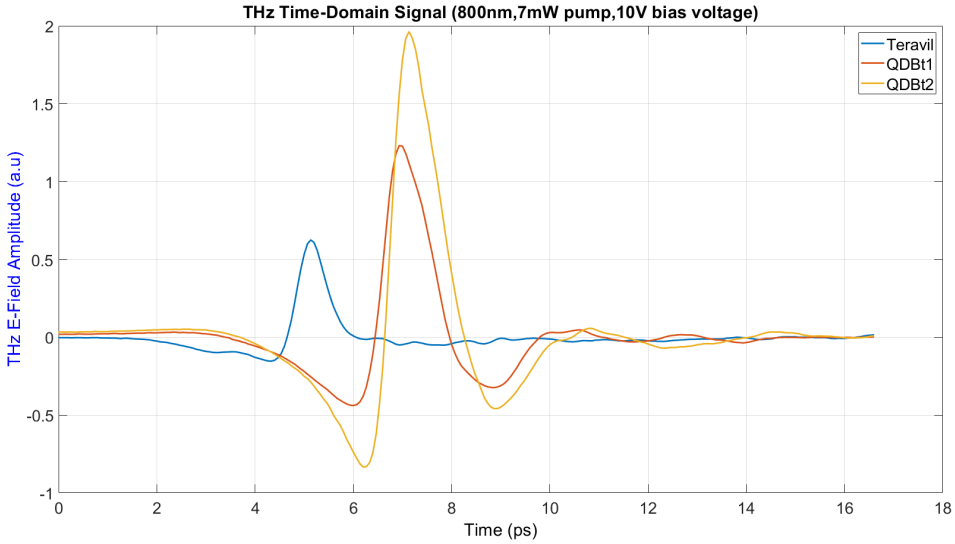

Figure 4.17: THz Time domain pulse at 7mW for 2v, 6V and 10V bias voltage

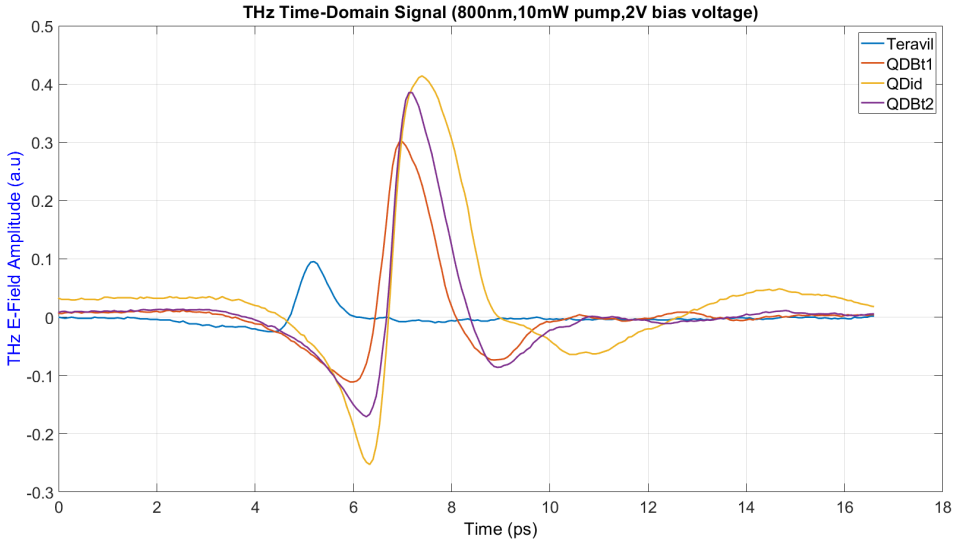

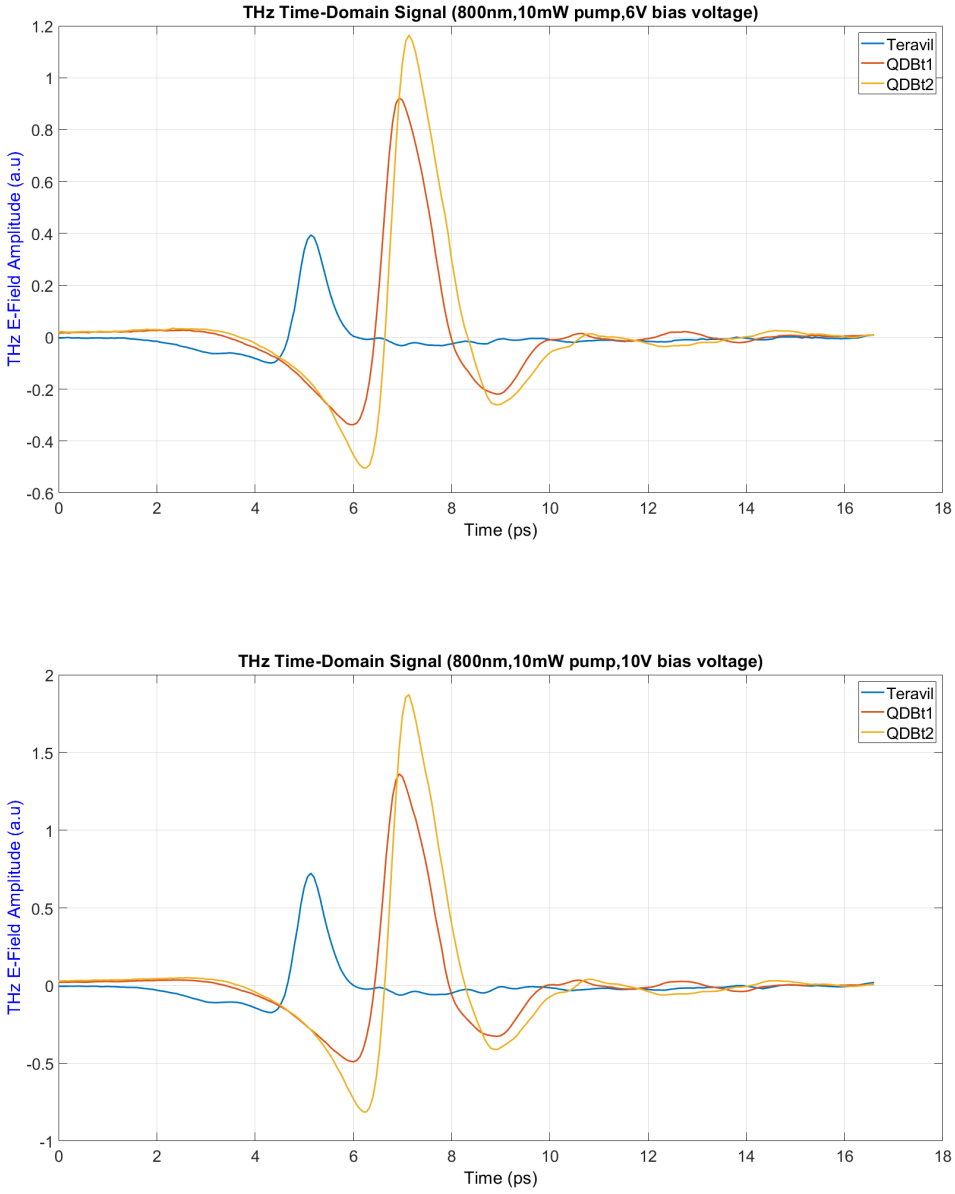

Figure 4.18: THz Time domain pulse at 10mW for 2v, 6V and 10V bias voltage

4.3.5 THz Time domain Pulse results discussion at 800nm

The electric field of the THz was measured through the photocurrent from the detector PCA as a function of the time-delay between the arrival of the THz and probe pulse at the detector antenna. The time domain pulse was recorded at 2V, 6V and 10V bias voltages for 1mW, 2mW, 3mW, 5mW, 7mW and 10mW as shown in figures 1-10. The QD_id antenna with inter-digitated electrodes had the highest THz E-field compared to the rest of the antennas, with a significantly higher difference for the relatively lower pumps. All the QD antennas shows a higher THz E-field amplitude than the Teravil Antenna with over 20 times higher THz E-field at 1mW and 2V bias voltage and over 4 times at 10mW and 2V bias voltage. Only the pulse amplitude is increased when increasing the bias voltage for each pump power, without any changes to the shape of the pulse. However, with increase in optical pump power the pulsewidth has been observed to decrease in time as the trend can be seen across figure 1-10 which can possibly be explained by the carrier lifetime shortening in the QD antennas due to Auger processes[117].

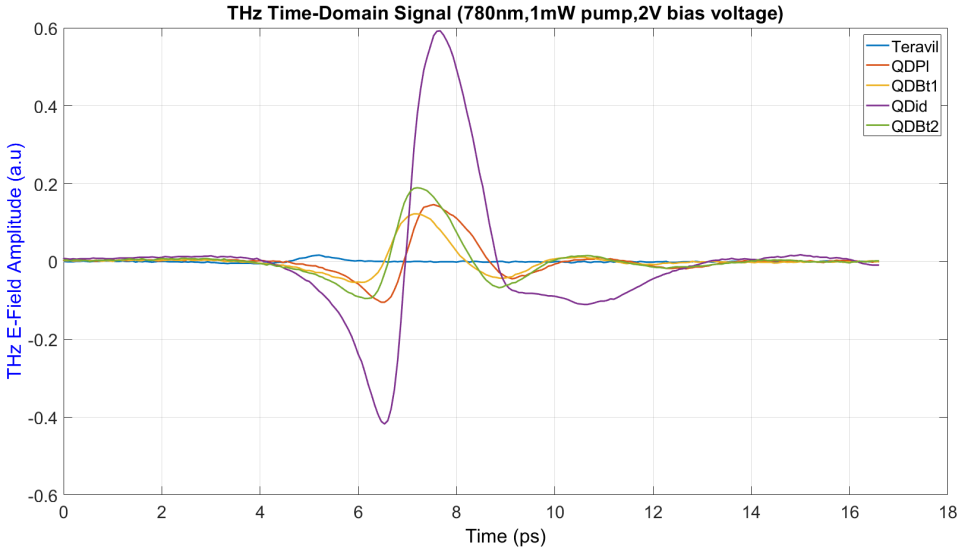

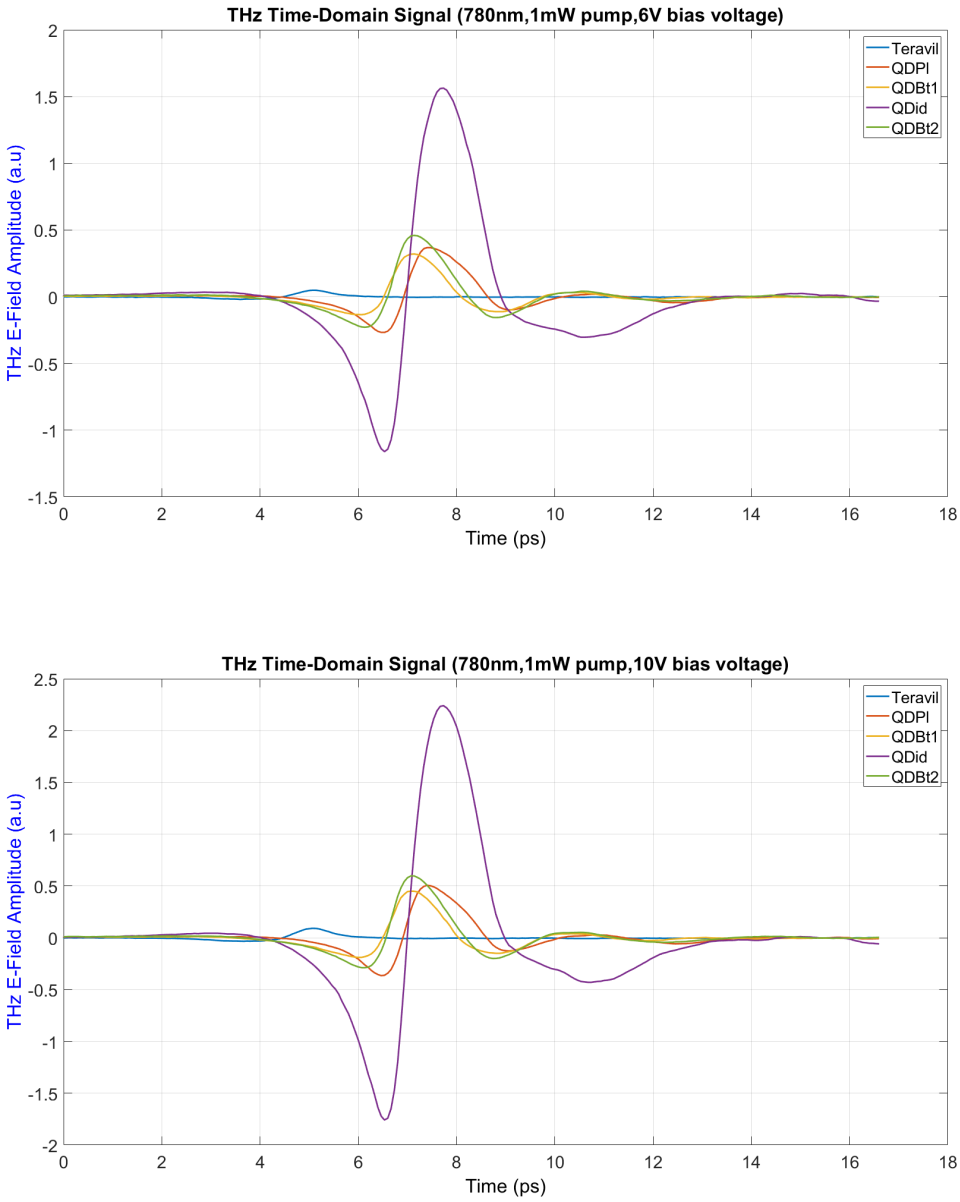

Figure 4.19: THz Time domain pulse at 1mW for 2v, 6V and 10V bias voltage

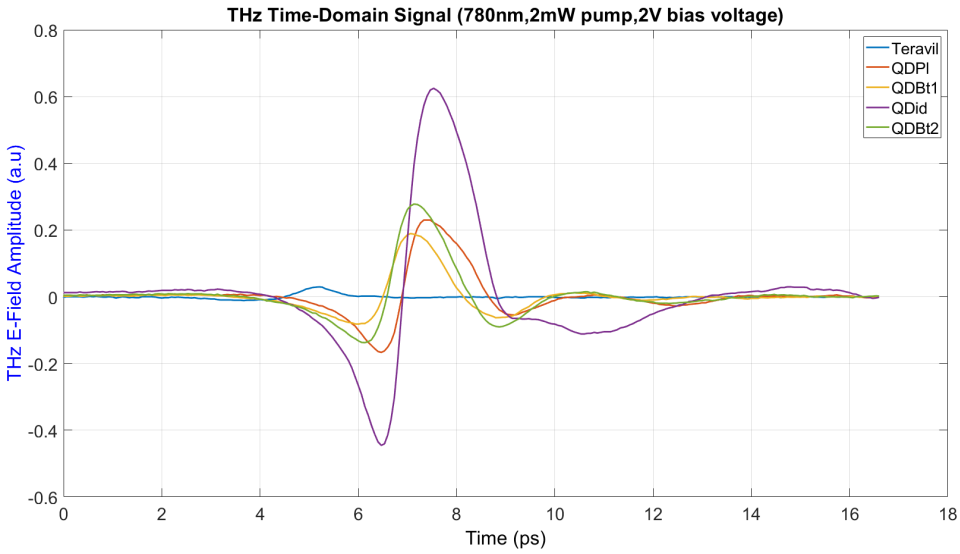
THz Time-Domain Signal (780nm,2mW pump,2V bias voltage)
THz E-Field Amplitude (a.u)
Time (ps)
Teravil
QDPI
QDBt1
QDid
QDBt2

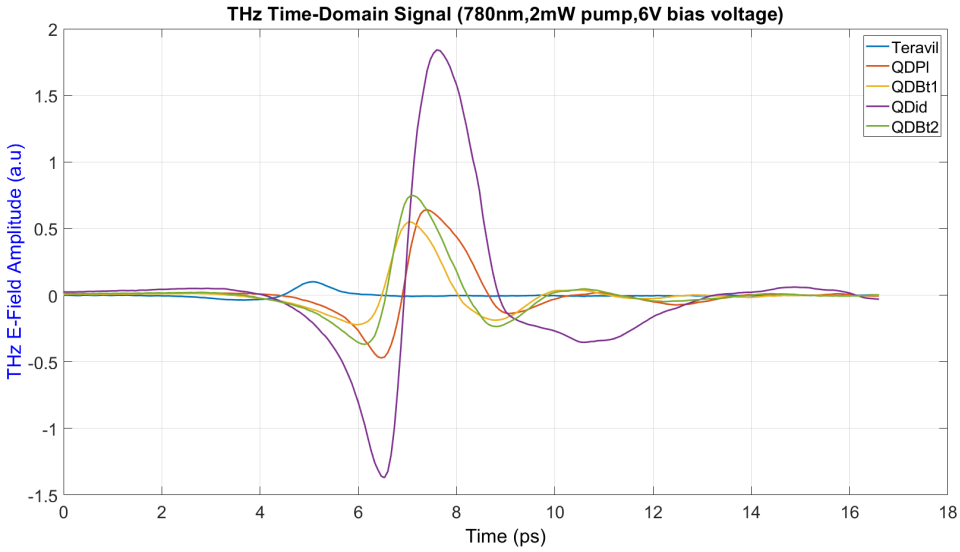
THz Time-Domain Signal (780nm,2mW pump,6V bias voltage)
THz E-Field Amplitude (a.u)
Time (ps)
Teravil
QDPI
QDBt1
QDid
QDBt2

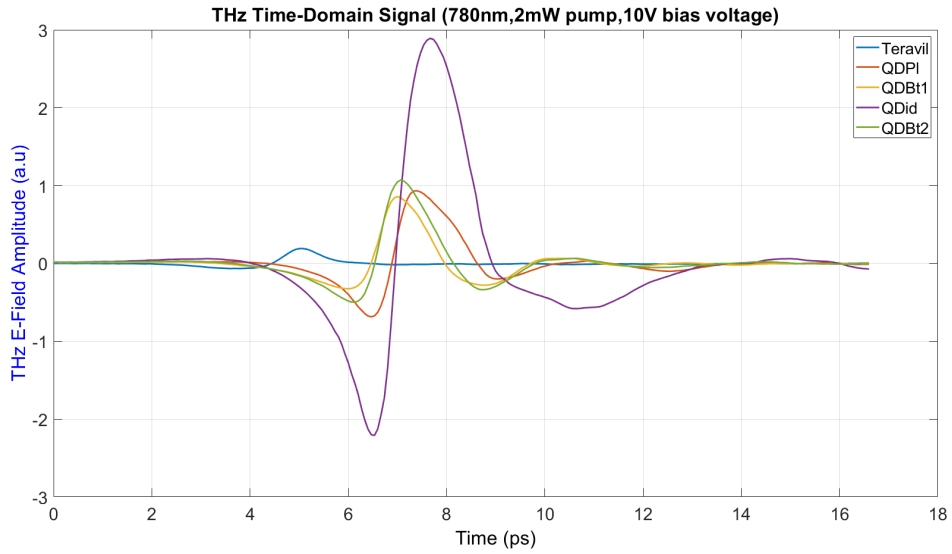

Figure 4.20: THz Time domain pulse at 2mW for 2v, 6V and 10V bias voltage

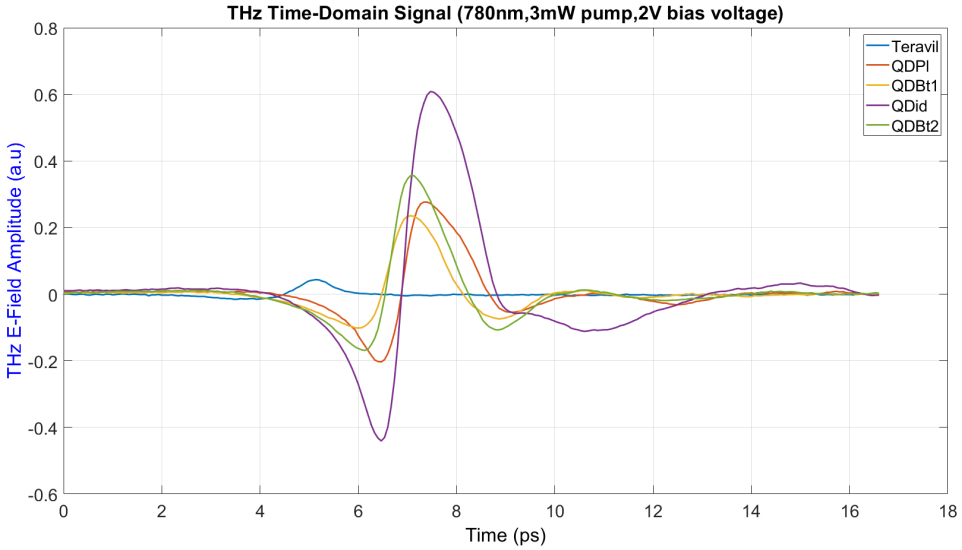

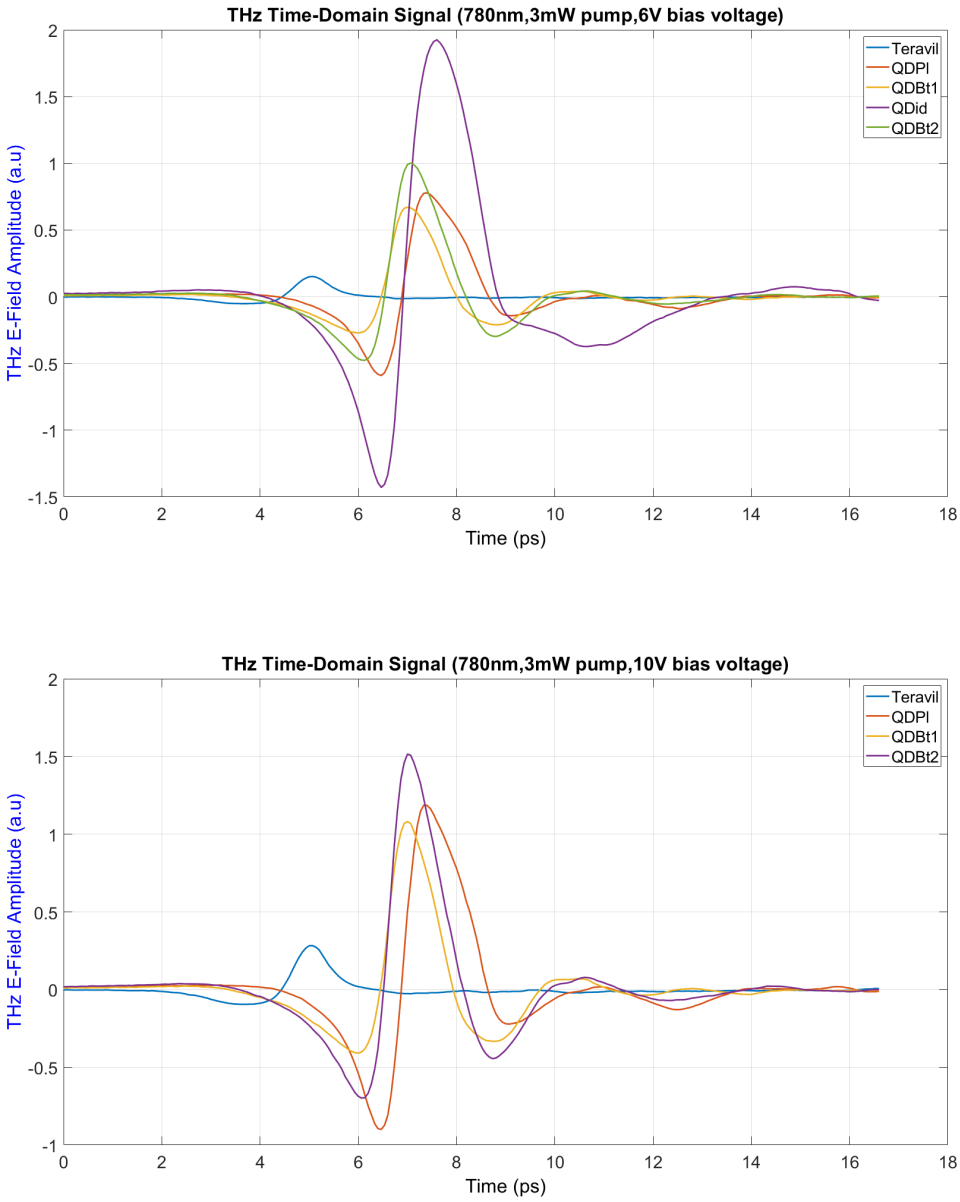

Figure 4.21: THz Time domain pulse at 3mW for 2v, 6V and 10V bias voltage

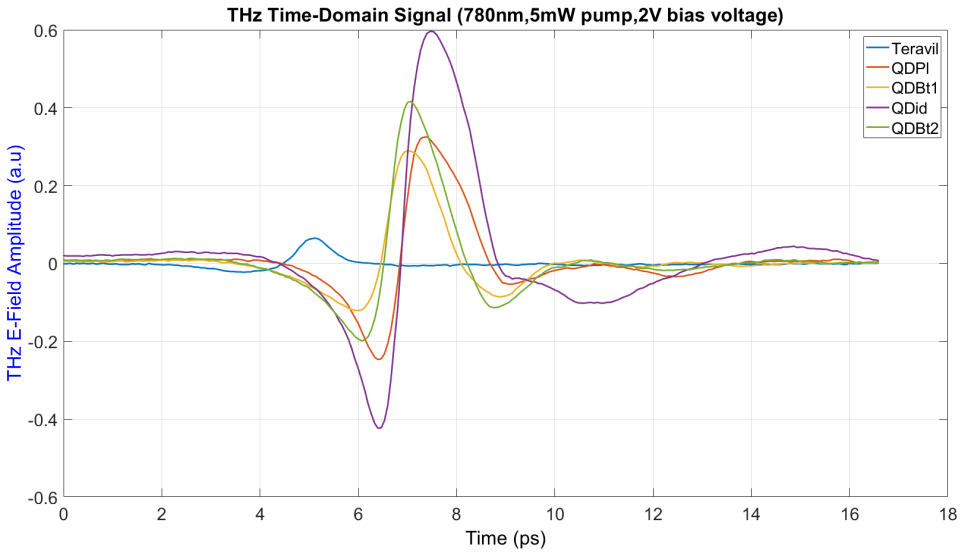
THz Time-Domain Signal (780nm,5mW pump,2V bias voltage)
THz E-Field Amplitude (a.u)
Time (ps)
Teravil
QDPI
QDBt1
QDid
QDBt2
0.6
0.4
0.2
0
-0.2
-0.4
-0.6
0
2
4
6
8
10
12
14
16
18

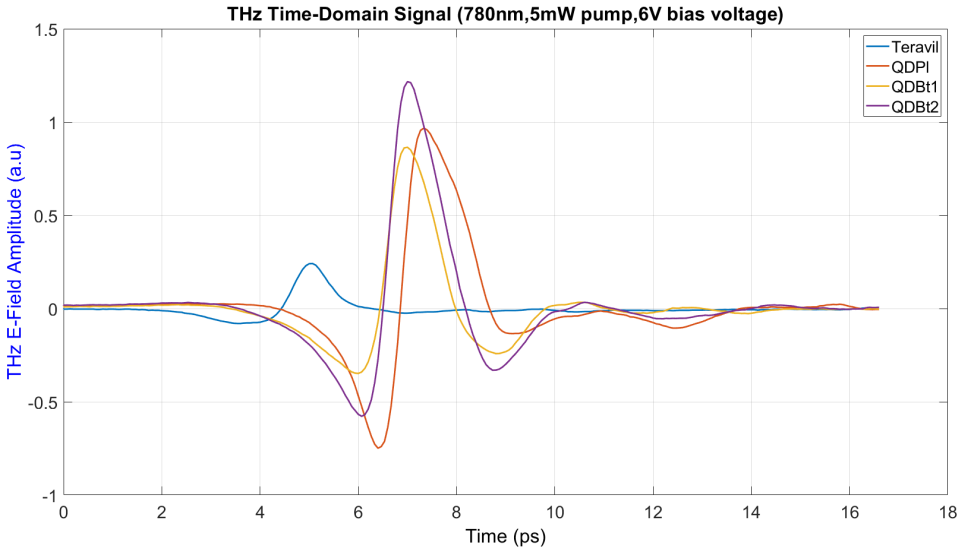
THz Time-Domain Signal (780nm,5mW pump,6V bias voltage)
THz E-Field Amplitude (a.u)
Time (ps)
Teravil
QDPI
QDBt1
QDBt2
1.5
1
0.5
0
-0.5
-1
0
2
4
6
8
10
12
14
16
18

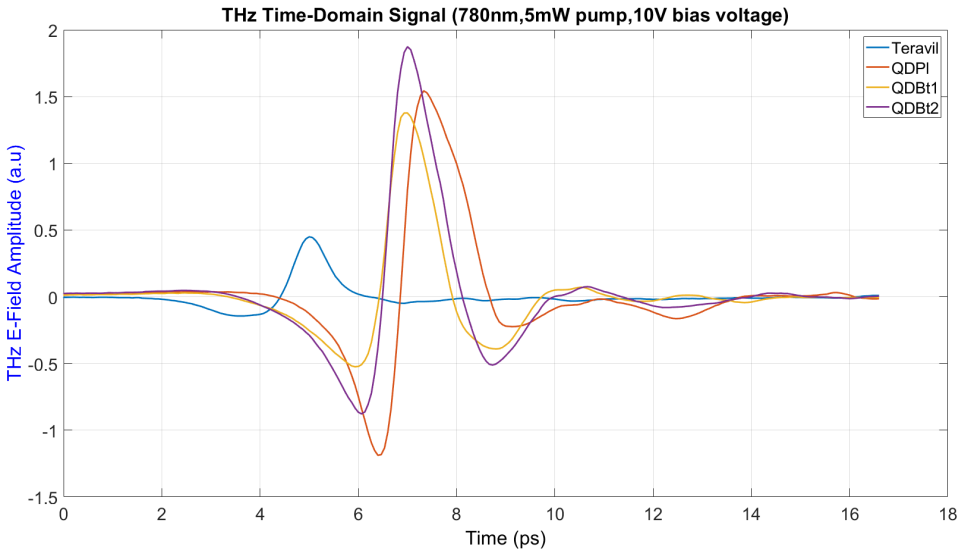

Figure 4.22: THz Time domain pulse at 5mW for 2v, 6V and 10V bias voltage

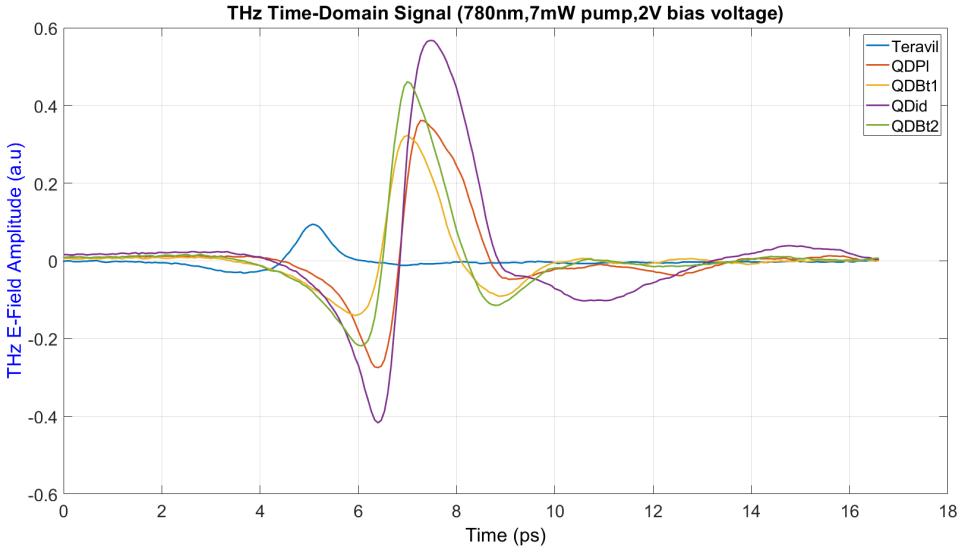

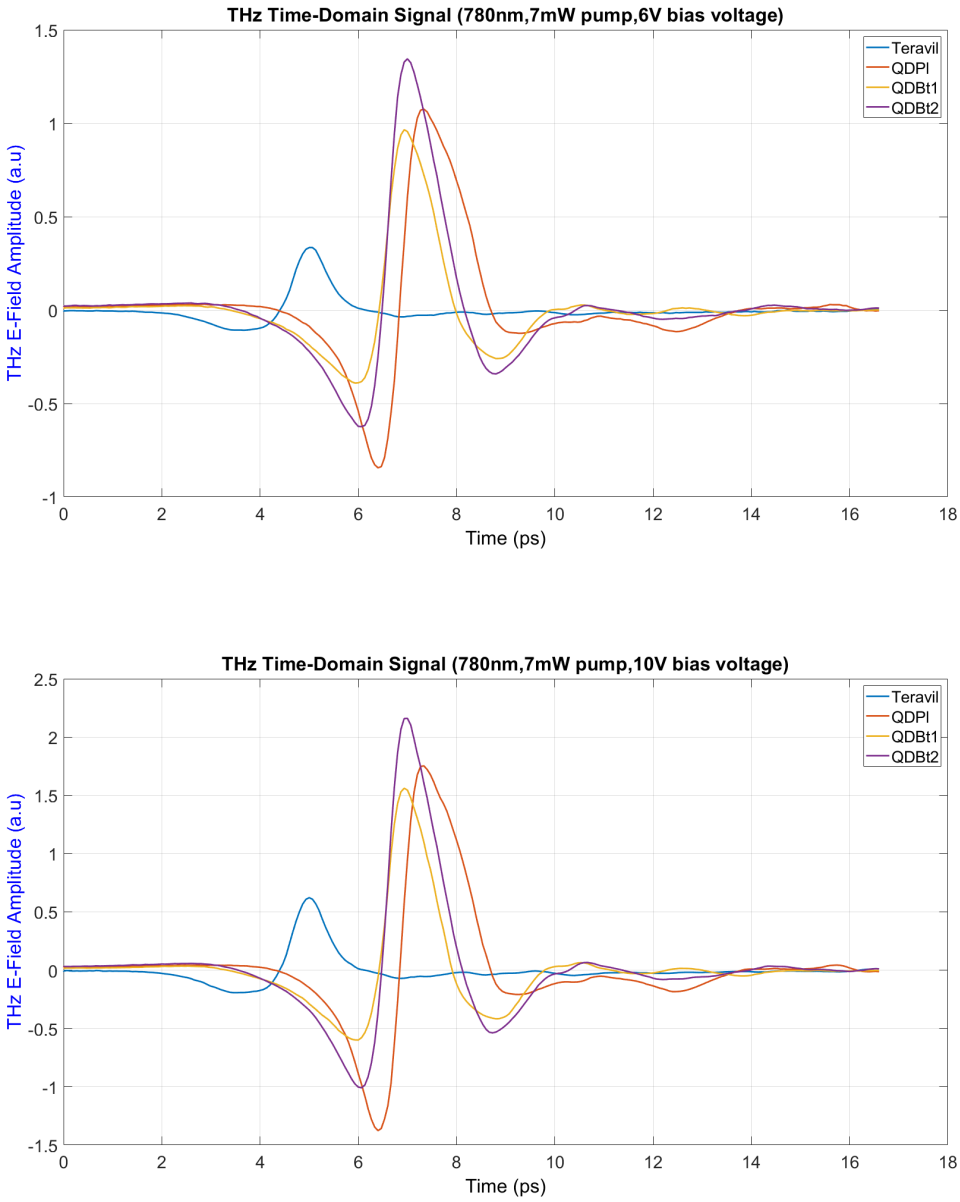

Figure 4.23: THz Time domain pulse at 7mW for 2v, 6V and 10V bias voltage

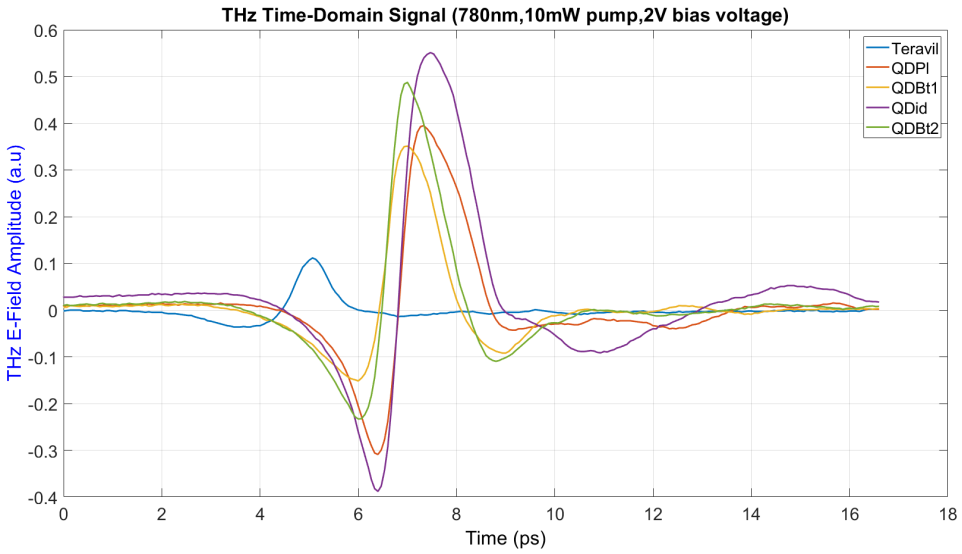
THz Time-Domain Signal (780nm,10mW pump,2V bias voltage)
THz E-Field Amplitude (a.u)
Time (ps)
Teravil
QDPl
QDBt1
QDid
QDBt2

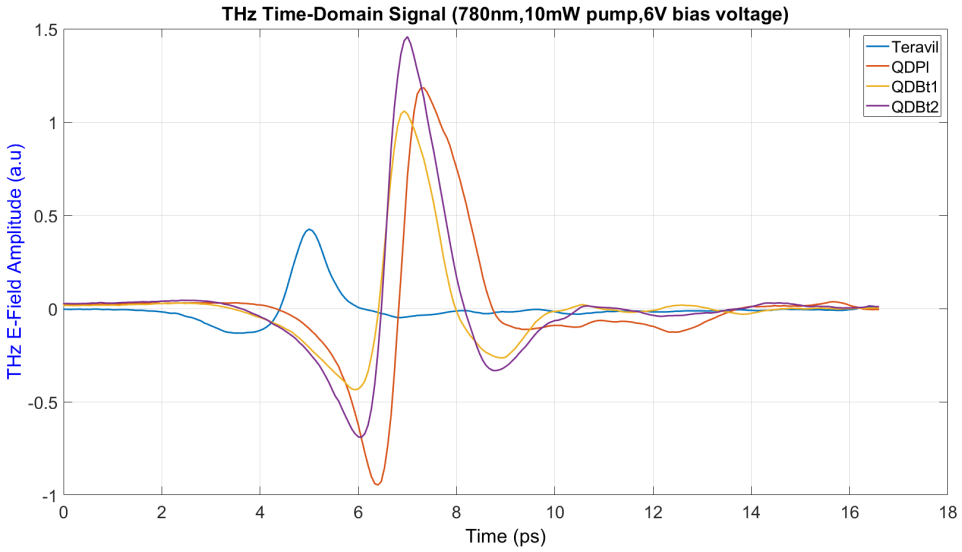
THz Time-Domain Signal (780nm,10mW pump,6V bias voltage)
THz E-Field Amplitude (a.u)
Time (ps)
Teravil
QDPl
QDBt1
QDBt2

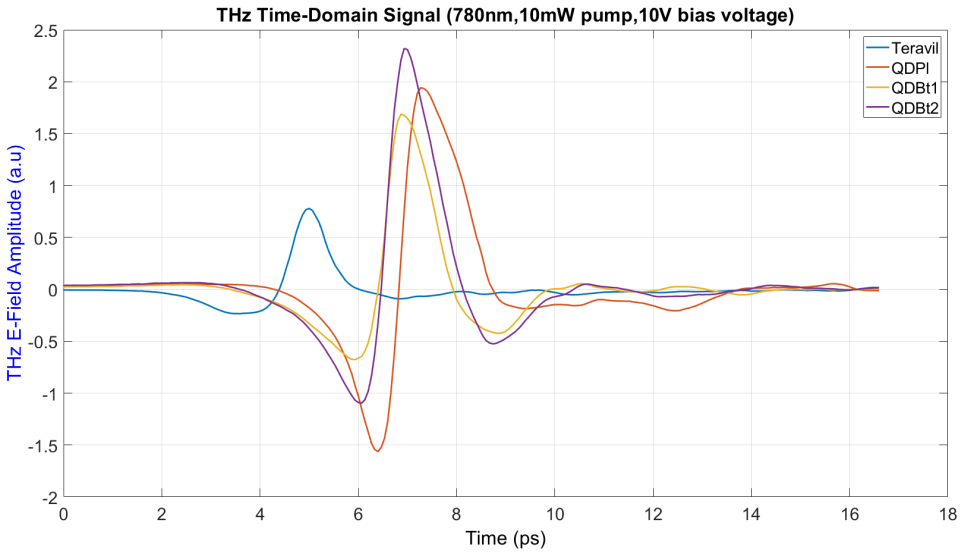

Figure 4.24: THz Time domain pulse at 10mW for 2v, 6V and 10V bias voltage

4.3.6 780nm Pulse results discussion

With similar experimental conditions, the same measurements were carried out at 780nm wavelength. The increase in THz E-field amplitude without affecting pulse shape in accordance to bias voltage increase at the same power level is similarly observed as reported for 800nm, also the same narrowing of pulse width with increase in pump powers was recorded. At the same pump power and bias voltage conditions the plasmonic QD_Pl antennas shows a wider pulse width than the non-plasmonic QD_Bt1 and QD_Bt2. The QD_Bt1 and QD_Bt2 shows a higher THz E-field amplitude at 780nm than at 800nm however the pulse width was slight narrower at 800nm. The adjustment of antenna position to maximise for the point of least resistance upon pump illumination results into slight spatial difference in antenna position which leads to temporal variation in the starting point of the THz pulse hence the reason for the THz pulses from the antennas not starting from the same point.

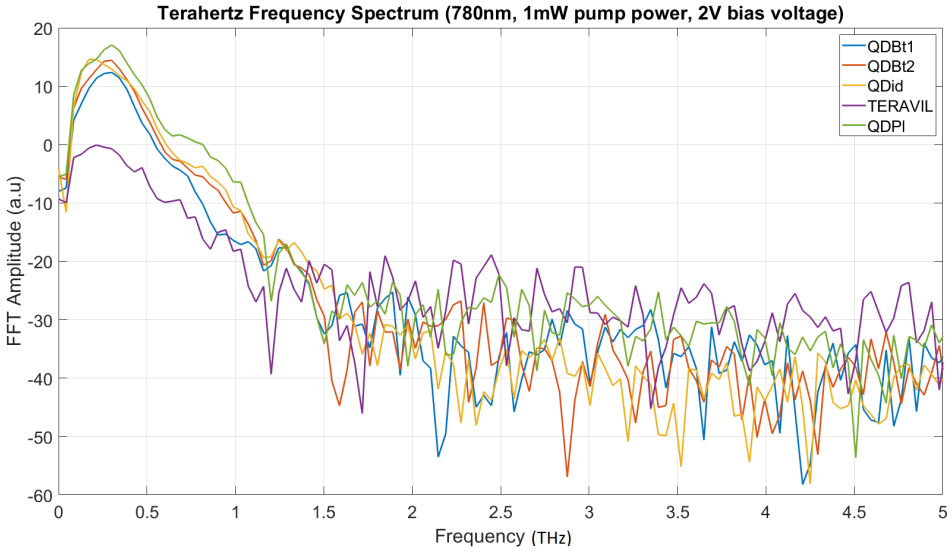
Terahertz Frequency Spectrum (780nm, 1mW pump power, 2V bias voltage)
QDBt1
QDBt2
QDid
TERAVIL
QDPI
FFT Amplitude (a.u)
Frequency (THz)
20
10
0
-10
-20
-30
-40
-50
-60
0
0.5
1
1.5
2
2.5
3
3.5
4
4.5
5

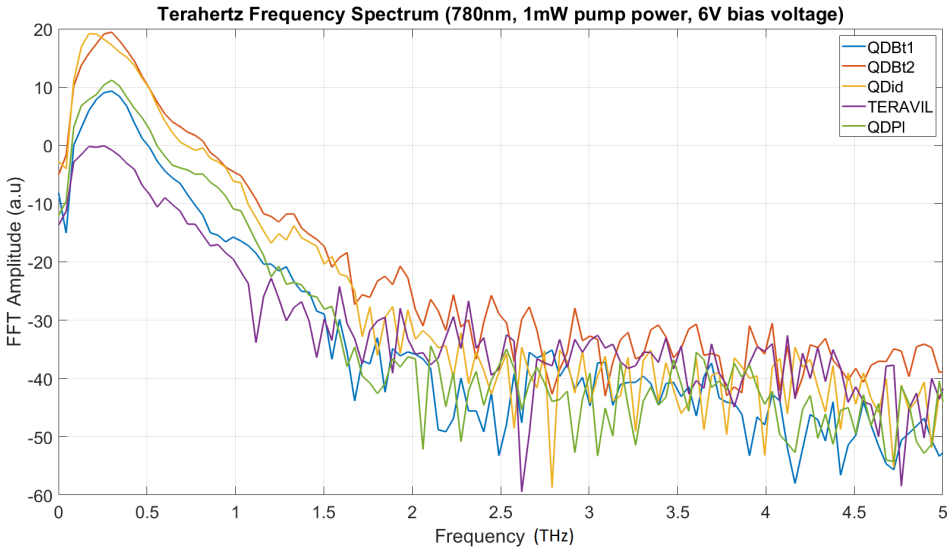
Terahertz Frequency Spectrum (780nm, 1mW pump power, 6V bias voltage)
QDBt1
QDBt2
QDid
TERAVIL
QDPI
FFT Amplitude (a.u)
Frequency (THz)
20
10
0
-10
-20
-30
-40
-50
-60
0
0.5
1
1.5
2
2.5
3
3.5
4
4.5
5

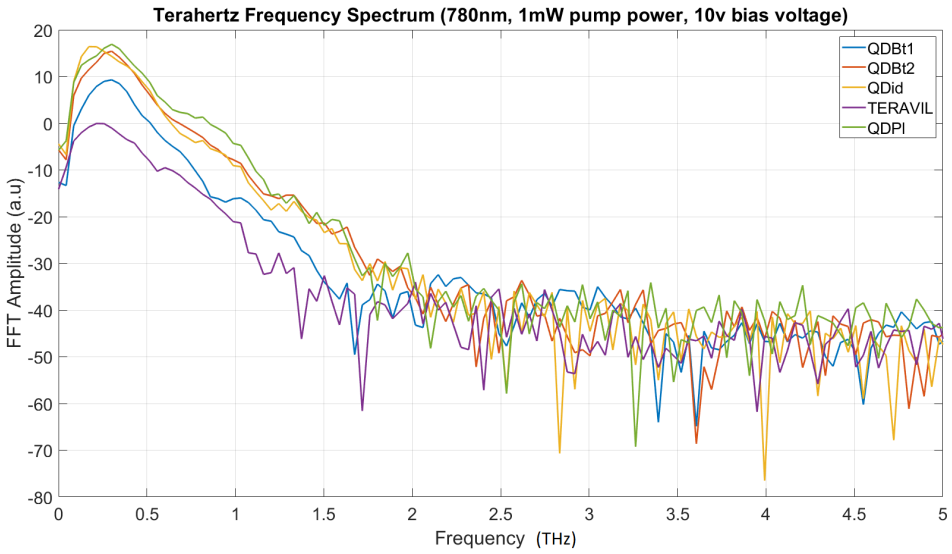

Figure 4.25: THz Frequency spectra of antennas at 1mW for 2v, 6V and 10V bias voltage

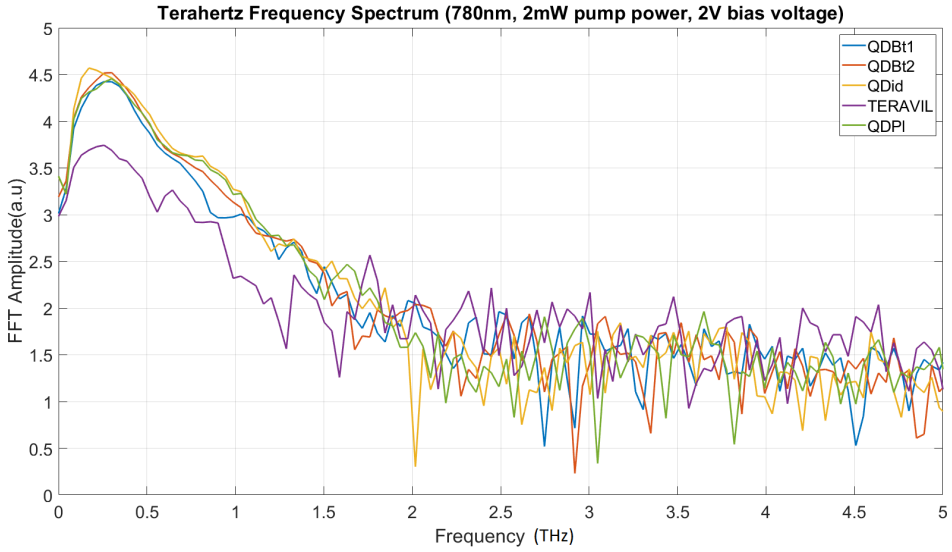

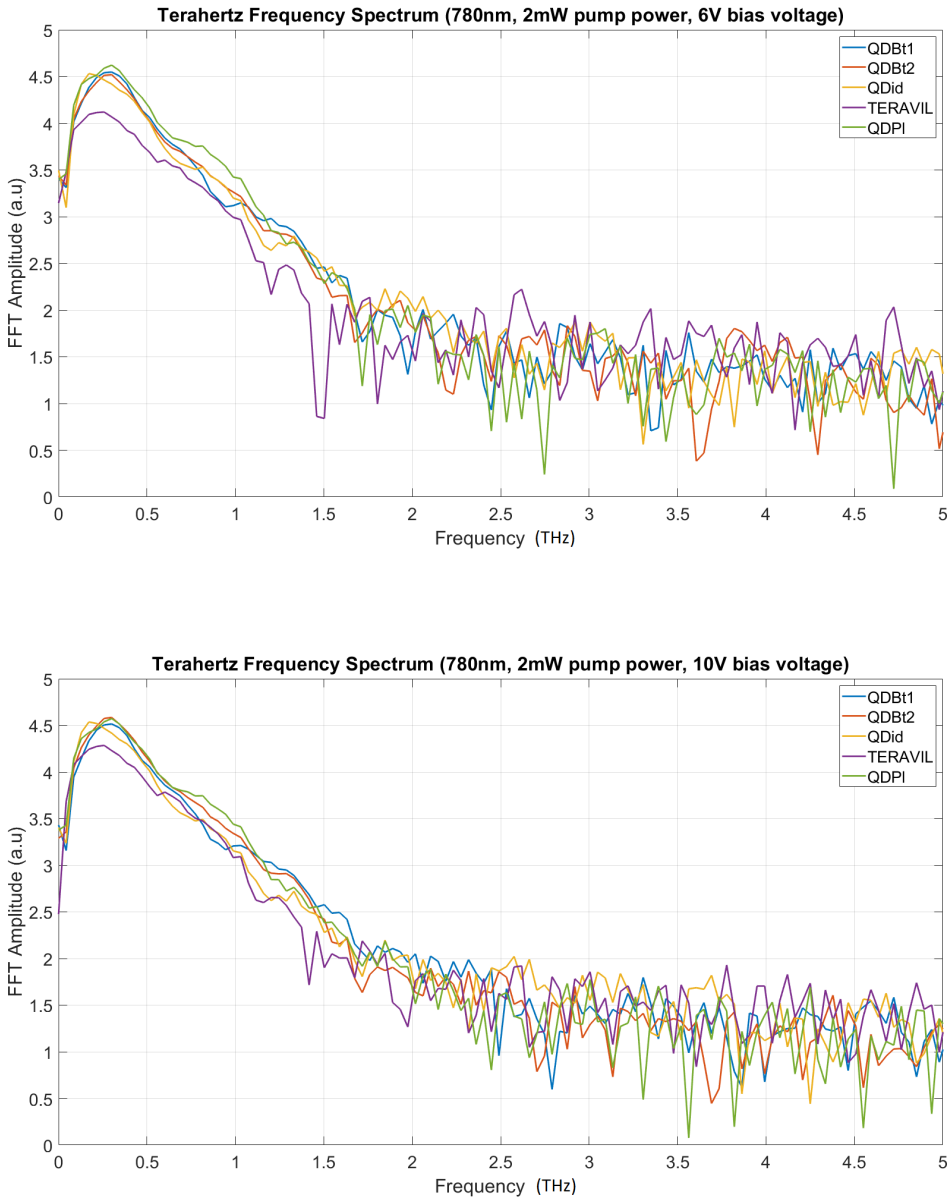

Figure 4.26: THz Frequency spectra of antennas at 2mW for 2v, 6V and 10V bias voltage

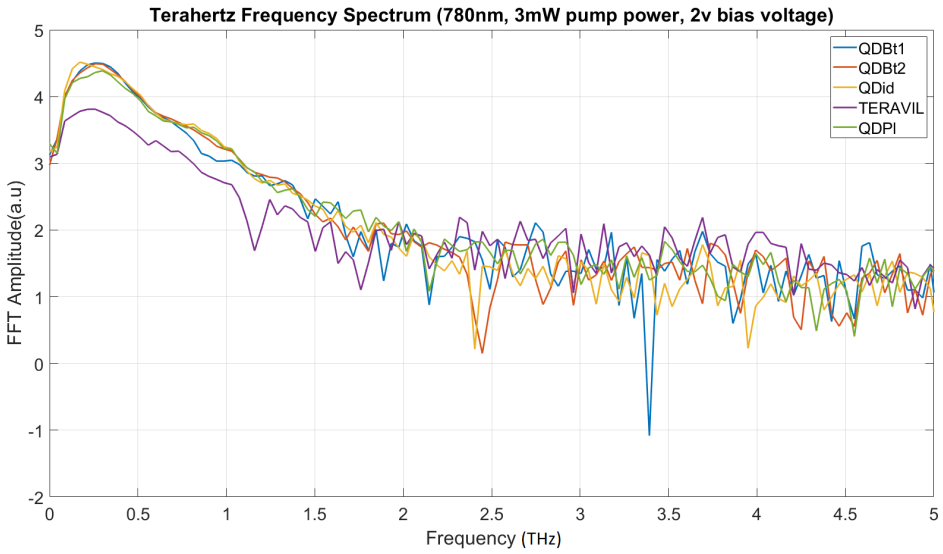
Terahertz Frequency Spectrum (780nm, 3mW pump power, 2v bias voltage)
QDBt1
QDBt2
QDid
TERAVIL
QDPI
FFT Amplitude(a.u)
Frequency (THz)

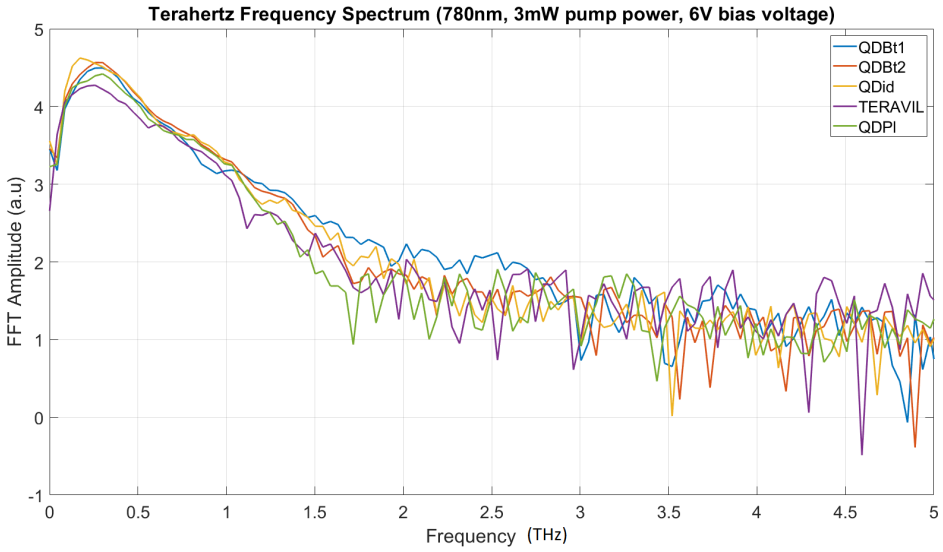
Terahertz Frequency Spectrum (780nm, 3mW pump power, 6V bias voltage)
QDBt1
QDBt2
QDid
TERAVIL
QDPI
FFT Amplitude (a.u)
Frequency (THz)

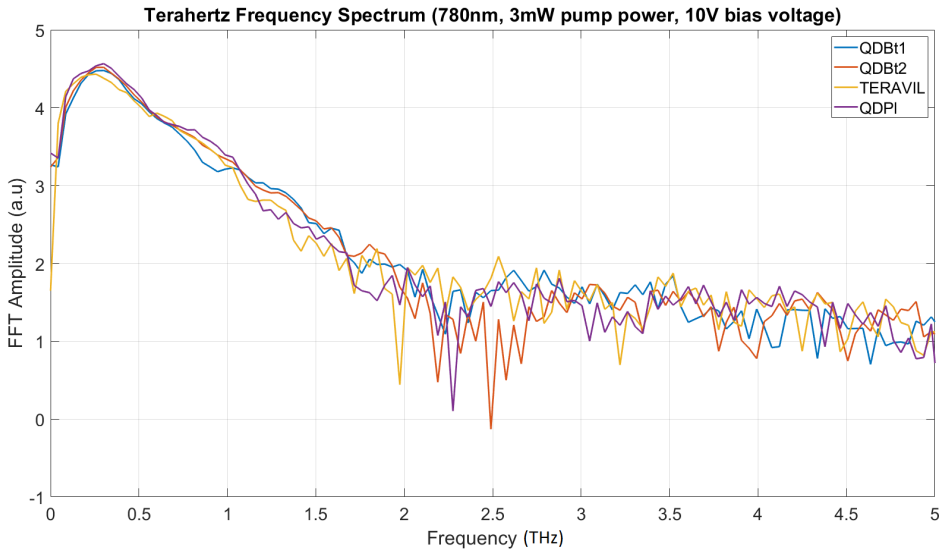

Figure 4.27: THz Frequency spectra of antennas at 3mW for 2v, 6V and 10V bias voltage

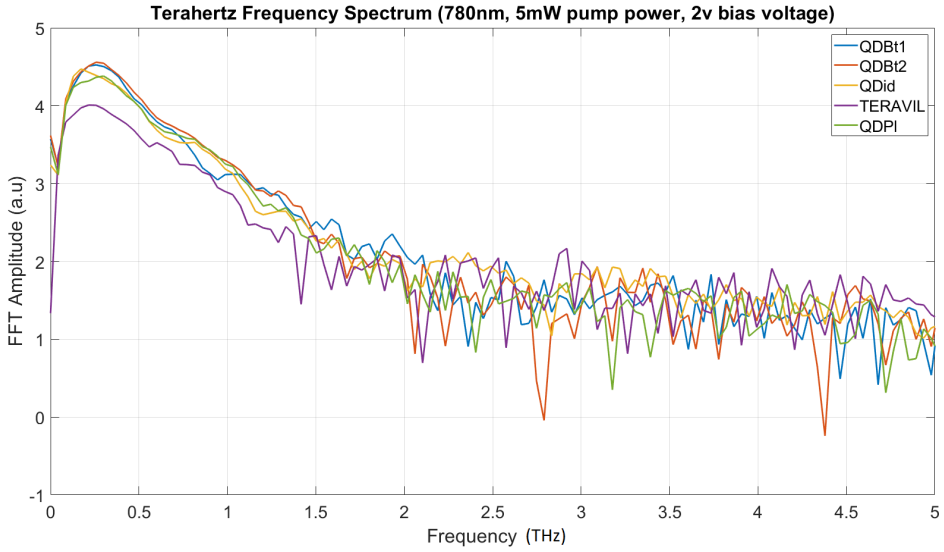

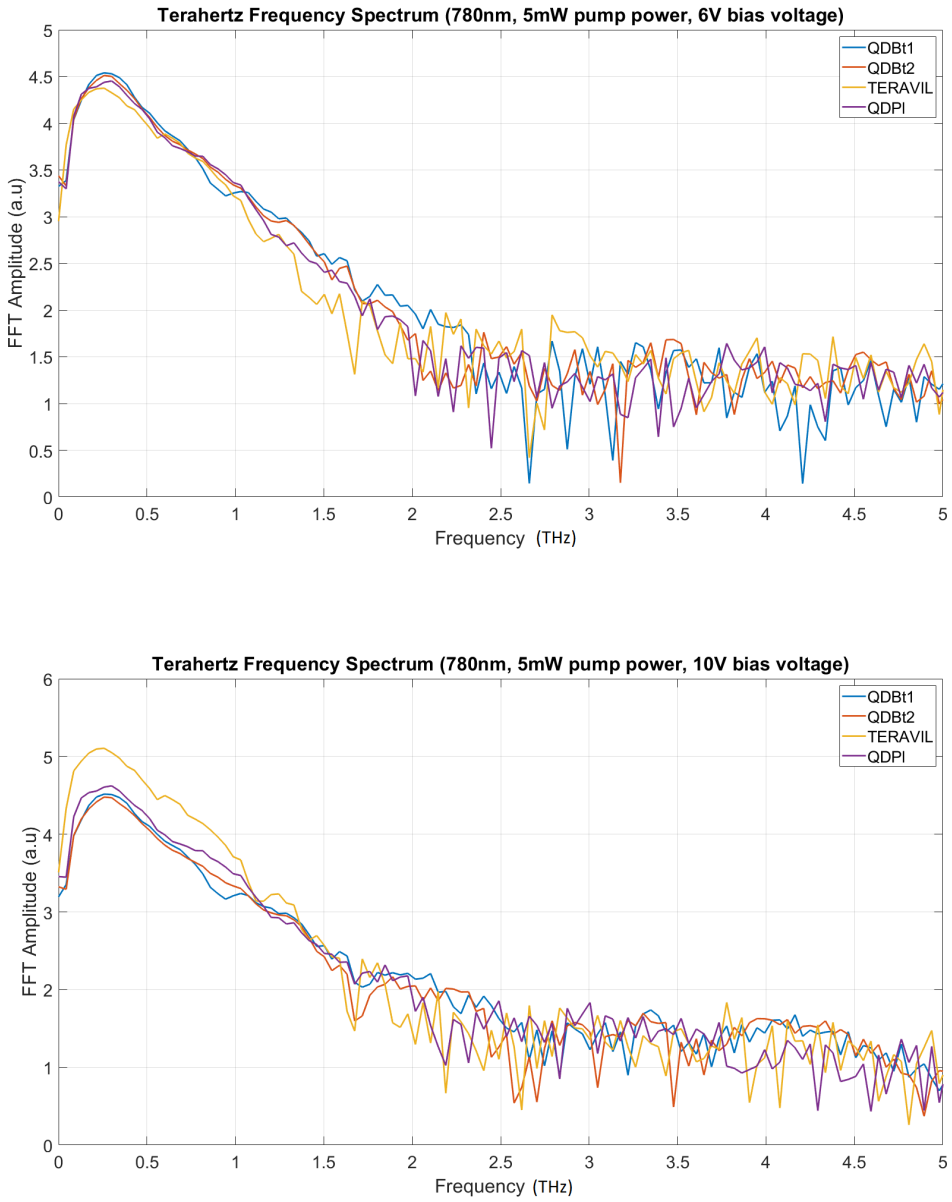

Figure 4.28: THz Frequency spectra of antennas at 5mW for 2v, 6V and 10V bias voltage

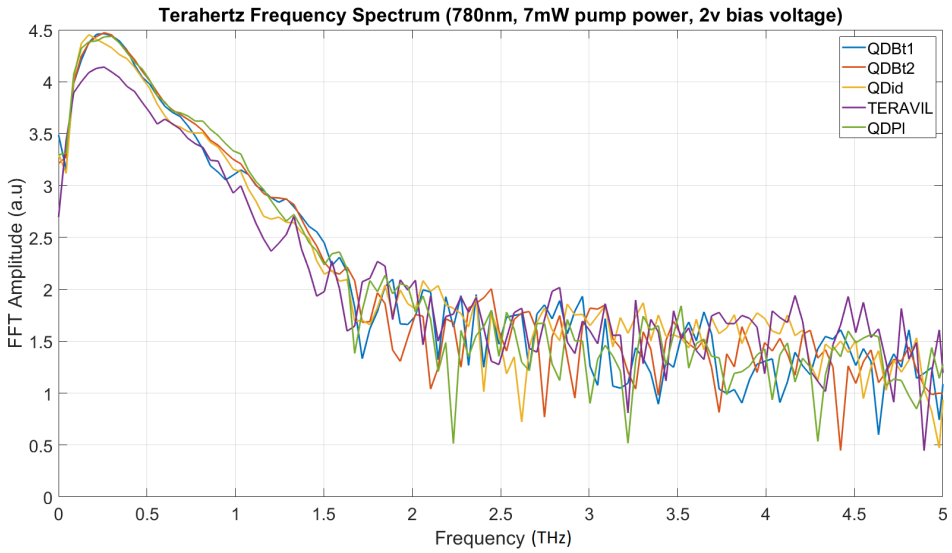
Terahertz Frequency Spectrum (780nm, 7mW pump power, 2v bias voltage)
QDBt1
QDBt2
QDid
TERAVIL
QDPI
FFT Amplitude (a.u)
Frequency (THz)
0
0.5
1
1.5
2
2.5
3
3.5
4
4.5
5

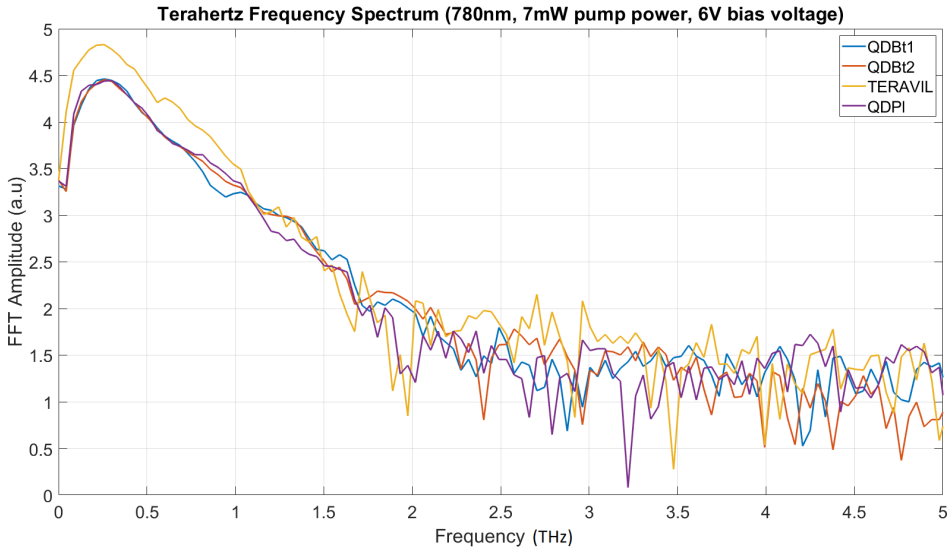
Terahertz Frequency Spectrum (780nm, 7mW pump power, 6V bias voltage)
QDBt1
QDBt2
TERAVIL
QDPI
FFT Amplitude (a.u)
Frequency (THz)
0
0.5
1
1.5
2
2.5
3
3.5
4
4.5
5

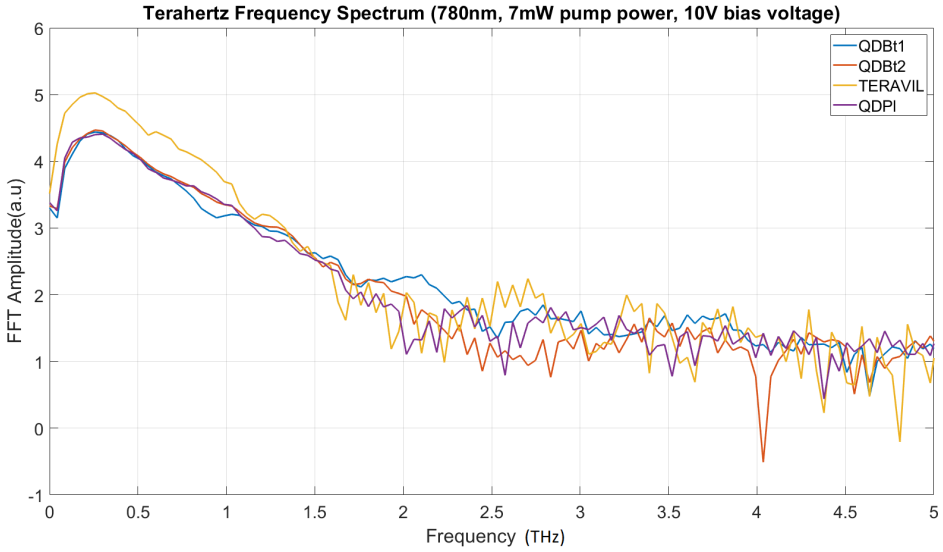

Figure 4.29: THz Frequency spectra of antennas at 7mW for 2v, 6V and 10V bias voltage

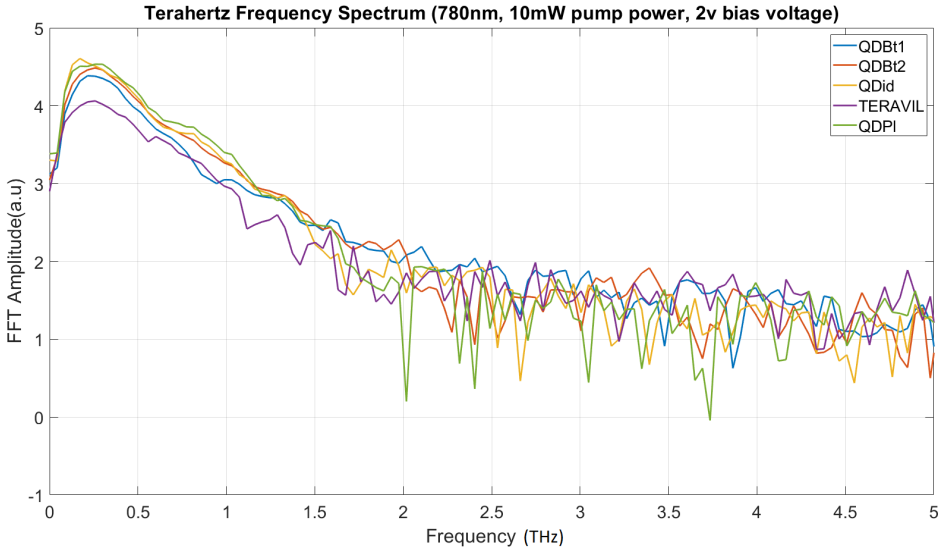

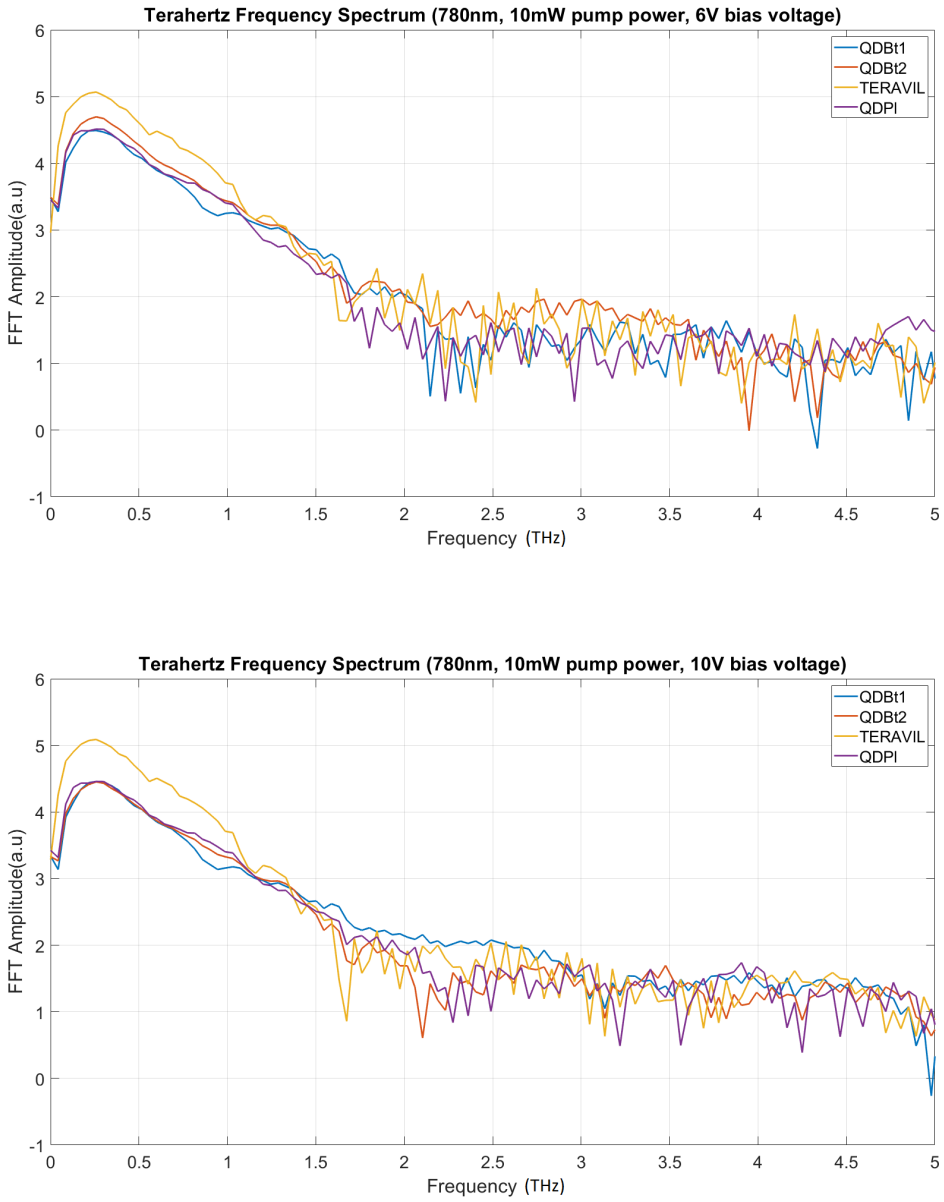

Figure 4.30: THz Frequency spectra of antennas at 10mW for 2v, 6V and 10V bias voltage

4.3.7 Discussion of Frequency domain properties at 780nm pump wavelength

To extract the frequency domain properties of the THz from the antennas, a fast fourier transform of the time domain pulses was carried out as shown in the results from Figures 4.19-4.24 presented above for 780nm, The Quantum dot antennas show higher normalised fft amplitudes and bandwidth than the teravil antenna

The SNR of the antennas at 780nm, 10mW pump power and 2V bias voltages was calculated from the top plot in fig 4.24 to be 49dB, 45 dB, 49 dB, 43 dB and 30dB with a frequency bandwidth of 1.89THz, 1.61THz, 2.2THz, 2.1THz,1.38THz for the QD_Pl, QD_id, QD_bt2, QD_bt1, and teravil antennas respectively. The frequency bandwidth can be seen to increase with increase in the optical pump power relative to the narrowing of the pulsewidth that was observed in the time domain.

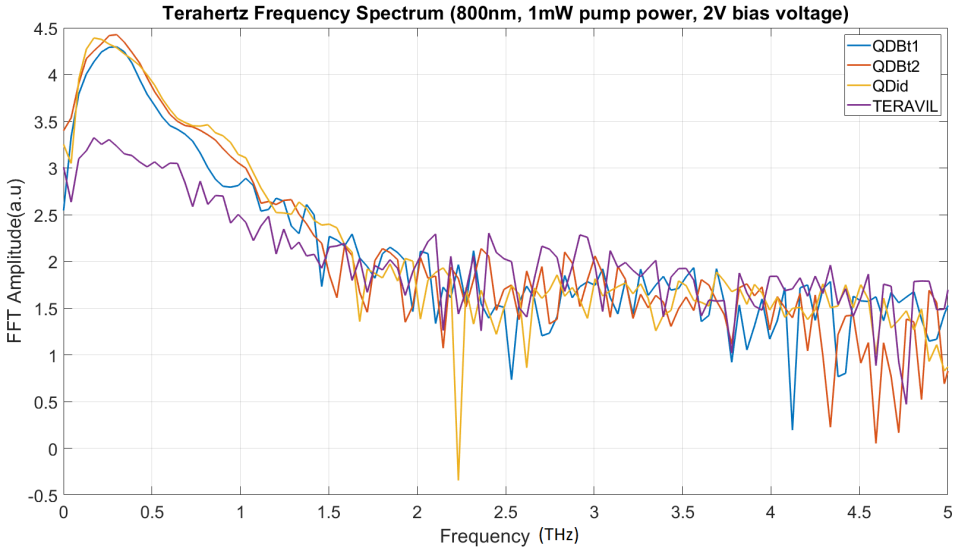

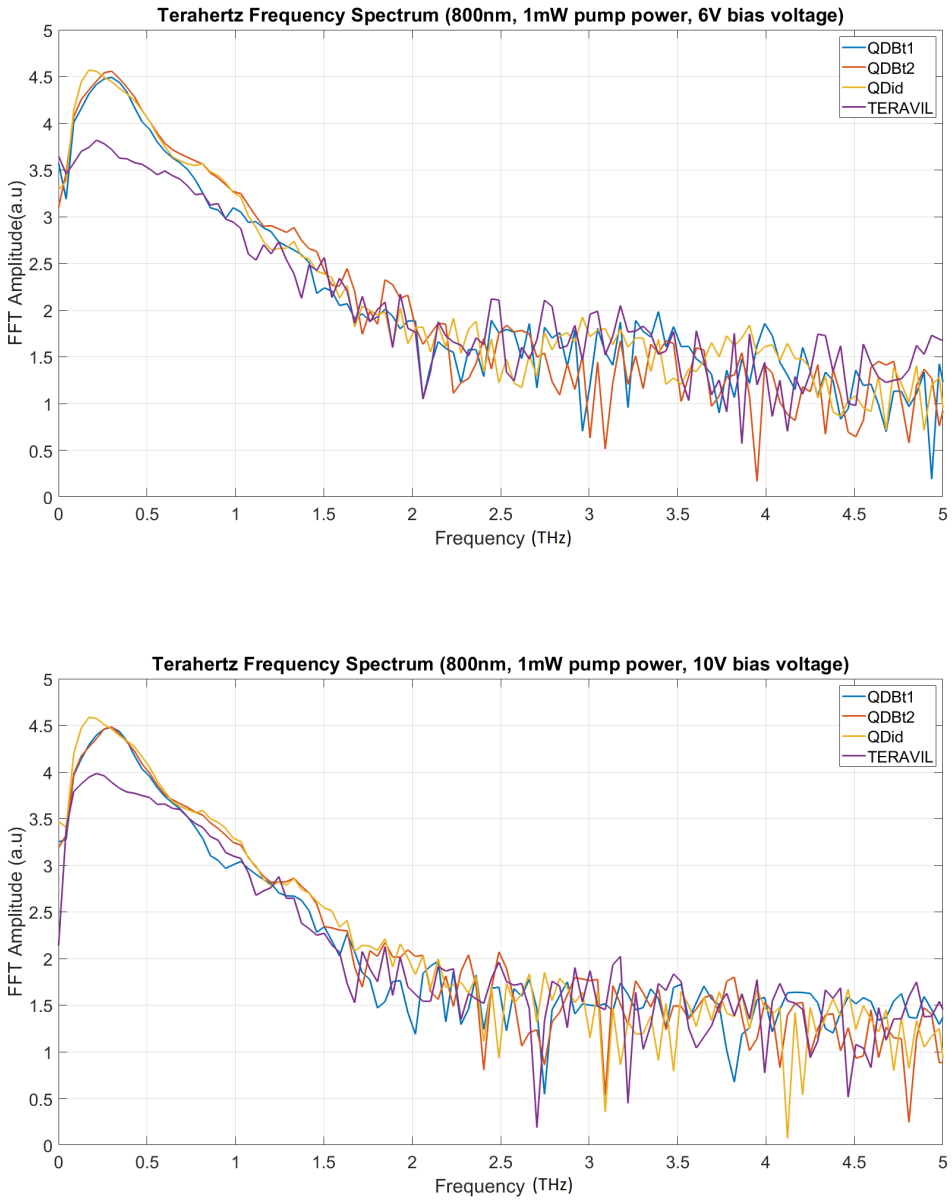

Figure 4.31: THz Frequency spectra of antennas at 1mW for 2v, 6V and 10V bias voltage

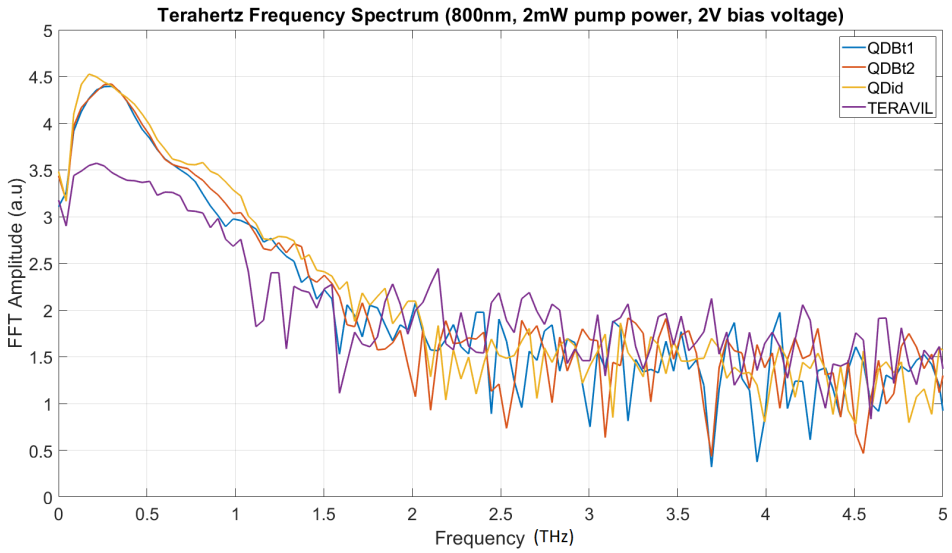
Terahertz Frequency Spectrum (800nm, 2mW pump power, 2V bias voltage)
QDBt1
QDBt2
QDid
TERAVIL
FFT Amplitude (a.u)
Frequency (THz)
0
0.5
1
1.5
2
2.5
3
3.5
4
4.5
5

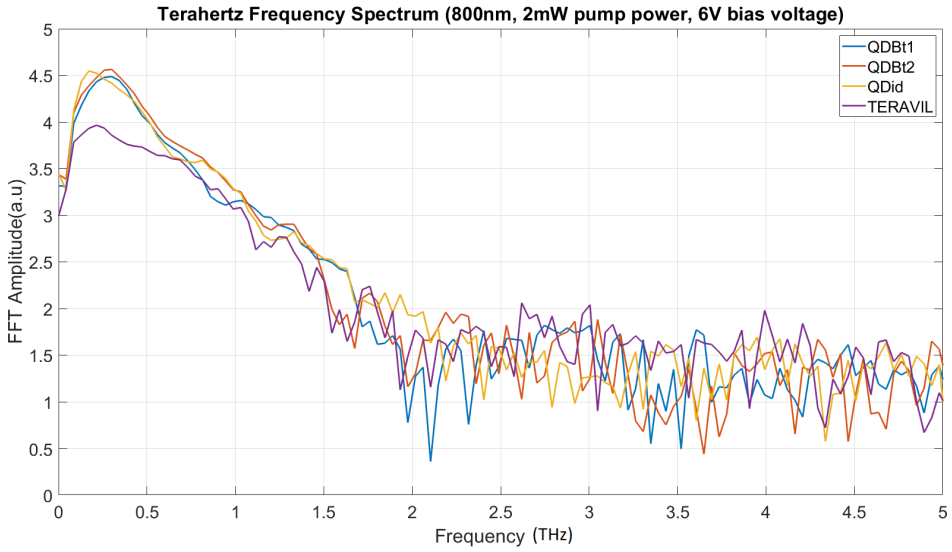
Terahertz Frequency Spectrum (800nm, 2mW pump power, 6V bias voltage)
QDBt1
QDBt2
QDid
TERAVIL
FFT Amplitude(a.u)
Frequency (THz)
0
0.5
1
1.5
2
2.5
3
3.5
4
4.5
5

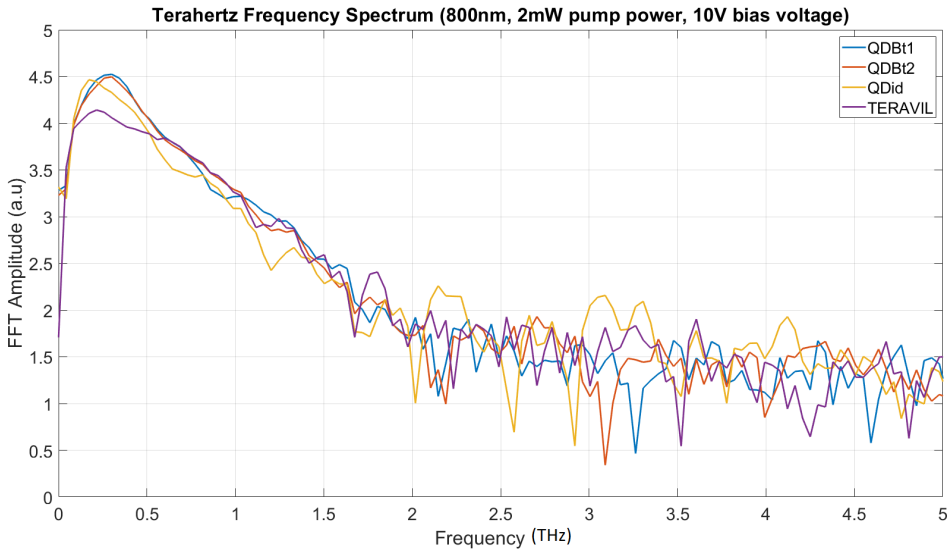

Figure 4.32: THz Frequency spectra of antennas at 2mW for 2v, 6V and 10V bias voltage

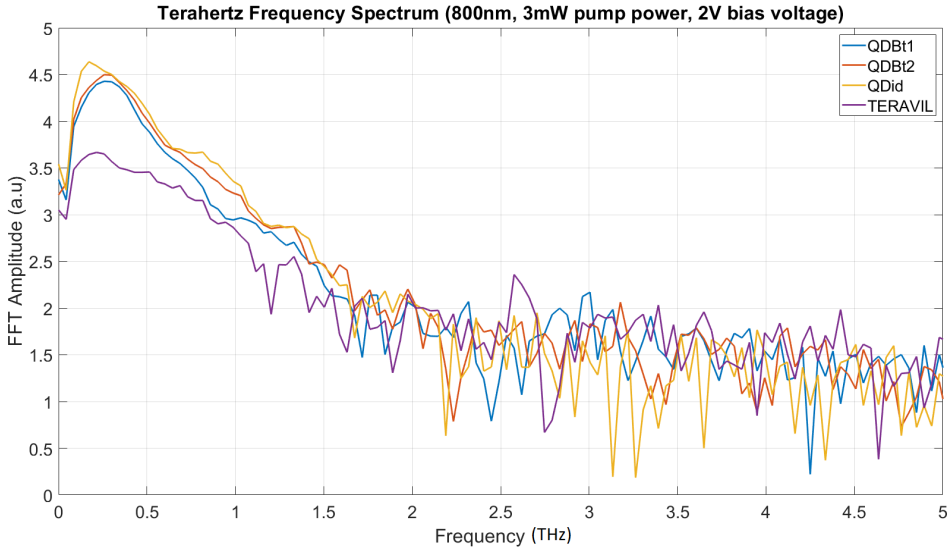

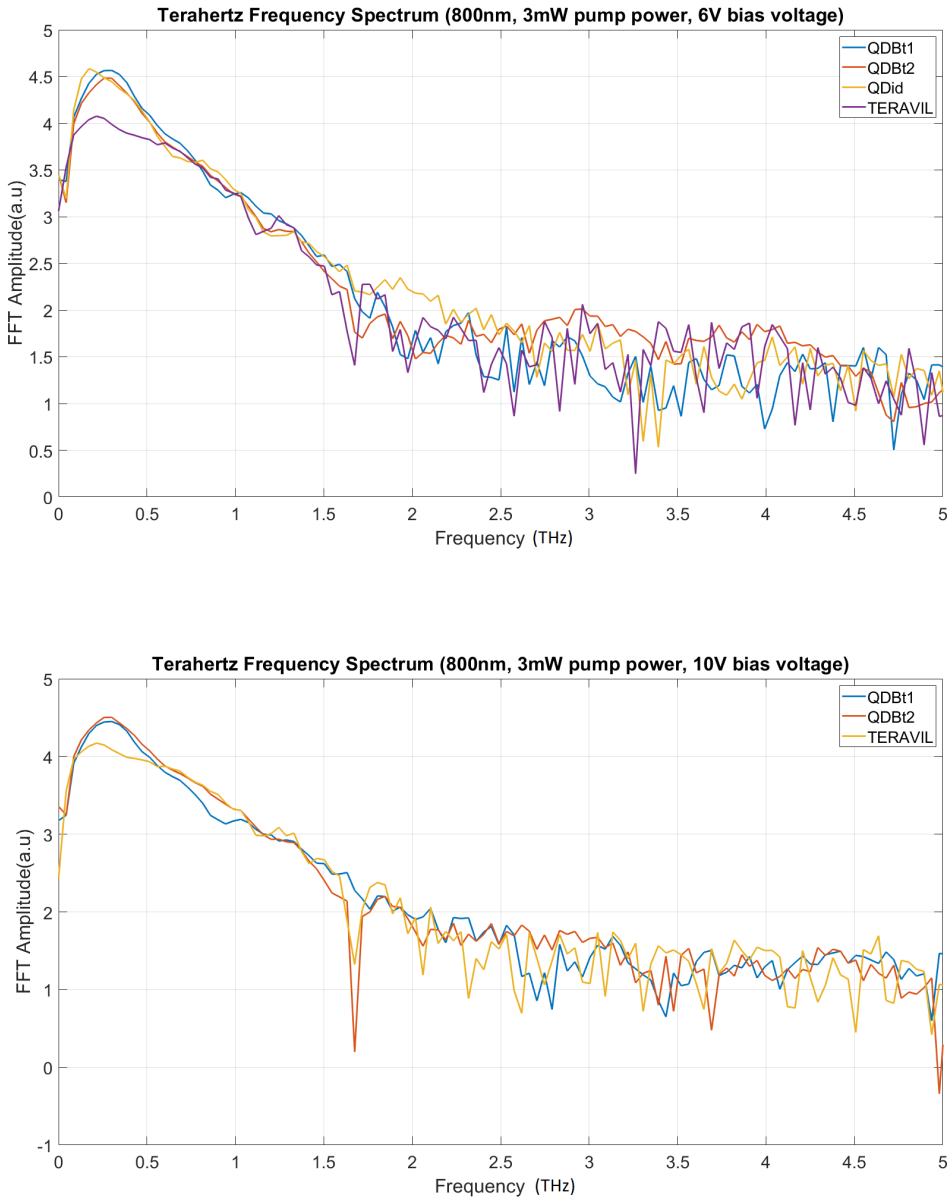

Figure 4.33: THz Frequency spectra of antennas at 3mW for 2v, 6V and 10V bias voltage

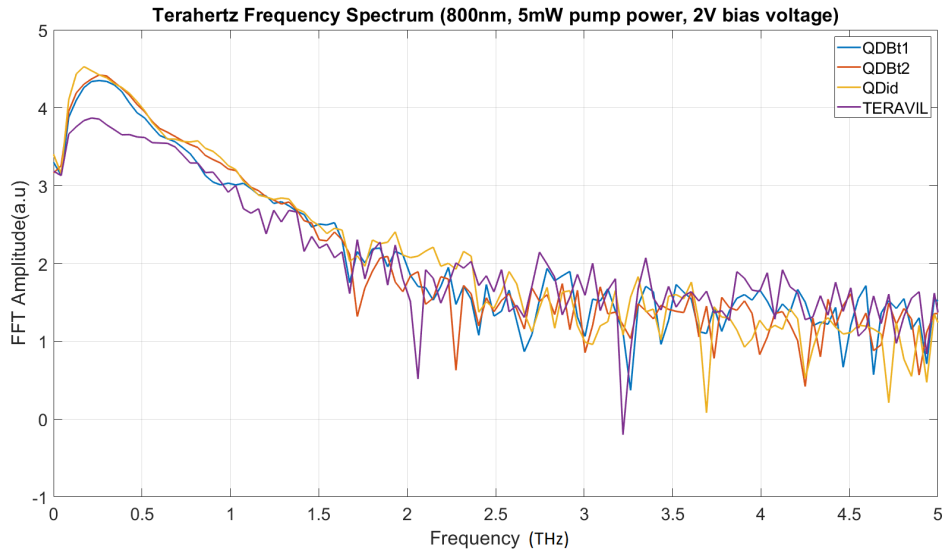
Terahertz Frequency Spectrum (800nm, 5mW pump power, 2V bias voltage)
QDBt1
QDBt2
QDid
TERAVIL
FFT Amplitude(a.u)
Frequency (THz)

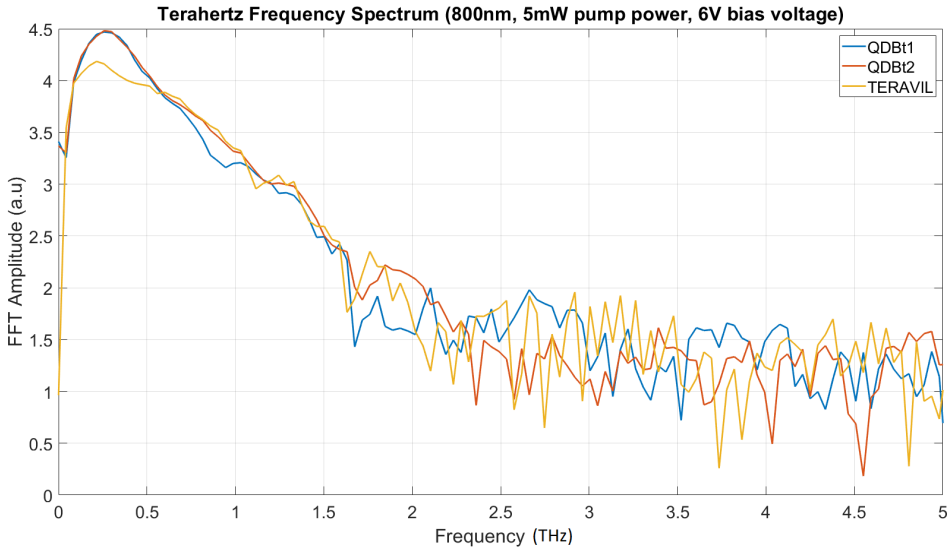
Terahertz Frequency Spectrum (800nm, 5mW pump power, 6V bias voltage)
QDBt1
QDBt2
TERAVIL
FFT Amplitude (a.u)
Frequency (THz)

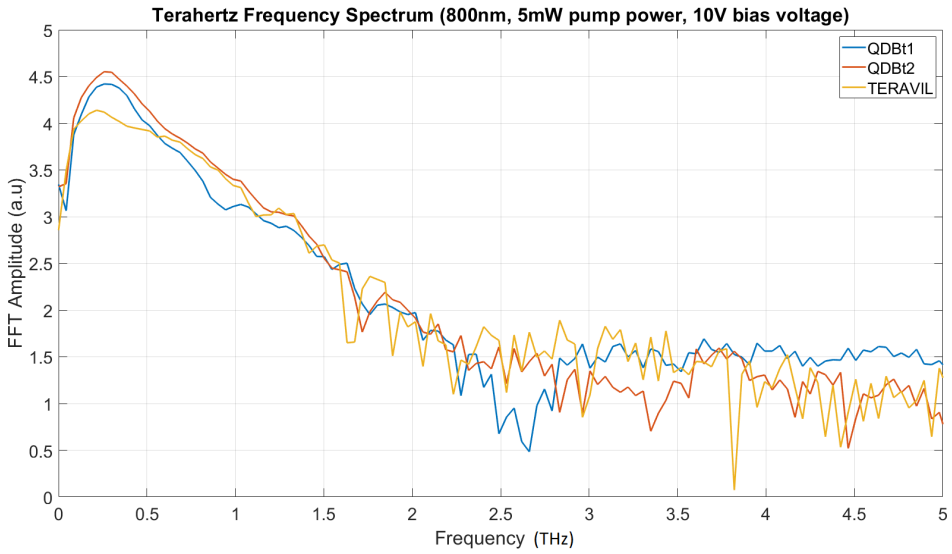

Figure 4.34: THz Frequency spectra of antennas at 5mW for 2v, 6V and 10V bias voltage

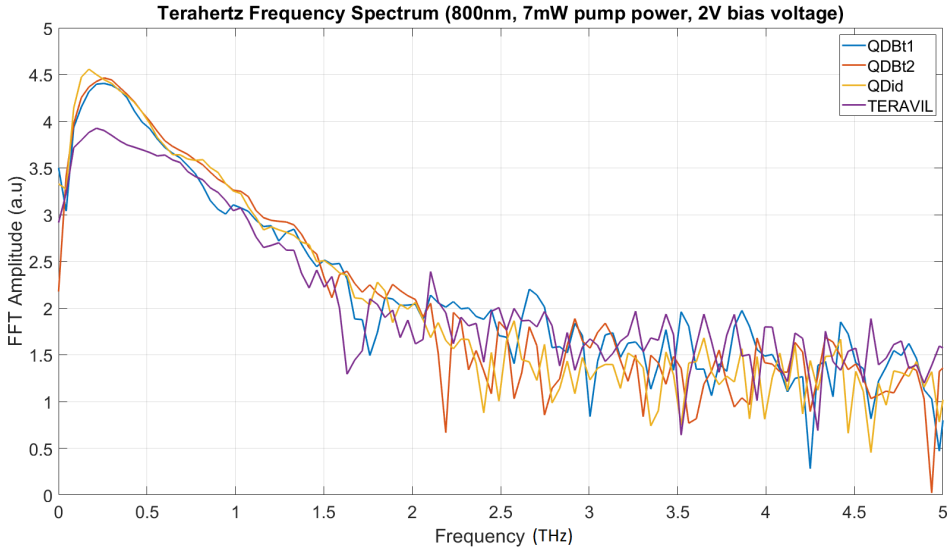

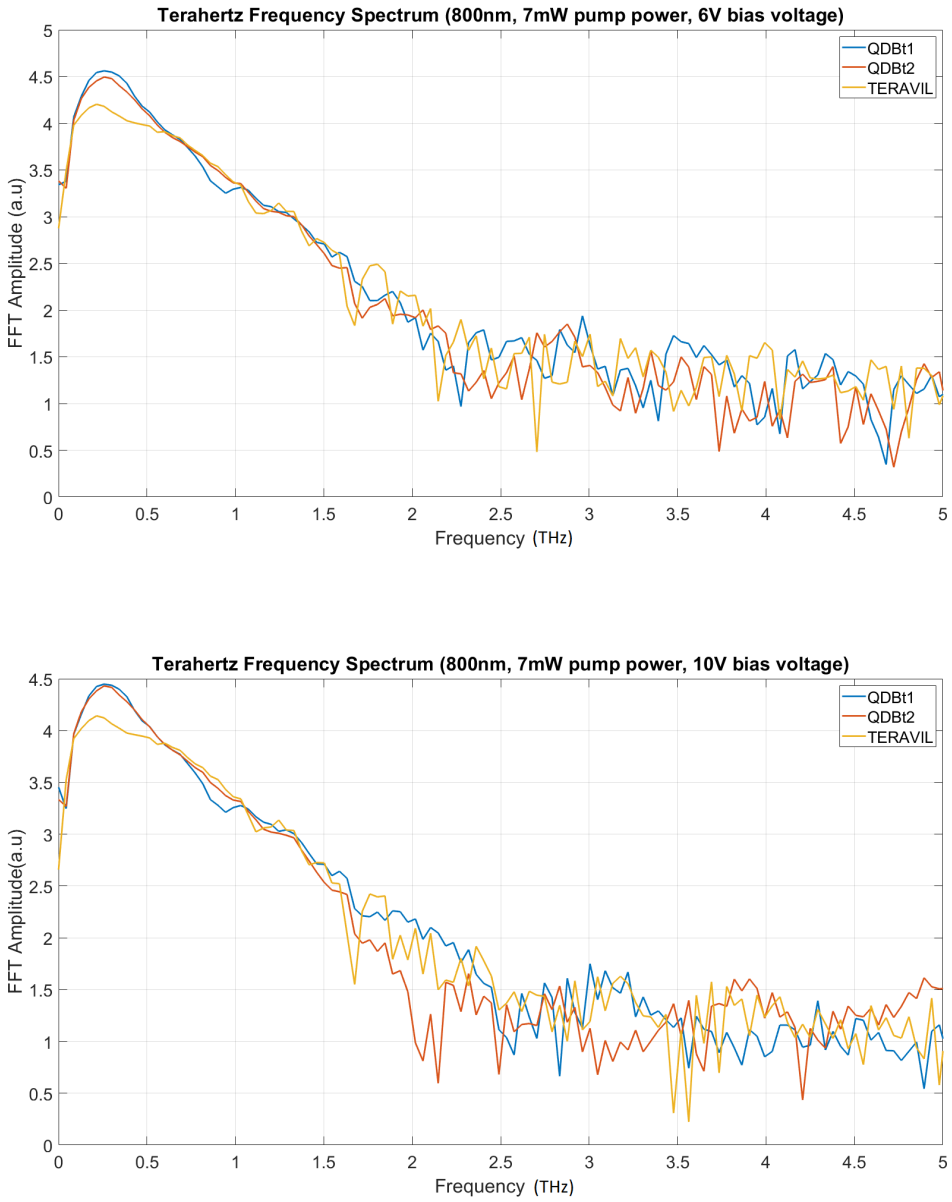

Figure 4.35: THz Frequency spectra of antennas at 7mW for 2v, 6V and 10V bias voltage

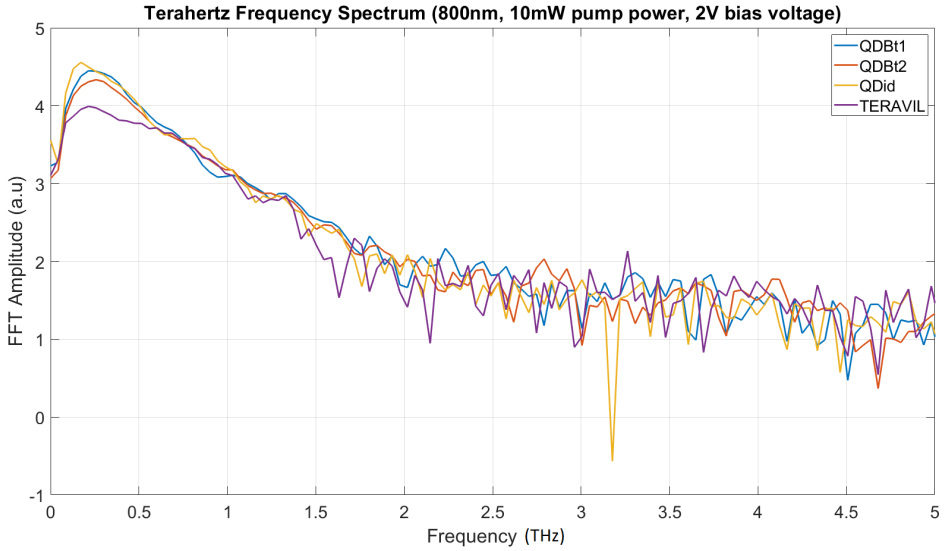
Terahertz Frequency Spectrum (800nm, 10mW pump power, 2V bias voltage)
QDBt1
QDBt2
QDid
TERAVIL
FFT Amplitude (a.u)
Frequency (THz)

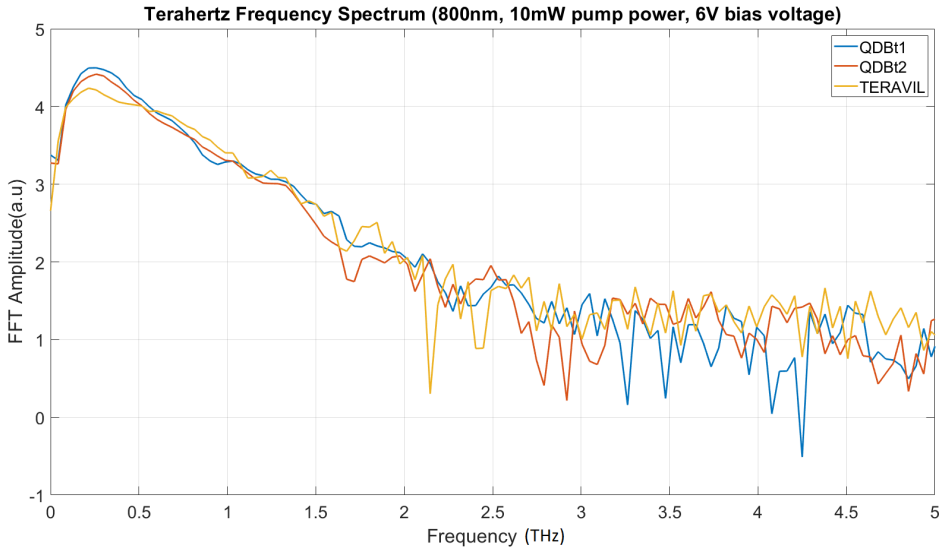
Terahertz Frequency Spectrum (800nm, 10mW pump power, 6V bias voltage)
QDBt1
QDBt2
TERAVIL
FFT Amplitude(a.u)
Frequency (THz)

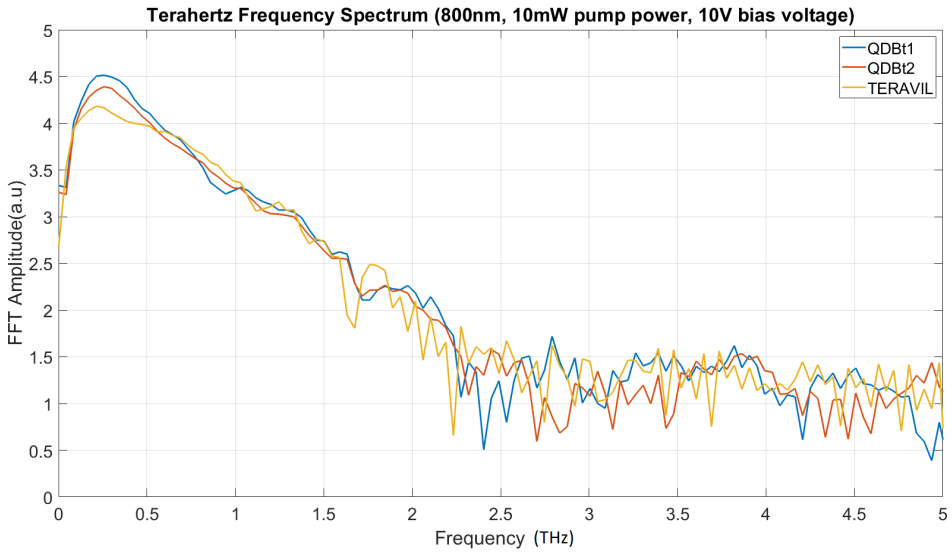

Figure 4.36: THz Frequency spectra of antennas at 10mW for 2v, 6V and 10V bias voltage

4.3.8 Discussion of Frequency domain properties at 800nm pump wavelength

Figure 4.26 (top plot) shows the Frequency spectrum of the fft of the entire temporal pulse length at 800nm wavelength, 2mW pump power and 2V bias voltage for the antennas. The results where normalised for comparison and it can be seen that the QD_id, QD_Bt2, QD_Bt1 and teravil antennas had an FFT amplitude of 4.5,4.4,4,4 and 3.55 (a.u) respectively. The precision and accuracy of the delay line movement eliminates pulse-pulse jitter and artefacts that can affect the fft of the signal, hence the absence of any abrupt artefacts in the frequency spectrum. The Figures 4.25 - 4.30 presented above shows the frequency spectrum of obtained from the fft of the THz time domain pulse at 800nm, the same parameters for the measurements at 780nm were carried out. Similar trends of increase in bandwidth with higher pump powers was recorded. The noise floor in 780nm is observed to be slightly higher than in 800nm at the relatively higher optical pump powers.

The results have consistently shown the increased THz output power from the Quantum dot antenna samples as compared to the Teravil antenna based on LT-GaAs. The antennas have been tested at 800nm wavelength

and 780nm wavelength at various pump powers and bias voltages as reported earlier in the chapter.

Chapter 5

5.1 Conclusion

This research project set out in the pursuit of compact terahertz sources, the utilization of Photoconductive antennas towards achieving this goal was identified due to their room-temperature operation, tunability and potential for integration of compact pump laser sources. The low optical pump to THz conversion efficiency was set out to be overcome by the utilisation of quantum dot structures in the antenna substrate, furthermore, the use of Quantum dots as the active region for compact optical source was established. The integration of quantum dot structures in lasers has enabled the development of lasers with the suitable requirements for the generation of continuous-wave terahertz. This research has demonstrated the appreciable properties of quantum dots towards realising a tunable, compact, room temperature continuous-wave terahertz source. A Quantum Dot external cavity laser emitting at two frequencies for continuous-wave terahertz emission in a Photoconductive Antenna (PCA) laser has been characterised. The external cavity QD Laser has been characterised with tunability of 152nm and a tuning range from 1143nm -1295.8nm that lies within the THz difference frequency for the generation of THz radiation from QD based PCAs The implementation of quantum dots in Terahertz Photoconductive antennas has been shown to yield various advantages in the Photoconductive antenna, the lack of defects in the quantum dot structures result in high carrier mobility and the quantum dots' action as carrier trapping sites shortens the lifetime of free carriers for more efficient PCAs. Antennas capitalising on quantum dot structures have been designed and tested for this research. The output terahertz was compared to a commercial antenna from teravil at various optical

pump and bias voltage parameters. The quantum dot antennas have shown a significant increase in THz output power at lower pump powers that are representative of the optical pump powers of semiconductor lasers that are planned to be integrated to the QD system towards an efficient compact THz system.The higher THz output powers obtained from the designed antennas for this research as compared to the commercial Teravil antenna paves the way for the utilisation of cheaper, low-power optical pump sources ($\sim$50mW) that effectively reduces the cost of the THz generation system. Non-resonant pumping of the antennas has shown a significant increase in THz output powers, the next step is for the design and development of Quantum dot lasers that will enable resonant pumping of the antennas at the bandgap energy of the QDs for a more efficient system. Due to the limitation of the antenna samples the operating parameters were set to be low, with more antenna samples in the future, the limiting parameters for the operation of the antennas will be measured for a more comprehensive characterization of the antennas.

Bibliography

[1] C. W. Berry, M. R. Hashemi, and M. Jarrahi, "Generation of high power pulsed terahertz radiation using a plasmonic photoconductive emitter array with logarithmic spiral antennas," *Applied Physics Letters*, vol. 104, no. 8, 2014.

[2] S. S. Dhillon, M. S. Vitiello, E. H. Linfield, A. G. Davies, M. C. Hoffmann, J. Booske, C. Paoloni, M. Gensch, P. Weightman, G. P. Williams, E. Castro-Camus, D. R. Cumming, F. Simoens, I. Escorcia-Carranza, J. Grant, S. Lucyszyn, M. Kuwata-Gonokami, K. Konishi, M. Koch, C. A. Schmuttenmaer, T. L. Cocker, R. Huber, A. G. Markelz, Z. D. Taylor, V. P. Wallace, J. Axel Zeitler, J. Sibik, T. M. Korter, B. Ellison, S. Rea, P. Goldsmith, K. B. Cooper, R. Appleby, D. Pardo, P. G. Huggard, V. Krozer, H. Shams, M. Fice, C. Renaud, A. Seeds, A. Stöhr, M. Naftaly, N. Ridler, R. Clarke, J. E. Cunningham, and M. B. Johnston, "The 2017 terahertz science and technology roadmap," *Journal of Physics D: Applied Physics*, vol. 50, no. 4, 2017.

[3] M. A. Belkin and F. Capasso, "New frontiers in quantum cascade lasers: High performance room temperature terahertz sources," *Physica Scripta*, vol. 90, no. 11, p. 118002, 2015.

[4] H A Hafez and X Chai and A Ibrahim and S Mondal and D Férachou and X Ropagnol and T Ozaki, "Intense terahertz radiation and their applications," *Journal of Optics*, vol. 18, no. 9, p. 93004, 2016.

[5] D. S. Sitnikov, S. A. Romashevskiy, A. V. Ovchinnikov, O. V. Chefonov, A. B. Savel'ev, and M. B. Agranat, "Estimation of THz field strength by an electro-optic sampling technique using arbitrary long gating pulses," *Laser Physics Letters*, vol. 16, p. 115302, 10 2019.

[6] A. Gorodetsky, K. A. Fedorova, N. Bazieva, and E. U. Rafailov, "Towards efficient and tunable generation of THz radiation from quantum dot based ultrafast photoconductive antennae (Conference Presentation)," in *Terahertz Emitters, Receivers, and Applications VII* (M. Razeghi, A. N. Baranov, J. M. Zavada, and D. Pavlidis, eds.), vol. 9934, p. 1, SPIE, 11 2016.

[7] Y.-S. Lee, *Principles of terahertz science and technology.* Springer, 1 ed., 2010.

[8] C. M. O'Sullivan and J. A. Murphy, *Field Guide to Terahertz Sources, Detectors, and Optics.* Bellingham: SPIE, first ed., 6 2012.

[9] K. A. Fedorova, A. Gorodetsky, E. U. Rafailov, and S. Member, "Compact All-Quantum-Dot-Based Tunable THz Laser Source," *IEEE Journal of Selected topics in Quantum Electronics*, vol. 23, no. 4, 2017.

[10] P. Siegel, "Terahertz technology," *IEEE Transactions on Microwave Theory and Techniques*, vol. 50, no. 3, pp. 910–928, 2002.

[11] M. Tonouchi, "Cutting-edge terahertz technology," *Nature Photonics*, vol. 1, no. 2, pp. 97–105, 2007.

[12] W. He, L. Zhang, D. Bowes, H. Yin, K. Ronald, A. D. R. Phelps, and A. W. Cross, "Generation of broadband terahertz radiation using a backward wave oscillator and pseudospark-sourced electron beam," *Applied Physics Letters*, vol. 107, no. 13, p. 133501, 2015.

[13] N. G. Gavrilov, B. A. Knyazev, E. I. Kolobanov, V. V. Kotenkov, V. V. Kubarev, G. N. Kulipanov, A. N. Matveenko, L. E. Medvedev, S. V. Miginsky, L. A. Mironenko, A. D. Oreshkov, V. K. Ovchar, V. M. Popik, T. V. Salikova, M. A. Scheglov, S. S. Serednyakov, O. A. Shevchenko, A. N. Skrinsky, V. G. Tcheskidov, and N. A. Vinokurov, "Status of the Novosibirsk high-power terahertz FEL," *Nuclear Instruments and Methods in Physics Research Section A: Accelerators, Spectrometers, Detectors and Associated Equipment*, vol. 575, no. 1, pp. 54–57, 2007.

[14] B. Williams, S. Kumar, Q. Hu, and J. Reno, "High-power terahertz quantum-cascade lasers," *Electronics Letters*, vol. 42, pp. 89–91, 1 2006.

[15] L. Li, L. Chen, J. Zhu, J. Freeman, P. Dean, A. Valavanis, A. G. Davies, and E. H. Linfield, "Terahertz quantum cascade lasers with ¿1 W output powers," *Electronics Letters*, vol. 50, no. 4, pp. 309–311, 2014.

[16] Menlo Systems, "TERA K15 Fibre-couple THz Time Domain Spectrometer."

[17] P. Tan, J. Huang, K. Liu, Y. Xiong, and M. Fan, "Terahertz radiation sources based on free electron lasers and their applications," *Science China Information Sciences*, vol. 55, pp. 1–15, 1 2012.

[18] E. L. Saldin, E. A. Schneidmiller, and M. V. Yurkov, "The physics of free electron lasers. An introduction," *Physics Reports*, vol. 260, no. 4, pp. 187–327, 1995.

[19] A. A. Andronov, V. A. Flyagin, A. V. Gaponov, A. L. Gol'denberg, M. I. Petelin, V. G. Usov, and V. K. Yulpatov, "The gyrotron: High-power source of millimetre and submillimetre waves," *Infrared Physics*, vol. 18, no. 5, pp. 385–393, 1978.

[20] V. A. Flyagin, A. G. Luchinin, and G. S. Nusinovich, "Submillimeter-wave gyrotrons: Theory and experiment," *International Journal of Infrared and Millimeter Waves*, vol. 4, pp. 629–637, 7 1983.

[21] G. Kozlov and A. Volkov, "Coherent source submillimeter wave spectroscopy," in *Millimeter and Submillimeter Wave Spectroscopy of Solids* (G. Grüner, ed.), pp. 51–109, Berlin, Heidelberg: Springer Berlin Heidelberg, 1998.

[22] A. Kozlov Gennadi
}and Volkov, "Coherent source submillimeter wave spectroscopy," in *Millimeter and Submillimeter Wave Spectroscopy of Solids* (G. Grüner, ed.), pp. 51–109, Berlin, Heidelberg: Springer Berlin Heidelberg, 1998.

[23] M. Micovic, A. Kurdoghlian, K. Shinohara, S. Burnham, I. Milosavljevic, M. Hu, A. Corrion, A. Fung, R. Lin, L. Samoska, P. Kangaslahti, B. Lambrigtsen, P. Goldsmith, W. S. Wong, A. Schmitz, P. Hashimoto, P. J. Willadsen, and D. H. Chow, "W-Band GaN MMIC with 842 mW output power at 88 GHz," in *2010 IEEE MTT-S International Microwave Symposium*, pp. 237–239, 2010.

[24] R. A. Lewis, *Terahertz Physics*. Cambridge: Cambridge University Press, 2012.

[25] S. I. Lepeshov, A. A. Gorodetsky, N. A. Toropov, T. A. Vartanyan, E. U. Rafailov, A. E. Krasnok, and P. A. Belov, "Optimization of Nanoantenna-Enhanced Terahertz Emission from Photoconductive Antennas," in *Journal of Physics: Conference Series*, 2017.

[26] S. Lepeshov, A. Gorodetsky, A. Krasnok, E. Rafailov, and P. Belov, "Enhancement of terahertz photoconductive antenna operation by optical nanoantennas," *Laser & Photonics Reviews*, vol. 11, no. 1, p. 1600199.

[27] M. Razeghi, "Toward realizing high power semiconductor terahertz laser sources at room temperature," vol. 8023, p. 802302, 5 2011.

[28] A. A. Khorami, A. Riahi, M. Ghahramani, and P. Bazvand, "Design and simulation of terahertz GaAs/AlGaAs quantum cascade laser for higher power performance," *Optik - International Journal for Light and Electron Optics*, vol. 127, pp. 1097–1099, 2 2016.

[29] M. Razeghi, "High-performance InP-based mid-IR quantum cascade lasers," *IEEE Journal on Selected Topics in Quantum Electronics*, vol. 15, no. 3, pp. 941–951, 2009.

[30] K. Ravi, W. R. Huang, S. Carbajo, E. A. Nanni, D. N. Schimpf, E. P. Ippen, and F. X. Kärtner, "Theory of terahertz generation by optical rectification using tilted-pulse-fronts," vol. 23, no. 4, pp. 5253–5276, 2015.

[31] S.-w. Huang, E. Granados, W. R. Huang, K.-h. Hong, L. E. Zapata, and F. X. Kärtner, "High conversion efficiency , high energy terahertz pulses by optical rectification in cryogenically cooled lithium niobate," *Optics Letters*, vol. 38, no. 5, pp. 796–798, 2013.

[32] M. Jewariya, M. Nagai, and K. Tanaka, "Enhancement of terahertz wave generation by cascaded $\chi\hat{}(2)$ processes in LiNbO_3," *Journal of the Optical Society of America B*, vol. 26, no. 9, p. A101, 2009.

[33] E. R. Brown, F. W. Smith, and K. A. McIntosh, "Coherent millimeter-wave generation by heterodyne conversion in low-temperature-grown

GaAs photoconductors," *Journal of Applied Physics*, vol. 73, pp. 1480–1484, 2 1993.

[34] D. H. Auston, K. P. Cheung, and P. R. Smith, "Picosecond photoconducting Hertzian dipoles," *Applied Physics Letters*, vol. 45, pp. 284–286, 8 1984.

[35] D. Saeedkia, B. Ung, M. Skorobogatiy, J. G. Rivas, Y. Zhang, A. Berrier, D.-S. Kim, Y.-M. Bahk, P. Planken, W. Knap, M. Dyakonov, J. F. Federici, L. Moeller, K. Su, J.-H. Son, S. Boppel, A. Lisauskas, H. Roskos, R. Singh, A. Azad, W. Zhang, M. Theuer, F. Ellrich, D. Molter, R. Beigang, A. Deninger, M. Nagel, H. Kurz, C. Matheisen, Y. Kawano, T. Ouchi, T. Yasui, M. Missous, T. Shibuya, K. Kawase, Riken, M. J. Bohn, D. T. Petkie, M. Reid, I. Hartley, T. Todoruk, Y.-C. Shen, B. B. Jin, K. Fukunaga, Y. Cai, Z. Wang, and D. Goyal, *Handbook of Terahertz Technology for Imaging, Sensing and Communications*. Woodhead Publishing Series in Electronic and Optical Materials, Elsevier, 2013.

[36] D. Klocke, A. Schmitz, H. Soltner, H. Bousack, and H. Schmitz, "Infrared receptors in pyrophilous ("fire loving") insects as model for new un-cooled infrared sensors," *Beilstein Journal of Nanotechnology*, vol. 2, pp. 186–197, 2011.

[37] Stanford Research Systems, "Model SR830 DSP Lock-In Amplifier," 2011.

[38] J. Neu and C. A. Schmuttenmaer, "Tutorial: An introduction to terahertz time domain spectroscopy (THz-TDS)," *Journal of Applied Physics*, vol. 124, no. 23, p. 231101, 2018.

[39] B. B. Hu and M. C. Nuss, "Imaging with terahertz waves," *Opt. Lett.*, vol. 20, pp. 1716–1718, 8 1995.

[40] D. D. Arnone, C. M. Ciesla, A. Corchia, S. Egusa, M. Pepper, J. M. Chamberlain, C. Bezant, E. H. Linfield, R. Clothier, and N. Khammo, "Applications of terahertz (THz) technology to medical imaging," in *Terahertz Spectroscopy and Applications II* (J. M. Chamberlain, ed.), vol. 3828, pp. 209–219, International Society for Optics and Photonics, SPIE, 1999.

[41] R. M. Woodward, V. P. Wallace, R. J. Pye, B. E. Cole, D. D. Arnone, E. H. Linfield, and M. Pepper, "Terahertz pulse imaging of ex vivo basal cell carcinoma.," *The Journal of investigative dermatology*, vol. 120, pp. 72–78, 1 2003.

[42] V. P. Wallace, A. J. Fitzgerald, S. Shankar, N. Flanagan, R. Pye, J. Cluff, and D. D. Arnone, "Terahertz pulsed imaging of basal cell carcinoma ex vivo and in vivo," *British Journal of Dermatology*, vol. 151, no. 2, pp. 424–432, 2004.

[43] E. Pickwell and V. P. Wallace, "Biomedical applications of terahertz technology," *Journal of Physics D: Applied Physics*, vol. 39, pp. R301–R310, 8 2006.

[44] P. H. Siegel, "Terahertz technology in biology and medicine," *IEEE Transactions on Microwave Theory and Techniques*, vol. 52, no. 10, pp. 2438–2447, 2004.

[45] H. J. Joyce, J. L. Boland, C. L. Davies, S. A. Baig, and M. B. Johnston, "A review of the electrical properties of semiconductor nanowires: insights gained from terahertz conductivity spectroscopy," *Semiconductor Science and Technology*, vol. 31, p. 103003, 9 2016.

[46] H. Shams, M. J. Fice, K. Balakier, C. C. Renaud, F. van Dijk, and A. J. Seeds, "Photonic generation for multichannel THz wireless communication," *Opt. Express*, vol. 22, pp. 23465–23472, 9 2014.

[47] G. Ducournau, P. Szriftgiser, A. Beck, D. Bacquet, F. Pavanello, E. Peytavit, M. Zaknoune, T. Akalin, and J.-F. Lampin, "Ultrawide-Bandwidth Single-Channel 0.4-THz Wireless Link Combining Broadband Quasi-Optic Photomixer and Coherent Detection," *IEEE Transactions on Terahertz Science and Technology*, vol. 4, no. 3, pp. 328–337, 2014.

[48] X. Wei, "China Sends World's First 6G Test Satellite Into Orbit," 2020.

[49] S. Gupta, M. Y. Frankel, J. A. Valdmanis, J. F. Whitaker, G. A. Mourou, F. W. Smith, and A. R. Calawa, "Subpicosecond carrier lifetime in GaAs grown by molecular beam epitaxy at low temperatures," *Appl. Phys. Lett.*, vol. 59, no. 25, pp. 3276–3278, 1991.

[50] A. C. Warren, N. Katzeneilenbogen, D. Grischkowsky, and J. M. Woodall, "Subpicosecond, freely propagating detection using GaAs : As epilayers electromagnetic pulse generation and," *Society*, pp. 1512–1514, 1991.

[51] P. P. Vasil'ev, "Picosecond optoelectronics," *Soviet Journal of Quantum Electronics*, vol. 20, no. April, pp. 209–227, 2007.

[52] F. J. Leonberger, "Applications Of InP Photoconductive Switches," no. July 1981, pp. 58–65, 1981.

[53] P. R. Smith, D. H. Auston, and M. C. Nuss, "Subpicosecond Photoconducting Dipole Antennas," *IEEE Journal of Quantum Electronics*, vol. 24, no. 2, pp. 255–260, 1988.

[54] M. Tani, M. Herrmann, and K. Sakai, "Generation and detection of terahertz pulsed radiation with photoconductive antennas and its application to imaging," *Measurement Science and Technology*, vol. 13, no. 11, pp. 1–4, 2002.

[55] C. W. Berry, N. Wang, M. R. Hashemi, M. Unlu, and M. Jarrahi, "Significant performance enhancement in photoconductive terahertz optoelectronics by incorporating plasmonic contact electrodes," *Nature Communications*, 2013.

[56] W. Shi, Z.-z. Zhang, L. Hou, and Z. Liu, "Terahertz generation from SI-GaAs photoconductive dipole antenna with different electrode gaps," vol. 7385, p. 73851P, 7 2009.

[57] M. Klos, R. Bartholdt, J. Klier, J.-F. Lampin, and R. Beigang, "Photoconductive antennas based on low temperature grown GaAs on silicon substrates for broadband terahertz generation and detection," vol. 974712, no. May 2016, p. 974712, 2016.

[58] N. M. Burford and M. O. El-Shenawee, "Review of terahertz photoconductive antenna technology," *Optical Engineering*, vol. 56, no. 1, p. 010901, 2017.

[59] C. Zhang, Y. Wang, J. Ma, B. Jin, W. Xu, L. Kang, J. Chen, P. Wu, and M. Tonouchi, "Temperature dependence of terahertz properties for InP," vol. 7277, no. February 2009, pp. 1–7, 2008.

[60] M. Y. Jeon, N. Kim, J. Shin, C. W. Lee, S.-p. Han, Y. A. Leem, D.-s. Yee, S. K. Noh, and K. H. Park, "Continuous Terahertz Wave Emission Using Tunable," *35th International Conference on Infrared, Millimeter, and Terahertz Waves*, pp. 3–4, 2010.

[61] M. Tani, S. Matsuura, K. Sakai, and S.-i. Nakashima, "Emission characteristics of photoconductive antennas based on low-temperature-grown GaAs and semi-insulating GaAs," *Appl. Opt.*, vol. 36, pp. 7853–7859, 10 1997.

[62] S. Yang and M. Jarrahi, "High-power continuous-wave terahertz generation through plasmonic photomixers," in *2016 IEEE MTT-S International Microwave Symposium (IMS)*, pp. 1–4, 2016.

[63] S.-P. Han, H. Ko, N. Kim, W.-H. Lee, K. Moon, I.-M. Lee, E. S. Lee, D. H. Lee, W. Lee, S.-T. Han, S.-W. Choi, and K. H. Park, "Real-time continuous-wave terahertz line scanner based on a compact 1 {\texttimes} 240 InGaAs Schottky barrier diode array detector," *Opt. Express*, vol. 22, pp. 28977–28983, 11 2014.

[64] C. W. Berry, N. Wang, M. R. Hashemi, and M. Jarrahi, "Plasmonic photoconductive antennas for high-power terahertz generation and high-sensitivity terahertz detection," in *The 8th European Conference on Antennas and Propagation (EuCAP 2014)*, pp. 2643–2646, 2014.

[65] N. Vieweg, M. Mikulics, M. Scheller, K. Ezdi, R. Wilk, H.-W. Hübers, and M. Koch, "Impact of the contact metallization on the performance of photoconductive THz antennas," *Opt. Express*, vol. 16, pp. 19695–19705, 11 2008.

[66] C. W. Berry, M. R. Hashemi, M. Unlu, and M. Jarrahi, "Nanoscale Contact Electrodes for Significant Radiation Power Enhancement in Photoconductive Terahertz Emitters," pp. 7–10, 2013.

[67] S. I. L. Rafailov, A. A. Gorodetsky, N. A. Toropov, T. A. Vartanyan, A. E. Krasnok, P. A. Belov, and E. U, "Novel Optimized Hybrid Terahertz Photoconductive Antennas," *Journal of Physics: Conference Series*, vol. 1092, no. 1, p. 12076, 2018.

[68] S.-G. Park, K. H. Jin, M. Yi, J. C. Ye, J. Ahn, and K.-H. Jeong, "Enhancement of terahertz pulse emission by optical nanoantenna.," *ACS nano*, vol. 6, pp. 2026–2031, 3 2012.

[69] P. J. Hale, J. Madeo, C. Chin, S. S. Dhillon, J. Mangeney, J. Tignon, and K. M. Dani, "20 THz broadband generation using semi-insulating GaAs interdigitated photoconductive antennas," *Opt. Express*, vol. 22, pp. 26358–26364, 10 2014.

[70] G. Matthäus, S. Nolte, R. Hohmuth, M. Voitsch, W. Richter, B. Pradarutti, S. Riehemann, G. Notni, and A. Tunnermann, "Microlens coupled interdigital photoconductive switch," *Applied Physics Letters*, vol. 93, p. 91110, 2008.

[71] A. Singh and S. S. Prabhu, "Plasmonic Interdigitated Photoconductive Antenna for THz Emission," in *12th International Conference on Fiber Optics and Photonics*, p. M4A.42, Optical Society of America, 2014.

[72] A. Singh and S. S. Prabhu, "Microlensless interdigitated photoconductive terahertz emitters," *Opt. Express*, vol. 23, pp. 1529–1535, 1 2015.

[73] S. Yang, M. R. Hashemi, C. W. Berry, and M. Jarrahi, "High-efficiency photoconductive terahertz antennas based on high-aspect ratio plasmonic electrodes," in *2014 IEEE Antennas and Propagation Society International Symposium (APSURSI)*, pp. 902–903, 2014.

[74] N. T. Yardimci and M. Jarrahi, "3.8 mW terahertz radiation generation over a 5 THz radiation bandwidth through large area plasmonic photoconductive antennas," in *2015 IEEE MTT-S International Microwave Symposium*, pp. 1–4, 2015.

[75] R. Leyman, D. Carnegie, K. Fedorova, N. Bazieva, S. Schulz, C. Reardon, E. Clarke, and E. U. Rafailov, *THz emission from quantum dot-based THz antennas pumped by a quantum-dot tunable laser diode*. 5 2013.

[76] E. U. Rafailov, R. Leyman, D. Carnegie, and N. Bazieva, "Highly efficient quantum dot-based photoconductive THz materials and devices," No. September 2013, p. 88460I, 9 2013.

[77] M. A. Reed, "Quantum Dots," *Scientific American*, vol. 268, no. 1, pp. 118–123, 1993.

[78] Y.-C. Xin, L. G. Vaughn, L. R. Dawson, A. Stintz, Y. Lin, L. F. Lester, and D. L. Huffaker, "InAs quantum-dot GaAs-based lasers grown on AlGaAsSb metamorphic buffers," *Journal of Applied Physics*, vol. 94, pp. 2133–2135, 7 2003.

[79] S. Raghavan, D. Forman, P. Hill, N. R. Weisse-Bernstein, G. von Winckel, P. Rotella, S. Krishna, S. W. Kennerly, and J. W. Little, "Normal-incidence InAs/In0.15Ga0.85As quantum dots-in-a-well detector operating in the long-wave infrared atmospheric window (8–12 μm)," *Journal of Applied Physics*, vol. 96, pp. 1036–1039, 6 2004.

[80] A. Zrenner, E. Beham, S. Stufler, F. Findeis, M. Bichler, and G. Abstreiter, "Coherent properties of a two-level system based on a quantum-dot photodiode," *Nature*, vol. 418, p. 612, 8 2002.

[81] R. Leyman, D. Carnegie, K. A. Fedorova, N. Bazieva, S. Schulz, C. Reardon, E. Clarke, and E. U. Rafailov, "THz Emission from Quantum Dot-Based THz Antennas Pumped by a Tunable Quantum-Dot Laser Diode," in *2013 Conference on Lasers and Electro-Optics - International Quantum Electronics Conference*, p. CC_P_5, Optical Society of America, 2013.

[82] J. J. Coleman, "The development of the semiconductor laser diode after the first demonstration in 1962," *Semiconductor Science and Technology*, vol. 27, no. 9, p. 90207, 2012.

[83] H. Park, J. Kim, E. Jung, W. Choi, J. Lee, and H. Han, "Enhanced terahertz emission from InAs quantum dots on GaAs," vol. 6352, p. 63521Z, 9 2006.

[84] E. U. Rafailov, *The Physics and Engineering of Compact Quantum Dot-based Lasers for Biophotonics*. Wiley, 2014.

[85] E. R. Brown, K. A. McIntosh, K. B. Nichols, and C. L. Dennis, "Photomixing up to 3.8 THz in low-temperature-grown GaAs," *Applied Physics Letters*, vol. 66, pp. 285–287, 1 1995.

[86] J. R. Demers, R. T. Logan, and E. R. Brown, "An Optically Integrated Coherent Frequency-Domain THz Spectrometer with Signal-to-Noise Ratio up to 80 dB," in *Microwave Photonics, 2007 Interntional Topical Meeting on*, pp. 92–95, 2007.

[87] S. Verghese, K. A. McIntosh, and E. R. Brown, "Optical and terahertz power limits in the low-temperature-grown GaAs photomixers," *Applied Physics Letters*, vol. 71, no. 19, pp. 2743–2745, 1997.

[88] M. Tani, P. Gu, M. Hyodo, K. Sakai, and T. Hidaka, "Generation of coherent terahertz radiation by photomixing of dual-mode lasers," *Optical and Quantum Electronics*, vol. 32, no. 4, pp. 503–520, 2000.

[89] R. N. Hall, G. E. Fenner, J. D. Kingsley, T. J. Soltys, and R. O. Carlson, "Coherent Light Emission From GaAs Junctions," *Phys. Rev. Lett.*, vol. 9, pp. 366–368, 11 1962.

[90] N. Ledentsov, V. M. Ustinov, A. Yu. Egorov, A. Zhukov, M. V. Maksimov, I. G. Tabatadze, and P. S. Kop'ev, *Optical properties of heterostructures with InGaAs-GaAs quantum clusters*, vol. 28. 1 1994.

[91] N. Kirstaedter, N. N. Ledentsov, M. Grundmann, D. Bimberg, V. M. Ustinov, S. S. Ruvimov, M. V. Maximov, P. S. Kop'ev, Z. I. Alferov, U. Richter, P. Werner, U. Gosele, and J. Heydenreich, "Low threshold, large T/sub o/ injection laser emission from (InGa)As quantum dots," *Electronics Letters*, vol. 30, no. 17, pp. 1416–1417, 1994.

[92] N. A. Naderi, F. Grillot, K. Yang, J. B. Wright, A. Gin, and L. F. Lester, "Two-color multi-section quantum dot distributed feedback laser," *Opt. Express*, vol. 18, pp. 27028–27035, 12 2010.

[93] M. Naftaly, M. R. Stone, A. Malcoci, R. E. Miles, and I. C. Mayorga, "Generation of CW terahertz radiation using two-colour laser with Fabry-Perot etalon ELECTRONICS LETTERS 3rd February 2005 ELECTRONICS LETTERS 3rd February 2005," *Electronics Letters*, vol. 41, no. 3, 2005.

[94] Z. Jiao, J. Liu, Z. Lu, X. Zhang, P. J. Poole, P. J. Barrios, D. Poitras, and J. Caballero, "Tunable Terahertz Beat Signal Generation From an InAs / InP Quantum-Dot Mode-Locked Laser Combined With External-Cavity," vol. 24, no. 6, pp. 518–520, 2012.

[95] D. Wandt, M. Laschek, A. Tünnermann, and H. Welling, "Continuously tunable external-cavity diode laser with a double-grating arrangement," *Opt. Lett.*, vol. 22, pp. 390–392, 3 1997.

[96] H. Lotem, Z. Pan, and M. Dagenais, "Tunable dual-wavelength continuous-wave diode laser operated at 830 nm," *Appl. Opt.*, vol. 32, pp. 5270–5273, 9 1993.

[97] K.-S. Lee and C. Shu, "Generation of widely tunable (65-nm) dual-wavelength picosecond pulses by harmonic and rational-harmonic mode locking of a Fabry–Perot grating-lens external-cavity laser," *J. Opt. Soc. Am. B*, vol. 16, pp. 710–716, 5 1999.

[98] C. Wang and C. Pan, "Tunable dual-wavelength operation of a diode array with an external grating-loaded cavity," *Applied Physics Letters*, vol. 64, no. 23, pp. 3089–3091, 1994.

[99] C.-L. Wang and C.-L. Pan, "Tunable multiterahertz beat signal generation from a two-wavelength laser-diode array," *Opt. Lett.*, vol. 20, pp. 1292–1294, 6 1995.

[100] P. Knobloch, C. Schildknecht, T. Kleine-Ostmann, M. Koch, S. Hoffmann, M. Hofmann, E. Rehberg, M. Sperling, K. Donhuijsen, G. Hein, and K. Pierz, "Medical THz imaging: an investigation of histopathological samples.," *Physics in medicine and biology*, vol. 47, pp. 3875–3884, 11 2002.

[101] L. Ricci, M. Weidemüller, T. Esslinger, A. Hemmerich, C. Zimmermann, V. Vuletic, W. König, and T. W. Hänsch, "A compact grating-stabilized diode laser system for atomic physics," *Optics Communications*, vol. 117, no. 5, pp. 541–549, 1995.

[102] A. S. Arnold, J. S. Wilson, and M. G. Boshier, "A simple extended-cavity diode laser," *Review of Scientific Instruments*, vol. 69, no. 3, pp. 1236–1239, 1998.

[103] Thorlabs, "DIFFRACTION GRATINGS TUTORIAL."

[104] W. E. L. Jr., "Theory of an Optical Maser," *Physical Review*, vol. 134, no. 6A, pp. 1429–1450, 1964.

[105] T. Andrzejewska, J. Badziak, A. Dubicki, and R. Wodnicki, "Nanosecond Pulse Generation In The Laser With The Pulsed Transmission Of The Q-Switch. Theory And Experiment.," No. March 1985, p. 39, 3 1985.

[106] P. F. Moulton, "Spectroscopic and laser characteristics of Ti:Al_2O_3," *Journal of the Optical Society of America B*, vol. 3, no. 1, p. 125, 1986.

[107] G. Loas, M. Romanelli, and M. Alouini, "Dual-frequency 780-nm Ti:Sa laser for high spectral purity tunable CW THz generation," *IEEE Photonics Technology Letters*, vol. 26, no. 15, pp. 1518–1521, 2014.

[108] P. J. Hale, J. Madeo, C. Chin, S. S. Dhillon, J. Mangeney, J. Tignon, and K. M. Dani, "Broadband THz generation using interdigitated photoconductive antennas with a 15 fs, high power oscillator," *2013 Conference on Lasers and Electro-Optics, CLEO 2013*, vol. 1, pp. 15–16, 2013.

[109] J. C. Chen, K. L. Yeh, M. J. Khan, J. Hebling, M. C. Hoffmann, S. Kaushik, and K. A. Nelson, "Terahertz Generation and Detection Using Frequency Conversion," *2009 Conference on Lasers and Electro-Optics and Quantum Electronics and Laser Science Conference (Cleo/Qels 2009), Vols 1-5*, pp. 1981–1982, 2009.

[110] F. Ahr, S. W. Jolly, N. H. Matlis, S. Carbajo, T. Kroh, K. Ravi, D. N. Schimpf, J. Schulte, H. Ishizuki, T. Taira, A. R. Maier, and F. X. Kärtner, "Narrowband terahertz generation with chirped-and-delayed laser pulses in periodically poled lithium niobate," *Optics Letters*, vol. 42, no. 11, p. 2118, 2017.

[111] V. Apostolopoulos and M. E. Barnes, "THz emitters based on the photo-Dember effect," *Journal of Physics D: Applied Physics*, 2014.

[112] K. S. Rao, M. Venkatesh, S. P. Tewari, and A. K. Chaudhary, "Generation of Terahertz Radiationin ZnGeP 2 by Difference Frequency Mixing Technique Using Femto Seconds Laser System," *International Conference on Fiber Optics and Photonics*, no. 3, pp. 2–4, 2012.

[113] J. Darmo, T. Müller, G. Strasser, and K. Unterrainer, "Voltage-controlled intracavity THz generator for self-starting Ti : Sapphire

lasers," *Summaries of Papers Presented at the Lasers and Electro-Optics. CLEO '02. Technical Diges*, pp. 3–5, 2002.

[114] J. Zhang, "Characterization of the terahertz photoconductive antenna by three-dimensional finite-difference time-domain method," 2014.

[115] F. D. J. Brunner, A. Schneider, and P. Günter, "High-efficiency terahertz generation in hydrogen-bonded organic nonlinear optical crystals," *34th International Conference on Infrared, Millimeter, and Terahertz Waves, IRMMW-THz 2009*, no. 3, p. 8093, 2009.

[116] R. J. B. Dietz, N. Vieweg, T. Puppe, A. Zach, B. Globisch, T. Göbel, P. Leisching, and M. Schell, "All fiber-coupled THz-TDS system with kHz measurement rate based on electronically controlled optical sampling," *Optics Letters*, vol. 39, no. 22, p. 6482, 2014.

[117] A. Gorodetsky, I. T. Leite, and E. U. Rafailov, "Operation of quantum dot based terahertz photoconductive antennas under extreme pumping conditions," *Applied Physics Letters*, vol. 119, no. 11, p. 111102, 2021.

Appendix A - Thesis Contribution

- Nasir G Bello, Semyon V Smirnov, Amit Yadav, Andrei Gorodetsky, Edik U Rafailov, ″THz generation comparison from a QD Photoconductive antenna and commercial antenna at low pump-power,″ Proc. SPIE 11827, Terahertz Emitters, Receivers, and Applications XII, 118270L (1 August 2021).

- Nasir G. Bello, Semen Smirnov, Andrei Gorodetsky, Edik U. Rafailov, ″Towards realisation of an efficient continuous wave terahertz source using quantum dot devices,″ Proc. SPIE 11124, Terahertz Emitters, Receivers, and Applications X, 111240G (6 September 2019).

- Nasir.G. Bello, S.Smirnov and E. Rafailov, External Cavity Continuous Wave Laser for All Quantum dot CW THz emission, IONS Exeter 2019, Poster Presentation.

- Nasir G. Bello, S.Smirnov and E. Rafailov,″ CW Laser for All Quantum dot CW THz emission″, SIOE 2019 Cardiff, Poster Presentation.

- Nasir G. Bello and E.Rafailov ″Methods of generating terahertz: A review″, Aston EAS Postgraduate conference 2018, Poster Presentation.

Appendix B - QD laser diode connection Schematic

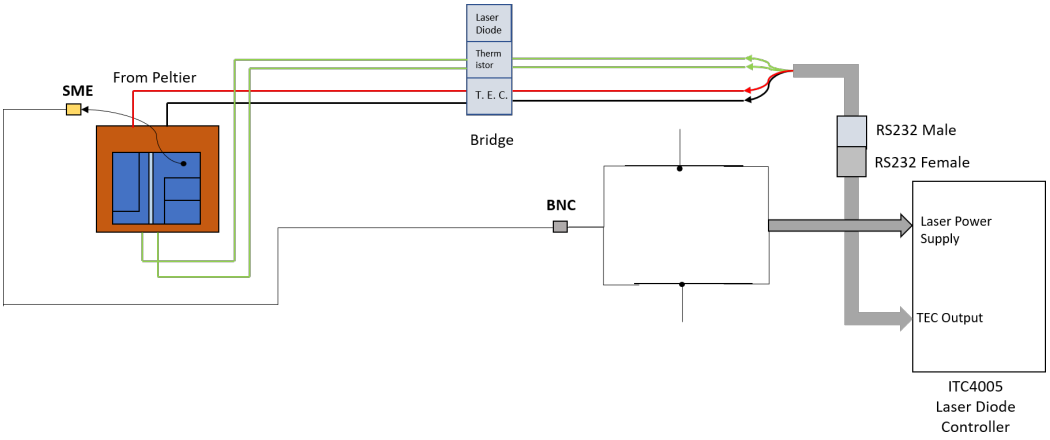

Figure 5.1: QD Laser connection schematic
The figure shows a schematic of the connection interface between the designed Quantum dot laser to a diode controller for power supply and temperature management.